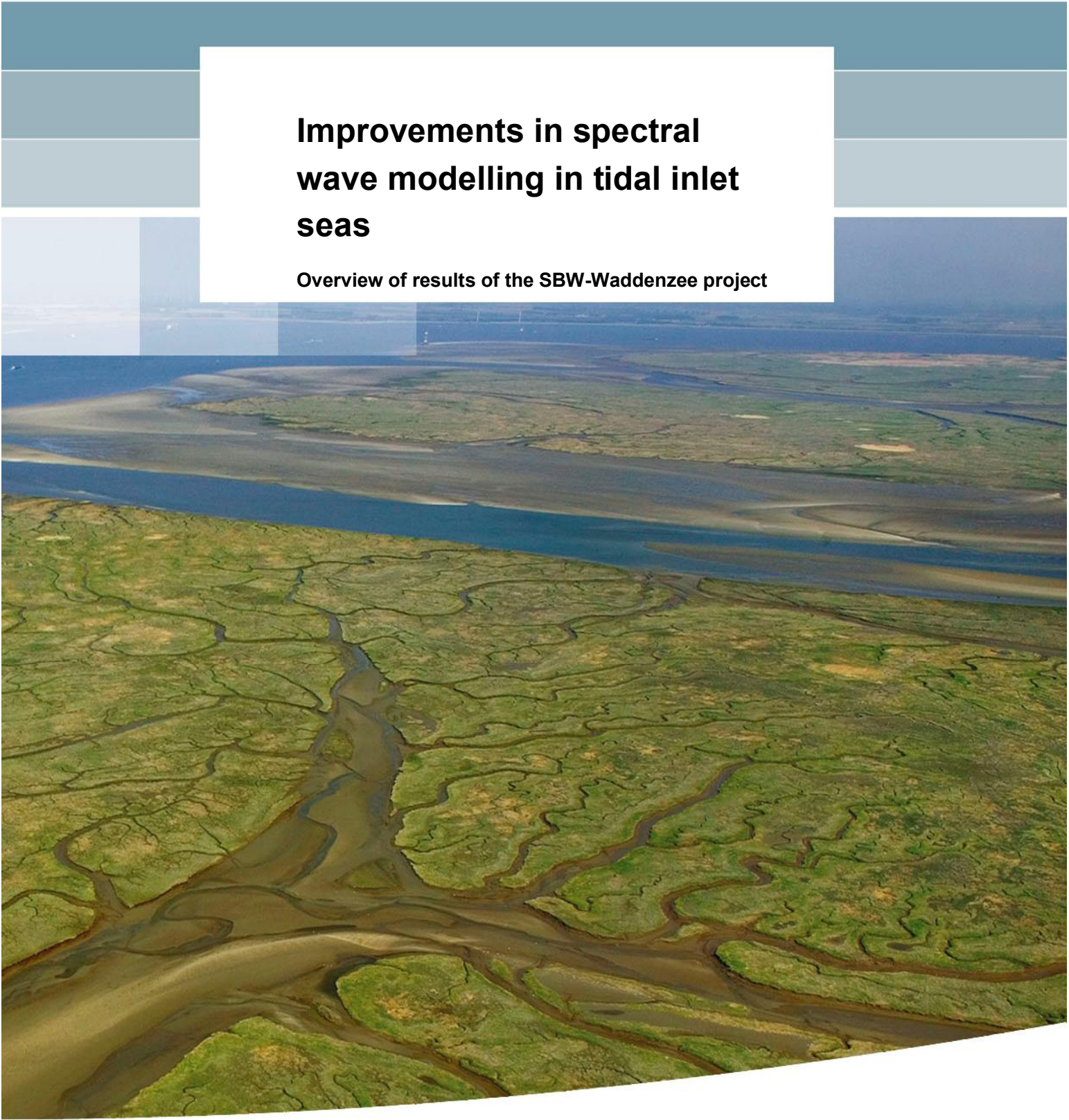


**Improvements in spectral
wave modelling in tidal inlet
seas**

Overview of results of the SBW-Waddenzee project



Improvements in spectral wave modelling in tidal inlet seas

Overview of results of the SBW-Waddenzee project 2006-2010

Andre van der Westhuysen
Ap van Dongeren
Joana van Nieuwkoop
Jacco Groeneweg
Sepehr Eslami Arab

1202119-006

Title

Improvements in spectral wave modelling in tidal inlet seas

Client	Project	Reference	Pages
Waterdienst	1202119-006	1202119-006-HYE-0003	42

Trefwoorden

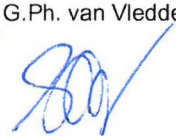
Wave modeling, Tidal inlets, SWAN, Wadden Sea, Spectral wave models, wave breaking dissipation, wave-current interaction.

Samenvatting

Over the last five years a research program has been carried out to assess the performance of the spectral wave model SWAN in the Wadden Sea so that it may be used for the transformation of offshore wave conditions to wave boundary conditions near the sea defenses (dikes and dunes). The assessment was done on the basis of extensive wave measurements conducted in the Ameland inlet and the Dutch Eastern Wadden Sea, as well as relevant data from other inlets, lakes and estuaries. We found that the 2006 default version of SWAN (version 40.51) performed reasonably well for storm conditions, but three aspects required further attention. First, over the tidal flats, the computed ratio of integral wave height over water depth showed an apparent upper limit using the conventional Battjes and Janssen (1978) depth-limited wave breaking formulation with default breaking parameter. Using the default settings, the wave height for a given water depth would be underpredicted near the sea defenses adjacent to nearly-horizontal flats. The problem has been largely solved using a new breaker formulation. The second area of model improvement concerns two processes related to wave-current interaction, namely the so-called wave age effect on waves generated in ambient current, and enhanced dissipation due to wave steepening in negative current gradients. Third, the variance density of lower-frequency wind waves from the North Sea penetrating into the inlet was underpredicted. Best results were obtained when the bottom friction coefficient was set at a lower value than the current default for wind seas. All these improvements have lead to a wave transformation model with which reliable wave conditions in the Wadden Sea and related complex areas can be determined.

Referenties

Project SBW-Waddenzee 1202119

Versie	Datum	Auteur	Paraaf	Review	Paraaf	Goedkeuring	Paraaf
1.0	Feb. 2011	A.J. v.d. Westhuysen et al.					
6.0	May 2011	A.J. v.d. Westhuysen, A.R. van Dongeren, J.L.L. van Nieuwkoop, J. Groeneweg, S. Eslami Arab		G.Ph. van Vledder 		M.R.A. van Gent 	

State
final

Contents

List of Tables	iii
List of Figures	v
1 Introduction	1
2 Observations	3
2.1 Monitoring network	3
2.2 SBW observational campaign	3
2.3 Other data sets used	7
2.3.1 Norderneyer Seegat	7
2.3.2 Eastern Scheldt	8
2.3.3 Lake IJssel and Lake Sloten	9
3 SWAN Wave action model formulation	11
3.1 Governing equations of SWAN	11
3.2 Default 2006 model formulations and settings	12
3.3 Proposed 2010 model formulations and settings	12
3.4 Qualitative and quantitative performance assessment	12
4 Results	15
4.1 Default model	15
4.2 Model innovations	15
4.2.1 Depth-induced breaking under finite-depth wave growth conditions	15
4.2.2 Wave-current interaction	18
4.2.3 Penetration of low-frequency wind wave energy	22
4.3 Results of the proposed model	24
5 Discussion	27
6 Conclusions	31
7 Outlook	33
7.1 Modeling	33
7.2 Information need	33
8 Acknowledgments	35
9 References	37
10 SBW Waddenzee research reports	41
Appendices	
A Figures	A-1

List of Tables

Table 2.1	Selection of stationary cases recorded in the Amelander Zeegat during the period 2004-2007. Computed wind speed and direction are mean values over domain. Water level at station Nes and maximum computed current speed u_{\max} in the inlet main channel. Acronyms: 'wp' = wave penetration, 'wci' = wave-current interaction and 'fdg' = finite-depth wave growth.	5
Table 2.2	Selection of stationary cases recorded in the Eastern Dutch Wadden Sea during the period 2006-2007. Computed wind speed and direction are mean values over domain. Water level at station Huibergat and maximum computed current speed u_{\max} in the inlet main channel. Acronyms: 'wp' = wave penetration and 'fdg' = finite-depth wave growth.	7
Table 2.3	Selected stationary case recorded in the Norderneyer Seegat. Computed wind speed and direction are mean values over domain. Water level at Riffgat (relative to German leveling datum Normal Null) and maximum computed current speed u_{\max} in the inlet main channel. Acronym: 'wci' = wave-current interaction.	8
Table 2.4	Selection of stationary cases recorded in the Eastern Scheldt. Computed wind speed and direction are mean values over domain. Water level at station BG2 and maximum computed current speed. These conditions are used for assessing wave penetration.	8
Table 2.5	Selection of stationary cases recorded in Lake IJssel. Water level represents the lake mean (Dutch: 'meetpeil') and currents were omitted. Wind speed and direction are lake means. Acronyms: 'fdg' = finite-depth wave growth.	9
Table 2.6	Selection of stationary cases recorded in Lake Sloten. Water level, wind speed and wind direction at station SL29. Currents were omitted. Acronyms: 'fdg' = finite-depth wave growth.	10

List of Figures

- Figure 1 Bathymetry of the Dutch Wadden Sea. Bed levels are given in m below NAP (Dutch leveling datum). The boxes indicate detail areas, shown in detail figures. Projection in Dutch Rijksdriehoek (RD) system
- Figure 2 Bathymetry of the Amelandier Zeegat region in the Dutch Wadden Sea, including the location of the wave buoys (circles), in the configuration of 2003–2006
- Figure 3 Bathymetry of the Amelandier Zeegat region in the Dutch Wadden Sea, including the location of the wave buoys (circles) in the configuration of 2007–present
- Figure 4 Bathymetry of the Dutch Eastern Wadden Sea, including the location of the wave buoys (circles)
- Figure 5 Observed spectra along the NW–SE array in the Amelandier Zeegat at three stages during a tidal cycle at the peak of the storm of 8–9 November 2007. Dash-dot line in bottom panels indicates wind direction.
- Figure 6 Observed spectra in the Eastern Dutch Wadden Sea at three stages during one half tidal cycle during the peak of the storm of 8–9 November 2007. Dash-dot line in bottom panels indicates wind direction.
- Figure 7 Bathymetry relative to MSL of the Norderneyer Seegat, including the location of the wave buoys (circles)
- Figure 8 Bathymetry of the mouth of the Eastern Scheldt, including the location of the wave buoys (circles)
- Figure 9 Bathymetry of Lake IJssel, including the measurement locations (circles)
- Figure 10 Bathymetry of Lake Sloten, including the measurement locations (circle)
- Figure 11 Scatterplots of model results of wave height and wave period versus observations for all cases and location for the default model (left) and proposed model (right)
- Figure 12 Scatterplots of model results of wave height and wave period versus observations for the cases of finite depth wave growth for the default model (left), and the proposed model with $c_{fjon}=0.067 \text{ m}^2/\text{s}^3$ (right)
- Figure 13 Nondimensional energy versus nondimensional depth (U_{10} -scaled) for the finite-depth wave growth dataset
- Figure 14 Nondimensional energy versus nondimensional depth (U_{10} - scaled) for the finite-depth wave growth dataset and Eq (3.9) by Young and Babanin (2006)

- Figure 15 Variance density spectrum of observations and SWAN default and proposed results for the field case of Lake Sloten
- Figure 16 Variance density spectra of observations and SWAN default and proposed results for the field case of Amelander Zeegat
- Figure 17 Variance density spectra of observations and SWAN default and proposed results for the field case of the Norderneyer Seegat
- Figure 18 Scatterplots of model results of wave height and wave period versus observations for opposing currents in the Amelander Zeegat. Left: Default model without currents. Right: Default model (with currents)
- Figure 19 Scatterplots of model results of wave height and wave period versus observations for following currents in the Amelander Zeegat. Left: Default model without currents. Right: Default model (with currents)
- Figure 20 Scatterplots of model results of wave height and wave period versus observations for opposing currents in the Amelander Zeegat. Left: Default model. Right: Proposed model, $cfjon=0.067 \text{ m}^2/\text{s}^3$
- Figure 21 Scatterplots of model results of wave height and wave period versus observations for following currents in the Amelander Zeegat. Left: Default model. Right: Proposed model, $cfjon=0.067 \text{ m}^2/\text{s}^3$
- Figure 22 Variance density spectra of observations and model results, for three cases of opposing currents in the Amelander Zeegat
- Figure 23 Variance density spectra of observations and model results, for three cases of following currents in the Amelander Zeegat
- Figure 24 Variance density spectra of observations and model results, for a case of North Sea wave penetration in the Eastern Scheldt
- Figure 25 Variance density spectra of observations and model results, for a case of North Sea wave penetration in the Eastern Scheldt
- Figure 26 Variance density spectra of observations and model results, for a case of North Sea wave penetration in the Eastern Wadden Sea
- Figure 27 Comparison dominant wave direction SWAN and radar. Left: depth; Right: difference in dominant wave direction vectors: black=dominant dir; red=SWAN dominant dir.
- Figure 28 Scatterplots of model results of wave height and wave period versus observations for cases of North Sea wave penetration. Left: Default model. Right: Proposed model
- Figure 29 Scatterplots of model results of wave height and wave period versus observations for cases of North Sea wave penetration. Left: proposed model with $cfjon=0.067 \text{ m}^2/\text{s}^3$. Right: Proposed model

1 Introduction

A significant part of the Netherlands lies below sea level and is protected from flooding by dunes and dikes. In compliance with the Dutch Flood Defenses Act ('Waterwet, 2009'), the safety of these Dutch primary sea defenses must be assessed every six years for the required level of protection. This assessment is based on the Hydraulic Boundary Conditions (HBCs), i.e. the loading conditions on the sea defense, and the Safety Assessment Regulations (VTV), a set of rules with which the sea defense resilience is assessed and which uses the HBCs. In order to compute the HBCs, the accepted procedure is to derive normative metocean conditions at the location of offshore water buoys, and transform these using the spectral wind wave model SWAN (Booij et al., 1999) to obtain wave conditions near the sea defenses.

Until 2006, this procedure could only be applied for sea defenses along the uninterrupted central Holland coast and the Scheldt estuaries in the southern part of the Netherlands. It was not applied in the Wadden Sea tidal inlet system in the north, since there were uncertainties regarding the quality of the model's performance. Instead, the hydraulic wave boundary conditions were derived from a collection of sea defense design data and sparse field data and observations: obviously an unwanted situation.

The Dutch Wadden Sea (Figure 1) is a complex coastal system, being enclosed by a series of barrier islands and the mainland coasts of the provinces of Friesland and Groningen. In this area many physical wave processes occur simultaneously. Tidal inlets are found between the barrier islands, each featuring an ebb tidal delta, one or more main tidal channels, and a complex system of smaller channels and flats extending into the Wadden Sea interior. Some of these inlets are relatively closed (e.g. Amelanders Zeegat, Figures 2 and 3), and some are relatively open (e.g. the mouth of the Eems-Dollard estuary, Figure 4). Apart from tidal channels, the Wadden Sea interior is shallow and flat, with tidally-modulated depths normally ranging between 0 m (drying) and 3 m. During extreme storms, storm surges can cause total water depths to increase by about 3 m over astronomical high water. In this region, young wind sea is generated locally under the influence of the finite depth.

The application of a spectral wind wave model in such a complex environment is a challenge, because a great number (if not all) of the known wave generation, propagation, redistribution and dissipation physical processes are important, at least in parts of a tidal inlet sea. Specifically, these processes include:

- fetch and/or depth-limited wave generation by wind,
- depth and current-induced refraction,
- wave dissipation by whitecapping, bottom friction, and current- and depth-induced breaking,
- nonlinear transfer due to triad and quadruplet interactions.
- diffraction (at the tidal flat-tidal channels edges).

These processes are all modeled with various degrees of parameterization in the phase-averaged spectral wind wave model SWAN, which is considered the most suitable tool to

compute the offshore-to-nearshore transformation of wave fields. Other types of models, notably non-hydrostatic or Boussinesq-type phase-resolving time-domain models, have a more complete description of the (nonlinear) wave transformation and can compute the wave shape, but are impractical to apply over such large domains at present.

Despite promising overall results using the SWAN model, Ris et al. (1999) showed some significant discrepancies between model results and (relatively sparse) observations in the Friesche Zeegat (the Netherlands) and the Norderneyer Seegat (German Wadden Sea, Figure 7). Similarly, Kaiser and Niemeier (2001) showed that SWAN performs reasonably well, but that it underestimates the penetration of lower-frequency wind sea from the North Sea into the tidal inlet of Norderney in the German part of the Wadden Sea. One of the reasons that the model could not be assessed thoroughly in the Dutch Wadden Sea was that up to 2002 very little wave data were available here. Wave observations had been conducted in similar geographical regions elsewhere (e.g. Danish Wadden Sea and Willapa Bay, USA), but nowhere was the data considered of sufficient quality or extent to validate SWAN for conditions occurring in the Dutch Wadden Sea.

Therefore, in 2003 an extensive measurement campaign was commenced in the tidal inlet of Ameland (Zijderveld and Peters, 2008) to fill this data need. In 2006 an additional set of measurement devices was deployed in the Eastern Dutch Wadden Sea. Furthermore, in 2006 the Dutch Public Works Department (Rijkswaterstaat Water Dienst) commenced a large program called SBW (Strengths and Loads of Sea Defenses). A part of this program was a five-year project ("SBW-Waddenzee") to assess and where possible improve the performance of the wave transformation model SWAN in the Wadden Sea, with a focus on the shallow water processes.

The objective of this report is to demonstrate the main results of the project and identify the remaining research topics. The report is structured as follows: first we describe the observational program, and a brief data analysis in Chapter 2. Chapter 3 states the wave action balance equations, the 2006 default model version and the newly-proposed model settings. Then, in Chapter 4, we will demonstrate the performance of the default model with respect to this data, discuss the improvements made within the framework of the project and show the performance of the proposed model against the data. We finalize with a discussion, conclusions and an outlook regarding further research.

This report focuses on three issues that required further attention based on the performance of the default version. First, over the tidal flats the computed ratio of significant wave height over water depth showed an apparent upper limit using the conventional Battjes and Janssen (1978) depth-limited wave breaking formulation using the default value of the breaker parameter γ . Secondly, two processes related to wave-current interaction are considered, namely the so-called wave age effect on waves generated in ambient current, and enhanced dissipation due to wave steepening in negative current speed gradients. Finally, the energy levels of low-frequency wind sea from the North Sea were underestimated as it penetrated into the Dutch Wadden Sea. Model improvements are proposed for all these issues, and the improved performance of the model is shown. The project results have led to a wave transformation model with which reliable wave conditions in the Dutch Wadden Sea and related complex areas can be determined.

2 Observations

2.1 Monitoring network

The observations used for the calibration and validation of SWAN for the Dutch Wadden Sea comprise of data from the long-term monitoring network along the Dutch coast and the special SBW measurement campaign that has been in operation in the Dutch Wadden Sea since 2003. The permanent metocean monitoring network along the Dutch coast was designed for collecting long-term statistical data for coastal management and design, but is also a source for model calibration and validation. This network features wave, water level and wind observation stations.

Wave monitoring in the Dutch Wadden Sea region includes data recorded by the Waverider buoys Eierlandse Gat (ELD) and Schiermonnikoog Noord (SON), located just offshore of the barrier islands at a depth of -26 m NAP and -20 m NAP (Dutch Leveling Datum) respectively (Figure 1). Observations from these buoys are available from 1979 onwards. This data provides the long-term statistics (extrapolated to occurrences of 1/4000 per year values) from which the offshore boundary values for the HBC wave transformation into the Wadden Sea are derived.

Water levels (tide and surge) are monitored in the Dutch Wadden Sea area at a large number of stations, both offshore and inside the barrier islands (Figure 1). The present data coverage has been achieved in the 1970s to 1980s, although some stations have been active much longer (e.g. Delfzijl since 1879). Winds are monitored at several locations in and around the Wadden Sea (Figure 1) as part of the monitoring network of the Royal Dutch Meteorological Institute (KNMI), and is available since 1949. However, except for the Huibertgat (indicated as HUIBGT), all these stations are situated on land, and may not be representative for conditions on open water.

In 2008, the monitoring network was extended with two permanent measurement masts near the mainland dikes: one in front of the Frisian coast at Wierumerwad (WRW1, Figure 4) and one in front of the Groningen coast at Uithuizerwad (UHW1). Various hydraulic and meteorological data, including wave, water level and wind data are routinely being collected.

2.2 SBW observational campaign

The observational campaign of the SBW project started in 2003, to extend the instrument coverage into the Dutch Wadden Sea in aid of model validation. The wave measurement component presently employs more than 20 wave buoys, both directional and non-directional Waveriders, spread out inside as well as just outside the Dutch Wadden Sea area. The initial focus of the campaign was the penetration of waves from the North Sea through the tidal inlets, in part to evaluate the concerns of wave penetration raised by Kaiser and Niemeyer (2001). The Amelander Zeegat (see inset in Figure 1, and Figures 2 and 3) was selected as a typical, relatively shielded inlet. Initially a single transect (2003-2006, Figure 2), and

subsequently a double transect (2007-present, Figure 3) of wave buoys were laid out through the inlet, covering the ebb tidal shoal, tidal channels and the shoals inside the Wadden Sea. From 2007, additional wave buoys were deployed in the eastern part of the Wadden Sea (Figure 4), which is more exposed to North Sea waves than the Amelander Zeegat. In addition, a number of locations were chosen to provide wave observations as close as possible to the dikes (e.g. at the Afsluitdijk at the border of Lake IJssel) (not shown). From 2010, these in-situ observations have been complemented by an X-band radar deployed on the light house at Ameland (indicated on Figure 3), with a range covering the inlet and out to the ebb tidal delta (Figures 1 and 3). Using commercial (www.SeaDarQ.com) analysis software, wave and current fields can be derived from these radar observations.

These observations, together with the wave, water level and wind monitoring data (Section 2.1), form a comprehensive data set for the calibration and validation of wave and hydrodynamical models. However, since current data was not observed, water level and current fields for the simulations presented here were computed using the Delft3D model, calibrated to the observed water levels. Also, since the wind stations discussed in Section 2.1 were mostly on land, the spatially-varying wind forcing was computed using the HIRLAM model. Due to the limited spatial extent of the Dutch Wadden Sea, and the typical wave energy travel times through the domain, wave conditions in a single inlet system are typically stationary and a spatially-uniform wind field is applied in the simulations. Table 2.1 presents a selection of stationary cases for hindcasting, taken from storm events recorded during the course of this campaign. These stationary cases were selected to capture significant phases during an event, such as flood, ebb and high tide. The table summarizes the key characteristics of each case, and indicates which physical process the case was selected to study (based on prevailing conditions).

Table 2.1 Selection of stationary cases recorded in the Amelander Zeegat during the period 2004-2007.

Computed wind speed and direction are mean values over domain. Water level at station Nes and maximum computed current speed u_{max} in the inlet main channel. Acronyms: 'wp' = wave penetration, 'wci' = wave-current interaction and 'fdg' = finite-depth wave growth.

Date and time	U_{10} (m/s)	U_{dir} (°N)	Water level (m NAP)	u_{max} (m/s)	Tidal phase	Significant physical process
08/02/2004, 20:00 ¹	13.5	314	1.0	2.3	flood	wp,wci
08/02/2004, 22:30 ¹	16.6	325	2.6	0.9	high w	wp,wci
09/02/2004, 01:30 ¹	16.3	328	1.8	1.7	ebb	wp,wci
16/12/2005, 10:00 ²	20.0	277	1.0	2.0	flood	wp,wci
16/12/2005, 23:30 ²	15.9	331	2.3	1.0	ebb	wp,wci
17/12/2005, 10:30 ²	15.4	339	2.0	0.5	high w	wp,wci
11/01/2007, 13:00 ³	19.5	228	1.0	0.7	high w	fdg
11/01/2007, 22:00 ³	17.9	275	0.9	0.6	flood	fdg
11/01/2007, 22:40 ³	18.8	279	1.3	0.7	flood	fdg
18/01/2007, 12:20 ³	21.1	233	0.8	1.3	ebb	fdg
18/01/2007, 14:00 ³	20.2	263	0.6	1.0	low w	fdg
18/01/2007, 17:20 ³	20.3	267	1.4	1.1	flood	fdg
18/01/2007, 20:40 ³	18.9	274	2.8	1.1	high w	fdg
18/03/2007, 10:00 ³	13.8	279	1.7	0.4	high w	fdg
18/03/2007, 14:40 ³	18.1	266	0.7	1.2	low w	wci, fdg
18/03/2007, 15:40 ³	17.9	271	0.6	0.8	low w	fdg
18/03/2007, 17:00 ³	17.1	268	1.2	1.1	flood	wci, fdg
18/03/2007, 19:20 ³	16.3	268	3.0	1.3	flood	wci, fdg
09/11/2007, 04:50 ⁴	17.3	322	1.2	1.3	flood	wp,wci, fdg
09/11/2007, 09:20 ⁴	18.4	326	2.7	0.7	high w	wp,wci,fdg
09/11/2007, 11:00 ⁴	18.5	328	1.7	1.3	ebb	wp, wci,fdg
09/11/2007, 17:20 ⁴	16.1	330	1.0	0.9	flood	wp,wci, fdg
28/01/2010, 03:58 ⁵	10.5	320	0.8	1.5	flood	wci, wp
28/01/2010, 06:39 ⁵	8.4	315	1.7	0.1	high w	wci, wp
28/10/2010, 09:49 ⁵	8.9	329	0.7	1.3	ebb	wci, wp

1. WL&Alkyon (2007)
2. Alkyon (2007)
3. Royal Haskoning (2008)
4. Witteveen+Bos (2008)
5. Deltares (2010)

Figure 5 presents a selection of the data presented in Table 2.1 above. Shown are the observed spectra along the NW-SE array through the Amelander Zeegat for the NW storm of 8-9 November 2007. Storm systems propagating over the North Atlantic and the North Sea generate waves which eventually reach shore. Typically, these North Sea storm waves have wave heights of 5 m or more, and contain wave energy in the range of 0.06-0.1 Hz, when they enter the tidal inlets. Figure 5 shows that the North Sea wave energy at the offshore peak frequency is strongly dissipated over the ebb tidal delta (AZB11) to AZB21, see Figure 3 for buoy locations). The vertical scale is reduced by a factor 20. Further along the channel (from AZB21 to AZB32 and AZB42), wave growth occurs at higher frequencies. In this regard, a clear enhancement of the wind wave growth in the opposing ebb current (9/11/2007 at 11:00) can be seen compared to the lower growth (in fact a reduction in variance) found in flood or 'following' (in the sense that the wave and current direction are aligned) current cases. This so-called 'wave age effect', where the ambient current alters the effective age of the wave field, is discussed in Section 4.2.2 below. Moving into the Wadden sea interior (AZB42 to AZB52/62), no significant penetration of wave energy in the North Sea frequency range is apparent. At the interior buoys AZB52 and AZB62, local wind sea growth (in finite depths) can be seen. The spectral directions at these buoys remain approximately aligned with the spatial mean local wind direction, although differences with the directions of the higher frequency components at AZB11 suggest some spatial variability in the wind field. Also, some differences are found at the locations AZB42 and AZB52 in the tidal channel, presumably due to bottom and current refraction (bottom panels).

The Eastern Dutch Wadden Sea region, featuring the mouth of the Eems-Dollard estuary, is situated north of the province Groningen in the Netherlands (Figures 1 and 4). The inlets in this region do not have such pronounced ebb tidal deltas as the Amelander Zeegat discussed above, and thus are more exposed to waves from the North Sea. Four directional Waverider buoys were deployed in this region as part of the SBW field measurement campaign during the period 2006-2007 (Figure 4): one offshore of the barrier islands at Westereems Oost (WEO1), and three inside the Wadden Sea at Pieterburenwad (PBW1), Wierumerwad (WRW1) and Uithuizerwad (UHW1) near the mainland coast. The latter three buoys are only operational during high tide (otherwise resting on the dry tidal flats). No waves were measured inside the Eems-Dollard estuary itself. As in the Amelander Zeegat, the water level and current fields, and uniform wind forcing are computed values by WAQUA and HIRLAM respectively. Table 2.2 presents a selection of stationary cases taken from one significant storm occurring during the observational period.

Table 2.2 Selection of stationary cases recorded in the Eastern Dutch Wadden Sea during the period 2006-2007. Computed wind speed and direction are mean values over domain. Water level at station Huibergat and maximum computed current speed u_{max} in the inlet main channel. Acronyms: 'wp' = wave penetration and 'fdg' = finite-depth wave growth.

Date and time	U_{10} (m/s)	U_{dir} (°N)	Water level (m NAP)	u_{max} (m/s)	Tidal phase	Significant physical process
09/11/2007, 06:20	17.3	326	1.9	0.7	low w	wp, fdg
09/11/2007, 07:00	19.9	326	2.3	0.8	flood	fdg
09/11/2007, 09:40	18.4	332	3.1	0.3	high w	wp, fdg
09/11/2007, 11:00	18.9	333	2.8	0.5	ebb	fdg
09/11/2007, 13:40	19.5	333	1.3	1.1	ebb	wp

Figure 6 shows the spectra from a selection of cases from Table 2.2, covering half a tidal cycle of the storm of 8-9 November 2007 (same storm as presented for the Amelander Zeegat in Figure 5). As with the Amelander Zeegat, high-energy spectra with a low peak frequency (0.07 Hz) arrive from the North Sea (e.g. at WEO1, vertical scale reduced by a factor 10). The wind wave energy at these lower frequencies (<0.2 Hz) is significantly reduced inside the barrier islands (e.g. PBW1, UHW1 and WRW1). The mean direction of these components remains approximately aligned with the local wind direction (bottom panels). However, in contrast to the relatively closed Amelander Zeegat, some energy remains at these frequencies at the nearshore buoys inside the Eastern Wadden Sea. The levels of energy remaining appear to be correlated with the water level, being the highest for the high tide case (09/11/2007 at 09:40). In addition to the energy entering from the North Sea, local, higher-frequency wind sea is generated landward of the barrier islands (e.g. PBW1, UHW1 and WRW1), as also found inshore of the Amelander Zeegat.

2.3 Other data sets used

In addition to the observations recorded during the SBW field campaign, further related data sets were used to increase the observed range of wave conditions in the Dutch Wadden Sea. These include observations in the tidal inlets of the Norderneyer Seegat (German Wadden Sea) and the Eastern Scheldt (Southwest Netherlands) to further study wave penetration and wave-current interaction. The shallow lakes IJssel and Sloten (Netherlands) were included to study local wave growth in finite water depths, as found in the Wadden Sea interior.

2.3.1 Norderneyer Seegat

The Norderneyer Seegat is situated between the islands of Juist (to the west) and Norderney (to the east) in the German Wadden Sea (see Figures 1 and 7). Several directional wave buoys were deployed in the region from which to derive the wave loads on the flood defenses of the Norderney Island. Wave buoy SEE is located well outside the inlet and served as a boundary condition to an inlet model. Station VST1 is located just outside the inlet main channel to the northeast. SGTNEY is inside the inlet system but exposed to outside waves, while RIFFGAT is located on the leeside of the island (given the predominant W-NW wind

directions during storms). The water level and current fields, and uniform wind forcing are computed values. One stationary case is considered here. Its characteristics are summarized in Table 2.3.

Table 2.3 Selected stationary case recorded in the Norderneyer Seegat. Computed wind speed and direction are mean values over domain. Water level at Riffgat (relative to German leveling datum Normal Null) and maximum computed current speed u_{max} in the inlet main channel. Acronym: 'wci' = wave-current interaction.

Date and time	U_{10} (m/s)	U_{dir} (°N)	Water level (m NN)	u_{max} (m/s)	Tidal phase	Significant physical process
05/02/1999, 03:36 ⁶	19.0	290	3.4	0.8	high w	wci

2.3.2 Eastern Scheldt

The second additional site is the Eastern Scheldt, where various wave-, wind and water level measurements are being carried out (Figure 8). The main source of the observations is the Hydrometeo Centre Zeeland (HMCZ), which is part of the Dutch Ministry of Transport, Public Works and Water Management. Table 2.4 shows the storm characteristics of three selected stationary cases. The water level fields are computed values from the WAQUA model. Spatially uniform wind fields are imposed, based on wind measurements at regional stations. In the hindcasts presented here, the wave observations of four non-directional Waverider buoys were used, namely: Schouwenbank (SCHB), Domburger Rassen (DORA) and Brouwershavensche Gat 2 (BG2) in the offshore area, and Oosterschelde 4 (OS4) in the mouth of the Eastern Scheldt. The latter buoy is located in a tidal channel just seaward of the Eastern Scheldt Storm Surge Barrier, which was open during all events.

Table 2.4 Selection of stationary cases recorded in the Eastern Scheldt. Computed wind speed and direction are mean values over domain. Water level at station BG2 and maximum computed current speed. These conditions are used for assessing wave penetration.

Date and time	U_{10} (m/s)	U_{dir} (°N)	Water level (m NAP)	u_{max} (m/s)	Tidal phase
26/12/2001, 09:00 ⁷	16.0	310	1.0	0.3	flood
26/12/2001, 12:00	13.0	315	1.5	0.5	high w
23/12/2003, 02:30	9.0	295	1.3	0.8	high w

6. Kaiser & Niemeyer (2001)

7. All cases in Svasek (2007)

2.3.3 Lake IJssel and Lake Sloten

As will be shown Section 3, data from shallow lakes are also relevant to the physical conditions in the Dutch Wadden Sea interior. Tables 2.5 and 2.6 present stationary cases selected from storms recorded in Lakes IJssel and Sloten as part of the wave monitoring network in the Dutch lakes. Lake IJssel (Figure 9) is approximately 20 x 60 km² in size with a typical depth of about 4–5 m, and has a fairly flat bottom. Wave and water level data for this lake have been observed at stations FL2, FL5, FL9, FL25 and FL26 using capacitance probes. Winds have been measured at FL2, FL25, FL26 and FL37, and their spatial average is determined as in Bottema (2007). This spatial average is applied uniformly over the model domain. The Lake Sloten (Figure 10) is approximately 4.5 x 3 km² in size and has a flat bottom with a characteristic water depth of about 1.7 m. Wave and water level data for this lake have been observed at the station SL29, also using capacitance probes. Winds have also been observed at this location. For both lakes, cases with relatively high wind speeds ($U_{10} = 15\text{--}24$ m/s) were chosen. No current fields were used in the SWAN hindcasts of these lakes, since wind-generated currents are expected to be weak, and hence wave-current interaction to be of minor importance (hence omitted in Tables 2.5 and 2.6).

Table 2.5 Selection of stationary cases recorded in Lake IJssel. Water level represents the lake mean (Dutch: 'meetpeil') and currents were omitted. Wind speed and direction are lake means. Acronyms: 'fdg' = finite-depth wave growth.

Date and time	U_{10} (m/s)	U_{dir} (°N)	Water level (m NAP)	Significant physical process
02/10/1999, 03:00 ⁸	15.2	215	-0.20	fdg
22/02/2002, 04:00	18.8	215	0.08	fdg
27/10/2002, 14:20	23.2	249	-0.26	fdg
08/01/2005, 13:00	19.9	246	-0.20	fdg
12/02/2005, 15:00	18.3	286	-0.39	fdg
18/01/2007, 12:00	22.4	237	0.06	fdg
18/01/2007, 19:00	23.5	267	0.10	fdg

8. Deltares (2008)

Table 2.6 Selection of stationary cases recorded in Lake Sloten. Water level, wind speed and wind direction at station SL29. Currents were omitted. Acronyms: 'fdg' = finite-depth wave growth.

Date and time	U_{10} (m/s)	U_{dir} (°N)	Water level (m NAP)	Significant physical process
12/02/2002, 13:00 ⁹	15.0	253	-0.43	fdg
26/02/2002, 14:00	20.8	243	-0.29	fdg
27/10/2002, 15:00	21.4	252	-0.45	fdg
20/03/2004, 20:00	19.4	241	-0.46	fdg
18/01/2007, 12:00	21.9	234	-0.46	fdg

9. Hindcast Alkyon (2008a) and Deltares (2008)

3 SWAN Wave action model formulation

3.1 Governing equations of SWAN

Discrete spectral wind wave models contain the physical formulations to simulate the processes relevant to the wave generation, propagation and dissipation in tidal inlets and shelf seas. Of this class of models SWAN (Booij et al., 1999) is the most widely-used in the scientific and engineering community, including the computation of the hydraulic (wave) loads on Dutch sea defenses. The model computes the evolution of wave action density N ($= E/\sigma$, where E is the variance density and σ the relative radian frequency) using the action balance equation:

$$\frac{\partial N}{\partial t} + \nabla_{x,y} \cdot [(\vec{c}_g + \vec{U})N] + \frac{\partial}{\partial \theta}(c_\theta N) + \frac{\partial}{\partial \sigma}(c_\sigma N) = \frac{S_{tot}}{\sigma} \quad (2.1)$$

with

$$S_{tot} = S_{in} + S_{wc} + S_{nl4} + S_{bot} + S_{brk} + S_{nl3} + S_{wc,cur} \quad (2.2)$$

where θ is direction..The terms on the left-hand side of (2.1) represent, respectively, the change of wave action in time, the propagation of wave action in geographical space (with \vec{c}_g the linear wave group velocity vector and \vec{U} the ambient current vector), depth- and current-induced refraction (with propagation velocity c_θ in directional space θ) and the shifting of the relative radian frequency σ due to variations in mean current and depth (with the propagation velocity c_σ). The right-hand side of (2.1) represents processes that generate, dissipate or redistribute wave energy, given by (2.2). In deep water, three source terms are traditionally used: the transfer of energy from the wind to the waves, S_{in} ; the dissipation of wave energy due to whitecapping, S_{wc} ; and the nonlinear transfer of wave energy due to quadruplet (four-wave) interaction, S_{nl4} . In shallow water, dissipation due to bottom friction, S_{bot} , depth-induced breaking, S_{brk} , and nonlinear triad (three-wave) interaction, S_{nl3} , are additionally accounted for. The final source term represents the enhanced breaking dissipation of waves on a current (Van der Westhuysen, 2011).

Since its introduction more than a decade ago, SWAN has been continuously developed, and improved versions have been published by Delft University of Technology, which maintains the code. It is therefore not possible to speak of *the* SWAN model, but rather of model versions, including their parameter settings. In this report we consider two versions, defined below.

3.2 Default 2006 model formulations and settings

We define the model version 40.51, current at the start of the project in 2006, as the *default version* for the purpose of this study. For this version, the following default settings were applied:

- Quadruplet interactions using the DIA formulation by Hasselmann et al. (1985).
- JONSWAP formulation for bottom friction with a coefficient set to $0.067 \text{ m}^2\text{s}^{-3}$ for fully-developed wind-sea conditions in shallow water as found by Bouws and Komen (1983).
- Depth-induced wave breaking according to Battjes and Janssen (1978).
- Triad interactions using the LTA formulations by Eldeberky (1996).
- The current-induced dissipation term $S_{wc,cur}$ is not activated.

In addition, the following two non-default options were applied, previously shown to produce improved results (see references below):

- Wind generation and whitecapping based on Van der Westhuysen et al. (2007), but corrected for an underprediction of swell (Van der Westhuysen, 2007).
- Based on Zijlema and Van der Westhuysen (2005)'s finding that the default convergence criteria can lead to poorly converged results with significant error, the number of required stationary iterations was fixed at 80 which ensures convergence (as has been verified).

3.3 Proposed 2010 model formulations and settings

The proposed version for the purpose of computing wave boundary conditions in the Wadden Sea is version 40.72ABCDE which differs from the settings described above in the following points:

- Depth-induced breaking under finite-depth wave growth conditions (Van der Westhuysen 2009, 2010), model parameter settings: $B = 0.96$, $\beta_{ref} = -1.3963$, $\nu = 500$.
- Enhanced whitecapping dissipation on negative current gradients according to Van der Westhuysen (2011), model parameter setting $C_{ds}'' = 0.8$.
- JONSWAP formulation for bottom friction with a coefficient set to $0.038 \text{ m}^2\text{s}^{-3}$.
- For all computations we force 80 iterations for complete convergence.

3.4 Qualitative and quantitative performance assessment

In order to assess the performance of SWAN in its default and proposed forms, we computed a total of 48 stationary hindcasts cases with the default SWAN version. Because there are a number of buoys per inlet, the total number of data points is 270. Of these hindcasts, the computed and observed variance density spectra were observed in order to qualitatively identify shortcomings in the model performance. Furthermore, scatter plots of integral properties were made and quantitative scoring indexes were defined. These are the scatter index and relative bias scores, which were computed for the significant wave height H_{m0} , and spectral periods $T_{m-1,0}$ and T_{m01} . The error measures are defined, respectively, as:

$$SCI_{\psi} = \frac{\sqrt{\frac{1}{N} \sum_{i=1}^N (\Psi_{SWAN}^i - \Psi_{obs}^i)^2}}{\frac{1}{N} \sum_{i=1}^N \Psi_{obs}^i} \quad (2.3)$$

and

$$\text{Rel. bias}_{\psi} = \frac{\sum_{i=1}^N (\Psi_{SWAN}^i - \Psi_{obs}^i)}{\sum_{i=1}^N \Psi_{obs}^i} \quad (2.4)$$

where ψ_{obs} is the observed significant wave height $H_{m0,obs}$ or spectral periods $T_{m-1,0,obs}$ or $T_{m01,obs}$, and ψ_{SWAN} is the corresponding modeled result $H_{m0,SWAN}$ or $T_{m-1,0,SWAN}$ or $T_{m01,SWAN}$, in a sample of size N .

We chose to assess the performance of the model based on these quantities because they are the most important wave parameters that are used as input in the water defense assessment rules. Wave direction is also used in the assessment. However, observations of wave directions are more scarce since they require directional instruments and therefore not considered in the error statistics. The computed and observed (where available) directions are shown in the spectral figures (see below).

4 Results

This section presents the hindcast results for the Dutch Wadden Sea and related regions, using the observational data presented in Section 2 and the two model variants described in Section 3. First, the performance of the default SWAN model is shown in Section 4.1, and subsequently a number of improvements to the model are discussed in Section 4.2. In Section 4.3 the overall improvement is discussed.

4.1 Default model

The scatter plots for all 270 data points (all buoys and all cases) in Figure 11 (left-hand column) show that the default version of SWAN performs quite well: most of the model-data points are around the 1:1 line of perfect prediction. The top left-hand panel shows integral significant wave height, the middle left-hand panel shows the mean period $T_{m-1,0}$ (related to the energy flux) and the bottom left-hand panel the mean period T_{m01} . The integral parameters of both the model and observations are calculated for the same frequency interval as available in the measurements (which varies from site to site). All panels on the left-hand side show a negative relative bias, which indicates an underprediction of integral values. The data points trend away from the unity line for larger values of wave height and period. Both aspects are of concern, since this means that SWAN in its default form would underestimate the hydraulic loads even already for these measured storm events. Scaled up to events with a small probability of exceedance (in the Dutch Wadden Sea area the dike safety assessment level is 1/4000 per year), the underestimation could increase and water defenses could pass the safety assessment erroneously (i.e. a false positive).

The right-hand column of Figure 11 shows the results using the proposed model, which is discussed below. The deficiencies in the default model will be illustrated in the remainder by comparing computed and observed integral parameters and spectra for specific field cases, discussing measures for error reduction, and showing each resulting improvement in the performance. We will return to the right-hand panels in Section 4.3.

4.2 Model innovations

Three model innovations are presented below, namely the improved modeling of depth-induced breaking in situations of finite-depth wave growth, such as found in the Wadden Sea interior (Section 4.2.1), model development related to wave-current interaction (Section 4.2.2), and improved modeling of wave penetration into the inter-tidal area of the Wadden Sea (Section 4.2.3).

4.2.1 Depth-induced breaking under finite-depth wave growth conditions

The first model improvement is related to local wave growth in the finite depths of the Wadden Sea interior. Specifically, it concerns the modeling of depth-induced breaking under such conditions. From De Waal (2001) and Bottema and Van Vledder (2009) it is known that

wave heights are underestimated in finite-depth wave growth situations in lakes. The expectation was that this model deficiency is relevant for the computation of HBCs in the Dutch Wadden Sea, since most sea defenses are adjacent to extensive tidal flat areas (Figures 1-4) dominated by local wind sea, as shown in Figures 5 and 6.

The left-hand panel of Figure 12 shows that the model results for the nearshore buoys AZB51, AZB61 and AZB62 (deployment 2007-present) in the Amelander Zeegat, and UHW1 and WRW1 in the Eastern Wadden Sea display an underestimation for the mean period $T_{m-1,0}$ and the ratio H_{m0}/d , which increases with increasing values of these variables. The default H_{m0}/d result appears to have an upper limit of about 0.38. As discussed in Van der Westhuysen (2010), this upper limit is due to a balance in the model between local wind wave growth and depth-induced breaking modeled using Battjes and Janssen (1978) with the default value of the breaking parameter. By contrast, observed H_{m0}/d ratios in the Dutch Wadden Sea flat areas reach values of up to 0.45 (with one outlier at UHW1, which includes low-frequency components). Apart from this point, the H_{m0}/d ratios are consistent with observed data from shallow lakes with a horizontal bathymetry, for example Lake IJssel and Lake Sloten in the Netherlands (Bottema and Van Vledder 2009) included in Figure 12.

The observations of Amelander Zeegat, Lake IJssel and Lake Sloten are replotted in Figure 13 as a function of the non-dimensional depth, defined as gd/U_{10}^2 , where U_{10} is the wind measured at 10 meters height. Added to these are data from Lake George, a shallow lake in Australia (Young and Verhagen, 1996). Lake Sloten and Lake IJssel can be identified as two distinct populations while the Amelander Zeegat (buoys AZB51, AZB61 and AZB62) and Lake George data cover both other populations. This last point is an important finding since it allows lake data to be used for the assessment of the wave model for the finite-depth wave growth aspect in the Wadden Sea (and vice versa). The reason for the two distinct populations for Lake IJssel and Lake Sloten is unknown at this point, but the hypothesis is that it has a relation with ripple heights in the bed in either lake which does not enter the scaling.

Comparing the observed data with the empirical finite-depth wave growth limit proposed by Young and Babanin (2006, Eq. 3.9) shows that this limit is not adequate to describe the Dutch Wadden Sea or Lake IJssel data (Figure 14). It is therefore not advisable to calibrate SWAN to this empirical relation, but rather to consider the individual field cases themselves. When considering the wave spectra of Lake Sloten and Amelander Zeegat (Figures 15 and 16 respectively), the default model shows less wave growth compared to the measured spectra, and thus a smaller wave height and higher peak period using the default model (dash-dotted lines). The computed mean wave directions are almost identical for each model version. Note that there are no observations of wave directions at these non-directional buoys.

In previous studies for Lake IJssel and Lake Sloten (e.g. De Waal et al., 1997, using HISWA (Holthuijsen et al., 1989)), either the value of the α parameter in Battjes and Janssen (1978) had to be decreased from unity, or the value of the breaking index γ parameter had to be increased from the default value of $\gamma=0.73$ to about $\gamma=0.8-0.9$. In other words, using the default breaking parameterization, a good model-data match could only be obtained after tuning of a parameter value which is then not universal anymore, which is an undesirable situation.

Van der Westhuysen (2009, 2010) found that the optimal value of γ , based on minimizing the bias and scatter index, can be clearly divided into two populations: one for sloping beaches (waves generated in deep water, subsequently breaking on a beach) and one for finite-depth wave growth (near-horizontal bed) cases. For both wave height and wave period, the sloping beach cases show a minimum error for γ values around 0.6-0.8, i.e. around the commonly-used default of $\gamma=0.73$, whereas for the cases with finite depth growth over nearly-horizontal beds the errors are monotonically decreasing with increasing γ . This indicates that the optimal result is reached when the Battjes and Janssen (1978) model parameter is tuned such that depth-limited wave breaking is effectively turned off. Thus, in the equilibrium balance, depth-limited breaking has a smaller contribution in the case of nearly-horizontal beds than in the case of sloping beaches. Here the wind input is balanced by other physical mechanisms such as bottom friction and whitecapping (steepness-induced breaking).

Van der Westhuysen (2010) proposes to modify the breaker formulation by Thornton and Guza (1983), itself a modification of Battjes and Janssen's (1978) formulation, to provide accurate modeling results in such conditions whilst retaining good performance over sloping beaches. Van der Westhuysen (2010) shows that the fraction of breaking waves in this expression can be expressed as a power law of the biphaseness of the wave field, which, along with the skewness and asymmetry, is a measure of the shallow water nonlinearity of the waves. As waves propagate from deeper water (where they are approximately sinusoidal) to intermediate depth, they become more "peaked" or skewed, but symmetrical (biphase = 0), and in shallow water they have a sawtooth shape and they become asymmetric (biphase $\rightarrow -\pi/2$) and break. Because SWAN is not a nonlinear wave-by-wave model, it can not compute the biphaseness of the waves. However, Doering and Bowen (1995) and Eldeberky (1996) related the biphaseness to the Ursell number, which can be computed by SWAN, so that the problem can be closed. The expression for total breaking dissipation is given by Van der Westhuysen (2010):

$$D_{tot} = -\frac{3\sqrt{\pi}}{16} \frac{B^3 \tilde{f}}{d} \left(\frac{\beta}{\beta_{ref}} \right)^n H_{rms}^3 \quad (4.1)$$

in which B is a proportionality coefficient, \tilde{f} the mean frequency, β the biphaseness of the self-interactions of the peak frequency, parameterized by Eldeberky (1996) as:

$$\beta = -\frac{\pi}{2} + \frac{\pi}{2} \tanh\left(\frac{0.2}{Ur}\right), \quad Ur = \frac{g}{8\sqrt{2}\pi^2} \frac{H_{m0} T_{m01}}{d^2} \quad (4.2)$$

and with β_{ref} the reference biphaseness at which all waves are breaking (see Section 3.3 for the parameter setting used here). The exponent n relates the biphaseness to the fraction of breaking waves. Van der Westhuysen (2009) shows this relation to be dependent on the mean steepness:

$$n = \frac{n_1 + n_2}{2} - \frac{n_2 - n_1}{\pi} \arctan\left[\nu \left(S_{loc} - \tilde{S}_{loc}\right)\right] \quad (4.3)$$

where $n_1 = 2$, $n_2 = 6$ and $\nu = 500$ are shape factors. The mean steepness S_{loc} is given by:

$$S_{loc} = \frac{H_{rms} \tilde{k}}{2\pi}, \quad \tilde{k} = \left[\frac{\iint k^{-\frac{1}{2}} E(\sigma, \theta) d\sigma d\theta}{E_{tot}} \right]^{-2} \quad (4.4)$$

with an average value of $\tilde{S}_{loc} = 0.038$. The source term is compiled from (4.1) assuming the dissipation per spectral component to be proportional to its variance density:

$$S_{brk} = D_{tot} \frac{E(\sigma, \theta)}{E_{tot}} \quad (4.5)$$

Figure 12 (right-hand column) shows the model results for the proposed SWAN version at shallow water locations near the dikes and in the lakes. Here the proposed version includes the breaker model (4.1)-(4.5). The bottom friction coefficient is held at $C_{f, JON} = 0.067 \text{ m}^2\text{s}^{-3}$ and enhanced dissipation on current gradients (discussed below) is not turned on ($C_{ds}'' = 0$), in order to evaluate only the effect of the change in breaker model. The scatter index and the relative bias of the considered parameters improve compared to the default. Large improvements can be observed for the H_{m0}/d ratio (bottom right). The apparent upper limit in the modeled H_{m0}/d values, seen in the lower panel of the left-hand column of Figure 12, virtually disappears when the breaker model of Van der Westhuysen (2009, 2010) is applied, and the model-data agrees better with the 1:1 line, especially for the higher values of this ratio. The relative bias reduces strongly, and the bias to a lesser extent.

The computed spectra of the proposed SWAN version for Lake Sloten and the Amelander Zeegat also compare much better to the observations than those of the default model (Figures 15 and 16, compare dash-dotted with dashed lines relative to the data). The computed wave spectrum at Lake Sloten significantly improves in the frequency range between 0.2 and 0.4 Hz (Figure 15). However, the high frequency flank is overestimated, similar to the default. This issue is therefore not resolved in this study. It can be partly resolved by replacing the quadruplet Discrete Interaction Approximation (DIA) as proposed by Hasselmann et al. (1985) with better approximations (Van der Westhuysen, 2007). The conditions shown for the Amelander Zeegat yield strong finite-depth wave growth ($gd/U_{10}^2 = 0.039$, where d is the depth at the buoy location). At the buoys AZB51/61/62 in the Wadden Sea interior, the Van der Westhuysen (2009, 2010) breaker model (dashed lines) produces more energetic spectra than the default model, significantly improving the model prediction of the observed variance density spectra (Figure 16). The modeled wave directions are similar for the frequency range with significant variance. Note that the buoys are non-directional and no observed wave direction is available. The remaining model variants included in the figure will be discussed in Section 4.3.

4.2.2 Wave-current interaction

The second area of model improvement concerns two aspects related to wave-current interaction. The first is the incorporation of currents, which changes the effective wave age, and the second is enhanced dissipation due to wave steepening in negative current gradients.

Wave age effect

As described in Chapter 1, Kaiser and Niemeyer (2001) reported that SWAN underestimated the wave conditions at the lee side of Norderney island at the RIFFGAT station. This finding cast doubt on the applicability of SWAN in such situations. The default model result for this case (Figure 17) shows that whereas the wave direction was predicted relatively accurately in

the frequency range with significant energy density, the predicted wind sea variance density is underdeveloped relative to the observations (compare default model (dashed line) and observations (solid line with dots)). A part of the reason is that Kaiser and Niemeyer (2001) used the default convergence criteria (at that time), which were rather lenient, resulting in only 15 iterations before run termination. Applying 80 iterations is more computationally intensive, but the results are better converged - in this case with higher energy levels in the wind sea spectrum (Figure 17, dotted line).

The remaining model-data disagreement can be explained by including residual tidal and wind-driven currents. Since the selected stationary case was at astronomical slack tide, Kaiser and Niemeyer (2001) did not take the currents into account. However, under these storm conditions, a significant wind-driven current was present. The modeled current field (Herman et al., 2006) (not shown) reveals that currents run across the inlet from southwest to northeast towards Norderney and close to the island turn in a counterclockwise fashion, where they have a more northerly and westerly direction and “jet” out of the inlet.

The results using the default model including currents and increased number of iterations show a marked improvement at station RIFFGAT (Figure 17, dash-dotted line in upper left panel). The spectrum now displays enhanced wind wave growth, with a lower peak frequency and greater total variance. This is because, in applying this current field, the local waves, driven by winds from the northwest, experience a mostly opposing current before they reach RIFFGAT, which alter (in this case decreasing) their effective wave age (e.g. Haus 2007):

$$\frac{\vec{U}_{cur} + \vec{c}_{rel}}{\vec{u}_*} \quad (4.6)$$

where \vec{U}_{cur} is the current velocity vector, \vec{c}_{rel} is the relative wave phase velocity vector and \vec{u}_* is the wind friction velocity vector. Hence, the wind is effectively blowing relatively harder over the wave field, causing enhanced wave growth. Note that the effect on the spectral mean period $T_{m-1,0}$ is opposite to what one would expect from a Doppler-shift in an opposing current without wind, represented by the fourth term on the LHS of (2.1).

The opposite also holds, namely that when the wind, wave and current direction are aligned, the wave age will increase and the modeled wave spectra will grow less than they would if no currents were included. The waves appear older due to the following current, and therefore grow less. This situation can occur, for instance, when a westerly wind blows over the Dutch Wadden Sea. Since the wave direction and the flow direction are more or less aligned, the following current over large distances causes an increase in the wave age, therefore less growth and a smaller period (relative to the case of “no current”). This would imply a reduction in wave period and wave height and hence a reduction in wave loads on the coastal defenses in this case.

The results for the remaining buoys inside and outside the inlet (SEE, SGTNEY and VST1, see Figure 7 for their locations) in Figure 17 show that the higher level of convergence (dotted lines) yields improved results relative to the default with 15 iterations (dashed lines) when compared with observations (solid lines with dots). The application of currents (dash-dotted lines) has a small effect at VST1. By comparison, at SGTNEY the currents have a large

effect, with the resulting stronger growth of the wind sea overshooting that of the observations. This is likely due to the buoy location in strongly turning currents, where errors in the hydrodynamic computation are likely to affect the wave model response. Furthermore, the waves at this location are exposed to North Sea waves. Results here are therefore also depended on the modeling of depth-induced breaking and bottom friction of these components. The errors here may also be related to errors in the computed current field used as model input. By contrast, the location RIFFGAT is sheltered, which means that the wave-age issue is dominant, and thus that inclusion of current effects is essential. Note the difference in scale between the results at SEE and VST1 and those at the innermost buoys (2 and 1 orders of magnitude respectively).

The effect of applying current fields in the Amelanders Zeegat is summarized in the scatter plots of Figures 18 and 19, for opposing and following current respectively, at locations AZB32/42/52. For our analysis, we define opposing currents that occur when the difference between the peak wave direction and the current direction is larger than 135 degrees (and for following currents, smaller than 45 degrees). Figure 18 shows that the inclusion of opposing current reduces the relative bias and scatter of the mean periods $T_{m-1,0}$ and T_{m01} . By contrast, for H_{m0} both these error statistics deteriorate with the addition of the opposing current. Here we see that wave heights are over-predicted in general (from negative to positive bias). This inaccuracy, related to the dissipation of wave energy in current gradients, is investigated in the next section.

For following current situations, the inclusion of the current fields improves the bias and scatter of H_{m0} , although still leaving a small positive bias and a large scatter (Figure 19). For the mean periods, the scatter increases and the relative bias changes from a relatively small positive to a relatively small negative value.

Enhanced dissipation on current gradients

The second aspect of wave-current interaction addressed is the effect of current gradients on the dissipation of wave energy. Ris and Holthuijsen (1996) showed that wave heights can be overestimated in near blocking, opposing current with a negative gradient. Similar, although less extreme, conditions exist in the tidal inlets of the Wadden Sea, where H_{m0} was found to be generally overestimated by the default model in the main channel of the Amelanders Zeegat (Figure 18 and, to a lesser extent, Figure 19). Considering these results, evidently a physical process causing wave energy dissipation is missing. Ris and Holthuijsen (1996) proposed that such overestimations are due to insufficient steepness dissipation (whitecapping) of waves on opposing currents with negative gradients. Their formulation for enhanced dissipation, based on the mean wave steepness, improved results, but also suppressed the growth of young seas (with inherent high steepness). The latter is a severe detrimental effect in tidal inlets, where both wave-current interaction and wind wave generation may take place at the same location.

Van der Westhuysen (2011) presents an alternative formulation for the enhanced dissipation of waves on current, based on the saturation-based whitecapping expression of Van der Westhuysen et al. (2007). In order to isolate the contribution of currents in the increased steepness and resulting dissipation, the degree of dissipation in this expression is scaled with the incremental shortening/steepening of the waves due to negative current gradients, which is related to the relative Doppler shifting rate c_σ/σ . In this way, the generation of young wind seas is not suppressed. The formulation reads:

$$S'_{wc,cur} = -C''_{ds} \max \left[\frac{c_{\sigma}(\sigma, \theta)}{\sigma}, 0 \right] \left[\frac{B(k)}{B_r} \right]^{p/2} E(\sigma, \theta) \quad (4.7)$$

where the propagation in sigma space c_{σ} is given by (e.g. Mei 1983):

$$c_{\sigma} = \frac{d\sigma}{dt} = \frac{\partial \sigma}{\partial d} \left[\frac{\partial d}{\partial t} + \vec{U} \cdot \nabla d \right] - c_g \vec{k} \cdot \frac{\partial \vec{U}}{\partial s} \quad (4.8)$$

in which s is the space coordinate in the propagation direction θ . The last term on the RHS of (4.8) is considered to be dominant in the cases considered here. The calibration coefficient $C''_{ds} = 0.8$ in (4.7) was found based on laboratory data, where the process could be isolated. A maximum function is included in order to take only relative increases in steepness into account in the enhanced dissipation. This formulation is suitable for both mature wave fields and young wind sea conditions. Note that negative current gradients occur both for accelerating opposing currents and decelerating following currents, both of which result in steepening of the waves (pers. comm. J.A. Battjes). The remaining parameters are as defined and calibrated in Van der Westhuysen et al. (2007): $B(k)$ is the spectral saturation and B_r is a threshold saturation level, which has been calibrated to $B_r = 1.75 \times 10^{-3}$. The parameter p is a function of the inverse wave age u^*/c , based on scaling arguments involving a spectral balance between the wind input, whitecapping and nonlinear interaction terms:

$$p(u^*/c) = 3 + \tanh \left[25 \left(\frac{u^*}{c} - 0.1 \right) \right] \quad (4.9)$$

Scatter plot results for opposing currents show that the enhanced dissipation removes the positive bias in H_{m0} (Figure 20 (top right panel)). The statistics of the mean period measures are similar to slightly improved. Similar, but somewhat smaller improvements are found for the following current cases (Figure 21). Note that the limited size of the dataset prevents the drawing of a definitive conclusion here.

Figures 22 and 23 present frequency spectra at the wave buoys AZB32 and AZB42 in the Ameland Zeegat for six stationary cases from Table 2.1: three for opposing and three for following currents, respectively. Figure 22 shows that the default model overestimates the observed variance density for frequencies higher than 0.15 Hz for two cases, but underestimates the energy for one case (09/11/2007 at 11:00). Application of the enhanced current-induced dissipation formulation (dashed lines) improves the prediction at buoy AZB42 for two of the three cases, although in one case (18/03/2007 14:40) the position of the peak frequency is not predicted well. The modeled and observed wave directions are in agreement for the frequency range with significant variance. Note that for the first case no observations of the wave direction were made. Figure 23 presents examples of frequency spectra for three stationary cases where a following current is present in the Ameland Zeegat. For one of the three cases, the default model reproduces the observed spectra fairly well, but overestimates the total variance somewhat for AZB42 on 18/03/2007 at 17:00, and underestimated the total

variance in the third case (18/03/2007 at 19:20). The model with enhanced dissipation (dashed lines) shows only small changes for most cases. The exceptions are the case 18/03/2007 at 17:00, which shows a reduction in variance relative to the default and closer to the measurements at AZB42, and 09/11/2007 at 04:50, which shows an increase in variance trending away from the measurements at AZB32. This is possibly due to a reduction in the level of depth-induced breaking dissipation over the ebb tidal delta in (4.1)-(4.5) relative to Battjes and Janssen (1978) of waves coming from the NW. The modeled and observed wave directions are in agreement for the frequency range with significant variance, except for the top right panel. Here all model variants predict waves from the WNW whereas they are observed from the WSW for this flood case. Clearly, the proposed model's predictions do not match the data which leaves room for further improvement.

4.2.3 Penetration of low-frequency wind wave energy

The Amelander Zeegat measurements shown in Figure 5 and discussed in Section 2 show very little North Sea-generated wave energy penetrating into the inlet under storm conditions. Here the ebb tidal delta functions as an efficient wave dissipator, and waves which do penetrate through the inlet gorge are quickly refracted out of the channels and dissipated over the flats. However, for more exposed inlets, e.g. in the Eems-Dollard estuary (Figure 4) and the Eastern Scheldt in the southwest of the Netherlands (Figure 8), significant wave penetration has been visually observed, already under frequently-occurring storm conditions.

The penetration of North Sea waves into the mouth of the Eastern Scheldt was investigated for a number of storms which had a pronounced offshore peak, and for which buoy measurements and a recent bathymetric survey were available. The results for the Eastern Scheldt cases (see Figures 24 and 25) show that the offshore wave spectral peak (around 0.12 Hz) is properly predicted by the default model (dash-dotted line) for the first three stations but that at the nearshore station OS4 the energy at this frequency is underestimated significantly (up to 50%). Note that the vertical scale (i.e. the energy density) has decreased significantly. Including the improvements discussed so far (breaker expression (4.1)-(4.5) and current gradient dissipation (4.7)-(4.9)) improve the results, especially in the high-frequency tail (dashed lines) but the prediction of the energy levels at the North Sea spectral peak is not improved significantly.

A similar result can be seen in the Eastern Dutch Wadden Sea during the peak of the storm of 8-9 November 2007 (Figure 26). Although the wind sea frequency range is consistently well-predicted, the low-frequency components are underpredicted at the location of the most shoreward buoys. At the outer buoy WEO1 the model-data agreement is reasonable but at all inner buoys there is a significant amount of energy below 0.2 Hz that the default model does not predict. The innovations so far (dashed lines) improve the results, but still the energy in the frequency range of the offshore peak remains underpredicted. Note again the change of vertical scale from the outer to the inner buoys. We verified that the low-frequency variance is not explained by lower-harmonic bound waves (Hasselmann, 1962; Herbers et al., 1994), which are not computed by SWAN.

The reduction of the offshore spectral peak was analysed by investigating the source terms and spectral evolution along dominant propagation paths (not shown). It was found that the

rapid change in the spectral shape did not occur when any source or sink terms (depth breaking, whitecapping, etc.) were locally large (Van Vledder et al., 2008). By elimination, this suggests that the cause of the mismatch is in the propagation terms and/or small-magnitude, but persistent, sink terms such as the bottom friction that act over large distances, both of which are discussed in more detail below.

The accuracy of the wave direction modeling in the tidal inlets (assumed to be dominated by propagation from the offshore) was investigated using data from an X-band marine radar deployed on the Ameland lighthouse overlooking the tidal inlet. Figure 27 presents spatial plots of simulated and radar-derived dominant wave directions in the Amelander Zeegat tidal inlet, for three tidal stages of a NW storm recorded in 28 January 2010. The dominant wave direction is defined as the direction of the energy bin with maximum wave energy, not to be confused with the peak wave direction. The left-hand panels compare vector plots of the computed and radar-derived directions, superimposed on the inlet bathymetry. The right-hand panels illustrate the differences in these results in terms of contour difference plots of the dominant wave direction. In addition, the peak directions recorded by the wave buoys in the vicinity are shown as the yellow circles.

The radar directional results (left-hand panels) show some typical propagation patterns, including waves entering over and around the ebb tidal shoal, refraction over the banks of the main tidal channel, wave trapping on the central shoal in the inlet and waves from the west crossing over the main tidal channel towards the head of Ameland. These features are generally well-reproduced by SWAN, and agree fairly well locally with the buoy observations. The right-hand panels show that the differences between the model results and observations are relatively small over the majority of the observed region. Some local discrepancies can be found (indicated by the black circles), in particular at locations with crossing seas. These areas are fairly consistent, although errors are somewhat greater during flood and ebb than when currents are weak (high tide). Note also that at some (random) locations, the radar wave direction is erroneously aliased by 180° , causing rather large differences in isolated areas. These results suggest that SWAN, utilizing only depth- and current-induced refraction (no diffraction) can adequately model wave propagation over complex inlets.

With respect to the sink terms, in the present formulation the bottom friction coefficient is a free parameter for which two default values are given by Booij et al. (1999). The first of these values was derived for swell conditions observed during the JONSWAP experiment (Hasselmann et al. 1973) which yielded a value $C_{f,JON} = 0.038 \text{ m}^2\text{s}^{-3}$. For fully-developed wind-sea conditions in shallow water a second value of $C_{f,JON} = 0.067 \text{ m}^2\text{s}^{-3}$ was found by Bouws and Komen (1983). However, a re-analysis of their paper reveals some inconsistencies in the determination of the friction coefficient for wind seas (Van Vledder et al., 2011). For the present purpose which concerns the penetration of low-frequency wind waves the “swell” value of $C_{f,JON} = 0.038 \text{ m}^2\text{s}^{-3}$ seems justified given the above-mentioned re-analysis.

With the reduction in bottom friction, the variance in the low-frequency flank of the spectra at the Eastern Scheldt's OS4 (Fig 24 and 25, thick solid lines) and at the Eastern Wadden Sea's UHW1 and WRW1 (Figure 26) is increased, relative to the default, but still falls short of the measurements, except at WRW1. Figure 28 compares the model results with observations in terms of scatter plots of H_{m0} , $T_{m-1,0}$ and T_{m01} for locations where wave penetration of longer-period North Sea waves is noticeable. For this analysis, the wave buoys AZB21 and AZB22 in

the Amelander Zeegat, BG2, DORA and OS4 in the Eastern Scheldt and PBW1, UHW1 and WRW1 in the Eastern Waddensea were used. The left-hand column shows the results of the default model, where a clear underprediction in H_{m0} , $T_{m-1,0}$ and T_{m01} is observed. The right-hand column of Figure 28 shows that using the proposed model (including the lower bottom friction) leads to a significant improvement in the statistics of the wave parameters: the bias is halved and the scatter greatly reduced. These results are consistent with independently-obtained results by Zijlema (2009).

To investigate the influence of the bottom friction on the results where wave penetration plays a role, the proposed SWAN version without the reduction of the bottom friction (therefore $C_{f,JON}=0.067 \text{ m}^2\text{s}^{-3}$) is compared to the proposed model itself (Figure 29). The results in the left-hand column shows a similar (slightly lower) underprediction of the wave parameters as was observed for the default model. Therefore, it can be concluded that the improved results at the lower frequencies and at the stations where wave penetration is relevant are in part due to the reduction of the bottom friction (judging from the reduction in the bias by about 50%) and in part due to other model changes.

4.3 Results of the proposed model

This section presents the overall performance of the proposed model, including the improvements listed in Section 3.3, and discussed individually in Section 4.2. The proposed model was run for all cases, and the improvements are shown in terms of scatter plots of integral parameters and variance density spectra (included as thick solid lines in the spectra figures presented in Section 4.2).

The scatter plots are shown in the right-hand column of Figure 11. The panels show that the proposed model consistently reduces the bias which was seen with the default model (left-hand column), and results in a smaller scatter index for all these parameters.

For the stations in the Wadden Sea interior (e.g. AZB 51/61/62 landward of the Amelander Zeegat) and in the shallow lakes (e.g. Lake Sloten), the improvement is due to the formulation for depth-induced breaking (4.1)-(4.5) that corrects the model behavior over nearly-horizontal slopes under wind forcing, and the reduction of the constant bottom friction coefficient (discussed in Sections 4.2.1 and 4.2.3 respectively). Apart from the integral properties (Figure 12), the improvement can also be seen in the spectra of Lake Sloten (Figure 15, thick solid line) and the inner buoys of the Amelander Zeegat (Figure 16). In the latter figure, the effect of a few intermediate steps in the model development are also shown. Results are shown for the default model (dash-dotted line) and the observations (solid line with dots), as well as simulations with the breaker model (4.1)-(4.5) model in combination with:

- high bottom friction dissipation without enhanced dissipation on current gradients (dashed),
- high bottom friction dissipation with enhanced dissipation on current gradients (dotted),
- low bottom friction dissipation without enhanced dissipation on current gradients (solid with crosses),
- low bottom friction dissipation with enhanced dissipation on current gradients (thick solid, the ultimately proposed model),

For the AZB51 and AZB61 buoys, only small differences between these model variants can be seen, the most important of which is the more enhanced low-frequency flank of the

spectrum in the cases of the lower bottom friction dissipation (which can be expected, since the lower-frequency waves will feel the bottom more than higher-frequency ones). The largest difference can be seen at AZB62 for the cases with and without enhanced dissipation on current gradients (compare the “solid with crosses” and thick solid lines). The enhanced dissipation tends to reduce the variance around the peak of the spectrum, tending away from the measurements in this case. This is due to the modeled strong current gradients at this location for this case: the current runs (practically alongshore) in the wind direction from southwest to northeast and has a value of about 0.8 m/s just upwind from AZB62 and near zero downwind due to the tidal channel, i.e. a case of a negative gradient in a following current. As there are no observations of currents in the Amelander Zeegat, we can not verify if such a gradient occurred in nature. A similar, but less pronounced effect can in fact also be seen at AZB51. However, there the reduction in variance due to enhanced dissipation on current gradients improves the results at the peak compared to the case with enhanced dissipation turned off. Since the conditions at the nearshore locations have a strong component of local wind sea, the wave period measures also improve, because they are coupled to the development of the total variance.

As discussed in the previous section, the effect of the reduced bottom friction on the penetration of lower frequencies from the North Sea is relatively modest when considering the total wave height results at, for example, the nearshore stations in the exposed Eastern Dutch Wadden Sea (PBW1, WRW1 and UHW1), see Figure 29. However, its influence is prominent in the results of the spectral mean period, in particular an improvement in $T_{m-1,0}$, which is weighted towards lower frequencies. This is important, since the Dutch dikes are assessed using criteria based on wave overtopping discharge rates, which are sensitive to this mean period measure.

The enhanced dissipation on negative current gradients (Section 4.2.2) has led to a general reduction in total significant wave height relative to the default, in part balanced by the lower bottom friction dissipation. This can be seen specifically at stations in the main tidal channel of the Amelander Zeegat inlet (e.g. AZB32/42, see Figures 22 and 23 thick solid lines), but also at interior stations, as discussed above.

Finally, for the “wave age” case evaluated at Norderney (Figure 17) the proposed model (thick solid lines) performs well at RIFFGAT, but results deteriorate at SGTNEY. The proposed model results show an increase in the frequencies below 0,1 Hz at SGTNEY, which are also higher than the default with currents (dash-dotted line). This is due to a combination of a decrease in breaking dissipation over the ebb tidal delta and reduced bottom friction of these offshore components arriving from the NW. We note that the errors here may also be related to errors in the computed current field used as model input.

Summarizing, it can be concluded from these results that the proposed model innovations have led to improved overall performance in the complex tidal inland field situations considered in this study.

5 Discussion

A number of innovations are proposed in this report to improve the nearshore wind-wave model SWAN for application to complex tidal inlet regions. It was shown that alterations to the default formulations for depth-induced breaking, the treatment of wave-current interaction and the settings for bottom friction reduces the overall model error. However, there are still a number of remaining challenges and information needs for wave modeling in these regions, and some reservations should be borne in mind when applying the results of this study.

First of all, the present effort focused on the Wadden Sea and similar environments on the northwest coast of Europe. While a wide range of conditions is considered here, the applicability of the proposed model formulation and settings should be verified for other regions as well.

A number of modeling challenges remain for tidal inlet areas such as the Wadden Sea. An important aspect identified here is the modeling of the penetration of low-frequency wind wave components into the complex system of channels and over the tidal flats. Comparison with available information derived from X-band radar data in the Amelander Zeegat suggests that the propagation aspect of the wave penetration is modeled relatively well, even under strong currents, at least over limited domains. This modeling of propagation is however complicated by the fact that the distance from the barrier islands to the mainland shore (where the predictions are required) is large, so that even small errors in the propagation direction can result in significant errors at these frequencies at the mainland coast. Further validation of this aspect requires continued spatial observation by X-band radar or, for greater range, High Frequency (HF) radar or Synthetic Aperture Radar (SAR) satellite data. In this regard, the preferred approach would be to choose situations where physical processes of wave growth and decay do not play a significant role or at least to isolate the lower-frequency (swell range) components from the observations, since the higher frequency wind sea components are correlated with the wind, and generally well-predicted, as shown above.

With respect to modeling propagation, it was found that limiting the amount of refraction (by limiting the c_0 term in (2.1)) of these low-frequency components, improves the prediction of the low-frequency wave height and period (Van Dongeren et al, 2011). A similar result was found previously by H. Vrijling of TU Delft who applied a predecessor of SWAN for the calculation of wave loads on the Eastern Scheldt barrier. However, limiting refraction has no physical basis and may not be generally applicable. Therefore, no low-frequency refraction limiter was applied in the proposed SWAN model. Nonetheless, it needs to be investigated what the effect of refraction modeling is on the results in the Wadden Sea, including comparing the results of the linear, phase-averaged model SWAN to nonlinear time-domain models.

The second aspect of modeling wave penetration is the associated dissipation. Analysis of spectral evolution (Section 4.2.3) suggested bottom friction to be the most important dissipation mechanism over the extensive tidal flats. The re-analysis of Van Vledder et al. (2011) lends support to the use of a lower constant bottom friction coefficient in the Hasselmann et al. (1973) bottom friction formulation for the Wadden Sea interior. However, a

more fundamental investigation of this issue is possible, using dynamic bed ripple modeling (e.g. Tolman 1994). Tolman (1994) concludes that in limited water depths, wind sea conditions can lead to the washing out of bed forms, resulting in lower levels of bottom frictions. Dynamic bed ripple formulations have recently been implemented in research versions of SWAN (Smith et al. 2011; Siadatmousavi et al. 2011), using as primary input the D_{50} grain size. Using available maps of the D_{50} grain size in the Dutch Wadden Sea, the bottom friction dissipation can be computed as a function of the local wave conditions, and the lower constant $C_{f,JON}$ used in this study can then be verified.

Regarding the enhanced dissipation of wave on negative current gradients (Section 4.2.2), it was noted that such gradients can occur in both accelerating (along the wave's propagation path) opposing current and decelerating following current. Whereas the former has been observed in the field and laboratory, to our knowledge no observations of the latter exist. Such observations would be a very useful addition to the subject of wave-current interaction modeling.

The current report does not discuss the accuracy of the input fields into SWAN, such as wind fields, bathymetry, and water level and current fields. The analysis of the accuracy of input fields and its effect on the wave field has been addressed in project reports (Deltares, 2008a and b). Wind fields applied here were mostly obtained from HIRLAM (High Resolution Limited Area Model ; <http://hirlam.org>), which is the state-of-the-art wind- and pressure field model. Still, deficiencies between the computed wind fields and local observations could be seen. This aspect will be addressed in future SBW projects. The bathymetry of the tidal inlet seas is measured during the summer months with intervals ranging from 1 to 4 years because of the expense of measurement campaigns. This is not ideal, because bathymetry data from different years had to be assembled, and the inlet bathymetry is highly-dynamic on time scales of months (summer to winter) and years. Despite these limitations, we are very fortunate to have had access to this unique bathymetric data set. The current and water level fields have been computed with surge models, such as Delft3D and WAQUA (Stelling, 1983). In the present study, these time-domain model results are calibrated against observations of water levels from local water level gauges (Figure 1). We have found that the surge peak was consistently underestimated by the surge models, the reason of which is still under investigation. For the present purpose, the water level and current fields used as input in the SWAN calculations were corrected for the discrepancies using linear interpolation techniques. Furthermore, even if the surge model showed perfect skill with regard to the water level data, this does not a guarantee that the modeled currents are modeled correctly. For this purpose, 3D current measurements are required in the tidal channels and, to capture the influence on the young wind sea, also on the tidal flats.

Finally, some observations regarding the use of the results of this study in applications such as the design and testing of sea defenses (the Dutch Wadden Sea HBC in this case). It should be noted that even though the observations in the Dutch Wadden Sea and elsewhere presented here includes some significant events over the observation period, they still represent only relatively mild storm conditions, and not the extreme events with return periods of at least 4000 years specified for the testing of the sea defenses in this region. This issue was addressed by evaluating results in terms of dimensionless relations such as that of Young and Babanin (2006) and limiting values of H_{m0}/d , under the assumption of their universal validity, also under extreme conditions. However, it may not be valid to assume that the physics under extreme conditions would be the same as under storm conditions

encountered in this study. An analogy with hurricane modeling is possible here: when applying empirical wind input formulations derived for moderate conditions to hurricane situations, significant overestimations of wave growth result (e.g. Jensen et al. 2006). Theory and observations suggest that the physics change under these extreme conditions, for example that an upper limit to the drag coefficient supported by the waves develops (e.g. Makin 2005; Donelan et al 2006). It is therefore possible that similar effects may influence the processes in the Dutch Wadden Sea under extreme conditions, currently not captured in the model.

6 Conclusions

This study presents the main results of a five-year research program to assess and where possible improve the performance of the wave transformation model SWAN in the Wadden Sea, with a focus on the shallow water processes. The end goal was to produce a model which may be used for the reliable transformation of offshore wave conditions to wave boundary conditions near the sea defenses (dikes and dunes).

In the course of the program, three main model innovations (depth-induced breaking, dissipation in ambient current gradients and bed friction) are proposed. These have been sequentially tested and compared to the default model results. The assessment was done on the basis of extensive wave measurements conducted in the Ameland Zeegat tidal inlet and the Eastern Dutch Wadden Sea, as well as relevant data from lakes and estuaries. On the basis of the results presented in this study, the following can be concluded:

- SWAN version 40.51, in its default form of 2006 (except for wind input and whitecapping modeled according to Van der Westhuysen, 2007)) was found to perform reasonably well for storm conditions. However, three aspects required further attention: (i) the modeling of depth-induced breaking under finite depth wave growth conditions, (ii) the modeling of wave-current interaction, through the inclusion of current fields and the enhanced dissipation on negative current gradients, and (iii) the penetration of low-frequency wind waves.
- Over the tidal flats, the computed ratio of significant wave height over water depth showed an apparent upper limit using the default version of SWAN, because the wave growth over finite depth is hampered by the Battjes and Janssen (1978) formulation of depth-induced wave breaking using a fixed breaker parameter γ , calibrated for sloping bed surf zones. The problem has been solved using a new breaker formulation of Van der Westhuysen (2009, 2010).
- Focusing on the main channel, a dissipation term was added in order to eliminate overprediction of the significant wave height in negative current gradients (opposing and following current). This has largely been achieved with a formulation for enhanced dissipation that is scaled with the degree of Doppler-induced steepening of the waves. Note, however, that the limited size of the dataset for following current prevents the drawing of a definitive conclusion.
- Currents should be included in the computations as they affect the wave age, which has consequences for the modeled variance spectra. In many (but not all locations considered here) this inclusion improved the model results.
- The primary spectral peak of North Sea waves penetrating into the inlet was underpredicted due to a combination of propagation and dissipation (bottom friction). On the basis of comparison with X-band radar derived results, the propagation components appears to be adequately modeled. Best results were obtained when the bottom friction coefficient was set at the lower value of the current two defaults ($C_{f, \text{JON}} = 0.038 \text{ m}^2\text{s}^{-3}$) which is consistent with a re-analysis by Van Vledder et al. (2011). Additional improvements are possible by reducing the amount of refraction of lower-frequency components, but this approach lacks physical basis, and is hence not proposed.

- As demonstrated in the simulations for the Norderneyer Seegat, wave computations should be performed using a sufficient number of iterations to ensure convergence. This confirms the findings of Zijlema and Van der Westhuysen (2005). In the present study 80 iterations was found to be sufficient.

All these improvements have resulted in reduced bias and scatter compared to the 2006 default model. The statistical error parameters are small enough that the proposed wave transformation model can determine reliable wave conditions in the Dutch Wadden Sea and related complex areas.

7 Outlook

In this report the major innovations in tidal inlet wave modeling in the framework of the SBW-Waddenzee project have been shown. In the project a number of issues have not been addressed, which need further attention:

7.1 Modeling

The project has not addressed the modeling of the non-linear quadruplet and triad interaction terms. The former is dominant in deeper water, but remains important during local wind sea growth over the tidal flats in the Wadden Sea. The latter becomes important as the waves propagate in very shallow water. The presently-implemented “Lumped Triad Approximation” (LTA) formulations by Eldeberky (1996) is a rather crude approximation which tends to overestimate variance levels at the first superharmonic of the spectrum. While computationally efficient, it should be investigated if an alternative model can be implemented and used in a practical way. Furthermore, the SWAN model currently has no modeled mechanism to redistribute energy from wind wave frequencies to subharmonic (infragravity wave) frequencies. This means that on shallow foreshores SWAN does not compute energy in the infragravity band which affects period measures. Such redistribution terms should be included in SWAN, which should also have the capability of propagating bound waves at the group speed (as opposed to the free wave celerity). Alternatively, models (such as non-hydrostatic or Boussinesq-type models) which do contain the modeled physics should be nested into the SWAN model.

Not all of the Dutch primary sea defenses consist of exposed dunes and dikes. In some cases the defense is part of a harbour or sluice complex and may consist of vertical walls. These circumstances present additional challenges to the computation of wave boundary conditions, such as local effects of diffraction, transmission of breakwaters and reflection from quay walls which are not addressed in the present study but warrant attention. In addition, some sea defenses are situated such that the conditions are strongly fetch-limited. These conditions have not been considered in this study explicitly, but do receive attention. SWAN tends to overpredict the wave energy at short fetches. (e.g. Bottema and Van Vledder, 2009).

Finally, the current method of sea dike assessment is based on overtopping discharge rates and uses as input the wave parameters and water levels at the instant of maximum water level. This instance may not coincide with the peak of maximum wave load. In addition, for other dike failure mechanism such as the stability of the seaward armouring blocks, the instance of maximum load may occur at a time instance earlier in the storm. Therefore, the effects of coupled non-stationary SWAN and surge computations should be investigated in the future.

7.2 Information need

During the project, a pilot deployment was made to record velocity profiles at three locations offshore and inside of the Amelanders Zeegat inlet. This information is useful in the

assessment of wave-current interaction modeling in SWAN, but also to the calibration and verification of hydrodynamic models in the Wadden Sea. The pilot deployment needs to be made permanent.

As final information need, the buoy data applied in this study can become less reliable in very shallow depths (less than about 1.5 m, pers. comm. Datawell), so that in these regions, it would be desirable to have independent observations from e.g. pressure gauges. In addition, observations of ripple formation and decay during a storm event over the tidal flats would significantly aid the bed friction modeling.

8 Acknowledgments

This study is part of the SBW (Strength and Loads on Water Defenses) project commissioned by Rijkswaterstaat Centre for Water Management in the Netherlands. The lead partner is Deltares in collaboration with Rijkswaterstaat's Data Division who collected data, and with researchers from universities and Dutch consultants Alkyon/Arcadis, Royal Haskoning, Svasek, Witteveen+Bos to perform hindcasts and analyze the results.

9 References

Battjes, J.A., and J.P.F.M. Janssen (1978). Energy loss and set-up due to breaking of random waves, Proceedings of 14th International Conference on Coastal Engineering, Hamburg, Germany, ASCE, 466-480.

Booij, N., R.C. Ris, and L.H. Holthuijsen (1999). A third generation wave model for coastal regions, Part I, Model description and validation. *J. Geophys. Res.*, 104, C4, 7649-7666.

Bottema, M. (2007). Measured wind-wave climatology Lake IJssel (NL). Main results for the period 1997-2006. Report RWS RIZA 2007.020, July 2007.

Bottema M., and G. Ph. Van Vledder (2009). A ten-year data set for fetch- and depth-limited wave growth. *Coastal Eng.*, 56, 703-725.

Bouws, E. and G. J. Komen (1983). On the balance between growth and dissipation in an extreme, depth-limited wind-sea in the southern North Sea. *J. Phys. Oceanogr.*, 13, 9, 1653-1658.

Deltares (2008a). Verification of water levels during storm events in the Wadden Sea. Deltares report H5107.35. Author: A. Luijendijk.

Deltares (2008b). Impact of bed level changes during an extreme storm on the wave characteristics at the Frisian dikes. Deltares report H5107.32. Authors: A. Mol and A. Luijendijk.

De Waal, J.P. (2001). Wave growth limit in shallow water. Proc. of 4th international symposium WAVES 2001, 560-569.

De Waal, J. P., D. Beyer, J. H. Andorka Gal, L. H. Holthuijsen, G. Ph. van Vledder, J. P. F. M. Janssen, and D. P. Hurdle (1997). Instellingen golfmodel HISWA, toe te passen bij productiesommen in het IJsselmeergebied (in Dutch). Model settings of the wave model HISWA, to be used in production runs for Lake IJssel. Werkdocument nr. 97.183X, RWS RIZA, November 1997.

Dietrich, J.C., M. Zijlema, J.J. Westerink, L.H. Holthuijsen, C. Dawson, R.A. Luetlich Jr., R.E. Jensen, J.M. Smith, G.S. Stelling, and G.W. Stone (2011). Modeling hurricane waves and storm surge using integrally-coupled, scalable computations. *Coastal Engineering*, 58, 45–65.

Doering, J.C. and A.J. Bowen (1995). Parametrization of orbital velocity asymmetries of shoaling and breaking waves using bispectral analysis, *Coastal Engineering*, 26, no. 1-2, 15-33.

Donelan, M. A., A. V. Babanin, I. R. Young, and M. L. Banner (2006), Wave-follower field measurements of the wind-input spectral function, part II: Parameterization of the wind input, *J. Phys. Oceanogr.*, 36, 1672–1689.

Eldeberky, Y. (1996). Nonlinear transformation of wave spectra in the nearshore zone. Ph.D. thesis, TU Delft, 203 pp.

Hasselmann, K. (1962), On the non-linear energy transfer in a gravity-wave spectrum: I. General theory, *J. Fluid Mech*, 12, 481– 500.

Hasselmann, K., T. P. Barnett, E. Bouws, H. Carlson, D. E. Cartwright, K. Enke, J. A. Ewing, H. Gienapp, D. E. Hasselmann, P. Kruseman, A. Meerburg, O. Müller, D. J. Olbers, K. Richter, W. Sell, and H. Walden (1973). Measurement of wind-wave growth and swell decay during the Joint North Sea Wave Project (JONSWAP). *Dtsch. Hydrogr. Z. Suppl.* 12(A8).

Hasselmann, S., K. Hasselmann, J. A. Allender, and T. P. Barnett (1985). Computations and parameterizations of the nonlinear energy transfer in a gravity-wave spectrum. Part 2: parameterization of the nonlinear transfer for application in wave models, *J. of Phys. Oceanogr.* 15, 1378-1391.

Haus, B. K. (2007). Surface current effects on the fetch-limited growth of wave energy. *J. Geoph. Res.*, 112, C03003, doi:10.1029/2006JC003924.

Herbers, T. H. C., S. Elgar, and R. T. Guza (1994). Infragravity-frequency (0.005–0.05 Hz) motions on the shelf: I. Forced waves, *J. Phys. Oceanogr.*, 24, 917– 927.

Herman, A., R. Kaiser, and H.D. Niemeier (2006). Medium-term wave and current modeling for a mesotidal Wadden Sea coast. *Proc. ICCE 2006, San Diego, USA*, 628-639.

Holthuijsen, L. H., N. Booij, and T.H.C. Herbers (1989). A prediction model for stationary, short-crested waves in shallow water with ambient currents. *Coastal Engineering*, 13, 23-54.

Jensen, R. E., V. J. Cardone and A. T. Cox (2006). Performance of Third Generation Wave Models in Extreme Hurricanes. *Proc. 9th International Workshop on Wave Hindcasting and Forecasting*. Victoria, Canada.

Kaiser, R. and H.D. Niemeier (2001). Analysis of directional spectra in shallow environment. Proc. of 4th international symposium WAVES 2001, San Francisco, USA, 944-952.

Makin, V. K. (2005). A note on the drag of the sea surface at hurricane winds. Bound.-Layer Meteorol., 115, 169-176.

Mei, C. C. (1983). The applied dynamics of ocean surface waves, Wiley, New York, 740 pp.

Ris, R.C. and L.H. Holthuijsen. (1996). Spectral modeling of current wave-blocking. Proceedings of 25th International Conference on Coastal Engineering, Orlando, USA, ASCE, 1247-1254.

Ris, R. C., L. H. Holthuijsen, and N. Booij (1999). A third-generation wave model for coastal regions, Part II: Verification, J. Geophys. Res., 104, C4, 7667-7681.

Siadatmousavi, S. M., F. Jose, and G.W. Stone (2011). The effects of bed friction on wave simulation: implementation of an unstructured third-generation wave model, SWAN. J. Coastal Res., 27(1), 140-152.

Smith, G., A. V. Babanin, P. Riedel, I. R. Young, S. Oliver, and G. Hubbert (2011). Introduction of a new friction routine in the SWAN model that evaluates roughness due to bedform and sediment size changes. Coastal Eng., 58, 4, 317-326.

Stelling, G.S. (1983). On the construction of Computational Methods for Shallow Water Flow Problems, Ph.D. thesis, TH Delft

Thornton, E.B. and R.T. Guza (1983). Transformation of wave height distribution, J. of Geophysical Research, vol. 88, no. C10, 5925-5938.

Tolman, H. L. (1994). Wind waves and movable-bed bottom friction. J. Phys. Oceanogr., 24(5), 994-1009.

Van der Westhuysen, A. J. (2007). Advances in the spectral modeling of wind waves in the nearshore, Ph.D Thesis, Fac. of Civil Engineering, Delft University of Technology.

Van der Westhuysen, A. J., M. Zijlema, and J. A. Battjes (2007). Nonlinear saturation-based whitecapping dissipation in SWAN for deep and shallow water. Coastal Engineering 54, 151-170.

Van der Westhuysen, A. J. (2009). Modeling of depth-induced wave breaking over sloping and horizontal beds. Proc. 11th International Workshop on Wave Hindcasting and Forecasting. Halifax, Canada.

Van der Westhuysen, A.J. (2010). Modeling of depth-induced wave breaking under finite-depth wave growth conditions. *J. of Geophys. Res.*, 115, C01008, doi:10.1029/2009JC005433.

Van der Westhuysen, A. J. (2011). Spectral modeling of wave dissipation on negative current gradients. *Submitted to J. Geophys. Res.*

Van Dongeren, A.R., A.J. van der Westhuysen, J. Groeneweg, G.Ph. van Vledder, J. Lansen, A. Smale, C. Gautier, H. Peters and I. Wenneker. (2011). Spectral wave modeling in tidal inlet seas: Results from the SBW Wadden Sea project. *Proceedings Of The International Conference On Coastal Engineering*, Hamburg, Germany, 1 (32). Retrieved from <http://journals.tdl.org/ICCE/article/view/970>

Van Vledder, G.Ph., J. Groeneweg and A. van der Westhuysen (2008). Numerical and physical aspects of wave modeling in a tidal inlet. *Proc. Of the International Conference on Coastal Engineering*, Hamburg, Germany, pp. 424-436.

Van Vledder, G.Ph., M. Zijlema and L.H. Holthuijsen (2011). Revisiting the JONSWAP Bottom Friction Formulation in Wind-Driven Storm Seas. *Proceedings Of The International Conference On Coastal Engineering*, Hamburg, Germany, 1 (32). Retrieved from <http://journals.tdl.org/ICCE/article/view/1395>

Young, I.R. and L.A. Verhagen (1996). The growth of fetch-limited waves in water of finite depth. Part 1. Total energy and peak frequency. *Coastal Engineering*, 29, 47-78

Young, I. R. and A. V. Babanin (2006). The form of the asymptotic depth-limited wind wave frequency spectrum. *J. Geophys. Res.*, 111, C06031, doi:10.1029/2005JC003398.

Zijderveld, A. and H. Peters (2008). Measurement programme Dutch Wadden Sea. *Proceedings International Conference on Coastal Engineering*, San Diego, USA, 404-410.

Zijlema, M. and A.J. van der Westhuysen (2005). On convergence behaviour and numerical accuracy in stationary SWAN simulations of nearshore wind wave spectra. *Coastal Engineering*, 52, pp. 237-256.

Zijlema, M. (2009). Multiscale simulations using unstructured mesh SWAN model for wave hindcasting in the Dutch Wadden Sea. in: M. Mizuguchi and S. Sato (Eds.), *Proceedings of Coastal Dynamics 2009*, World Scientific Publishing, Singapore, paper no. 2

10 SBW Waddenzee research reports

Alkyon (2008a). Analysis of SWAN hindcasts Wadden Sea, Oosterschelde Slotermeer; Investigation into low frequency wave energy, current effects and depth limitation. Alkyon Report A2085. Author: G.Ph. van Vledder.

Alkyon (2008b). SWAN hindcast in the Eastern Wadden Sea and Eems-Dollard estuary during the Storm of 9 November 2007. Alkyon Report A2191. Authors: J. Adema, G.Ph. van Vledder and O.R. Koop.

Deltares (2008). Observed finite-depth wave growth limit in the Wadden Sea. Deltares report H5107.35. Authors: A.J. van der Westhuysen and J.P. de Waal.

Deltares (2009a). Penetration of North Sea waves into the Wadden Sea - phase 3: fallback options. Deltares report report 1200114-002. Authors: A.R. van Dongeren, A.J. van der Westhuysen, G.Ph. van Vledder and I. Wenneker.

Deltares (2009b). SBW Wadden Sea, water level modeling; Study on sensitivity of applying spatially varying bed characteristics. Deltares report 1200114-005. Authors: J.-J. Schouten and A. van der Hout.

Deltares (2009c). SBW Wadden Sea 2009: Wave hindcast of the storm of 31 January 2008. Deltares report 1200114-005. Authors: A. van der Hout and C. Swinkels.

Deltares/Alkyon (2009). Wave propagation through tidal inlet systems. Deltares and Alkyon report 1200114-002-HYE-0006. Authors: A.J. van der Westhuysen, B. Huisman, F. Enet, O.R. Koop and G.Ph. van Vledder.

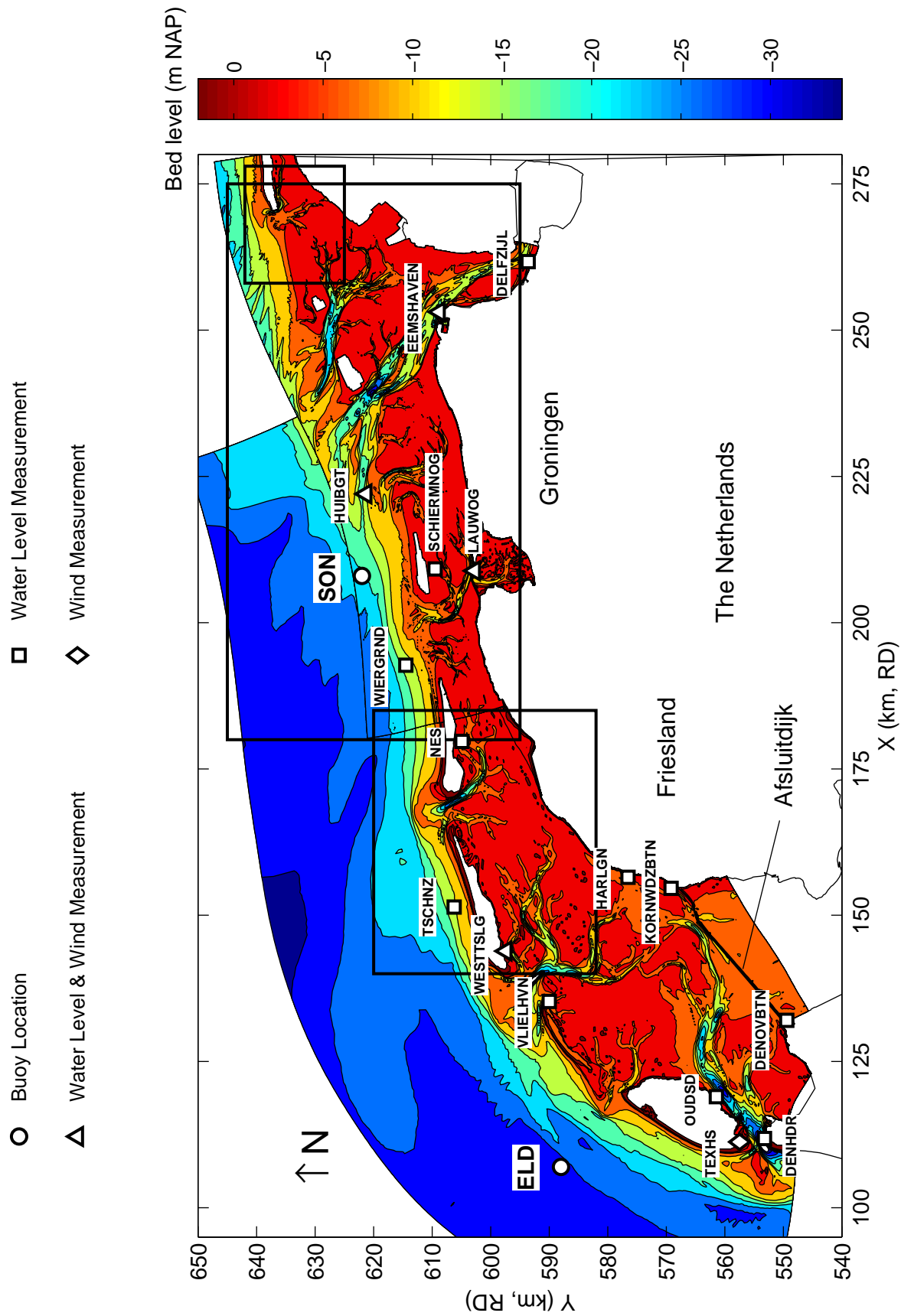
Deltares (2010). Wave propagation under the influence of currents. Deltares report 1202119-003-HYE-002. Authors: A.J. van der Westhuysen and C. Gautier.

Royal Haskoning (2008). Hindcast Ameland Zeegat storms January and March 2007 (revised). Royal Haskoning Report 9T5842.A0/R0004, October 2008. Authors: J. Lansen, S. Jacobse, M. Kluyver, E. Arnold.

Svasek (2007). Hindcast tidal inlet Eastern Scheldt, Storms December 2001 and December 2003, Svasek Report CG/1461/07542/A, December 2007 Authors: C. Gaultier and M. van de Boomgaard.

Witteveen+Bos (2008). Hindcast of the 8 and 9 November 2007 storm for the tidal inlet of Ameland. Witteveen en Bos Report DT-293-2. Authors: R. Zijlstra and A. Smale.

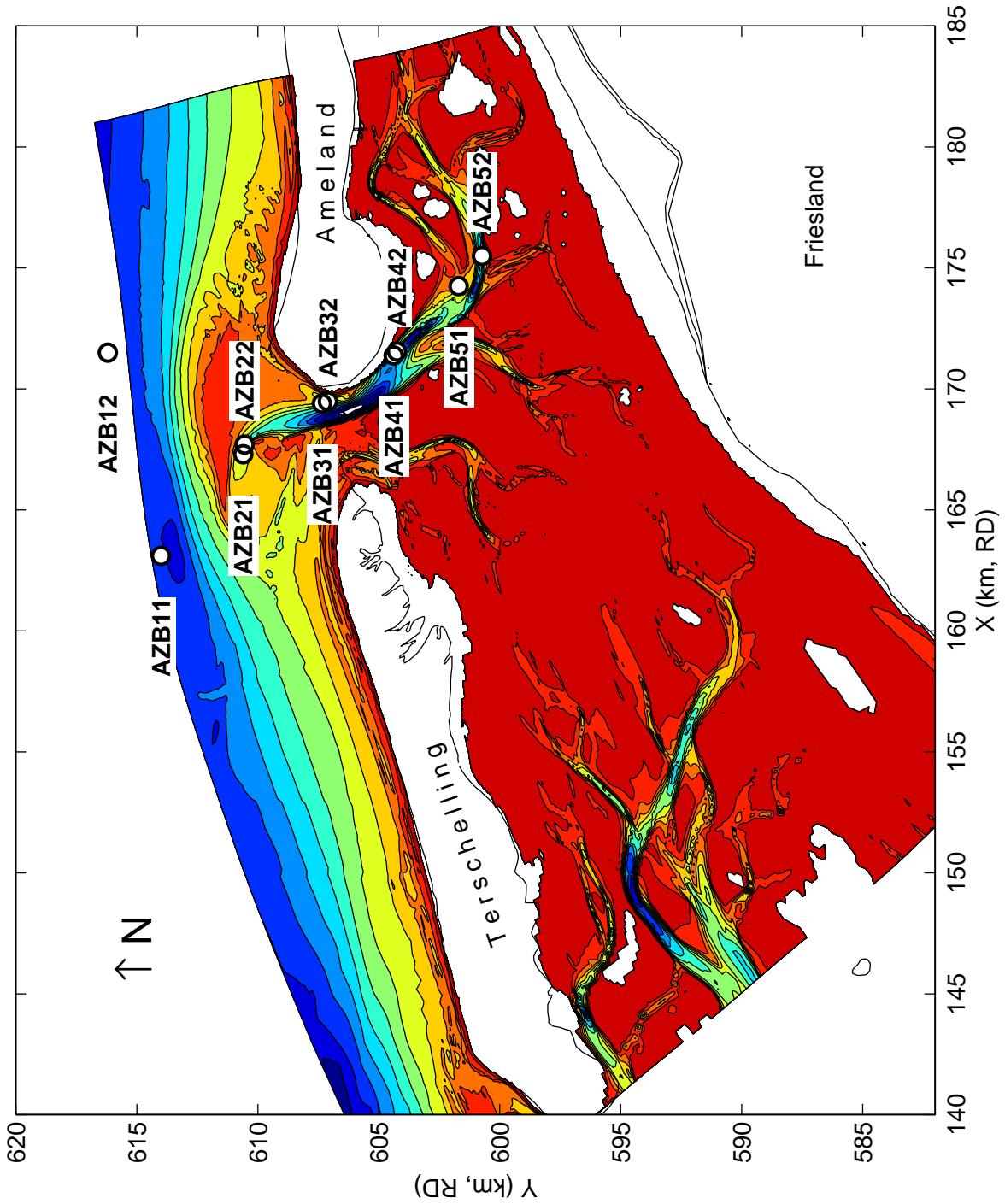
A Figures



Bathymetry of the Dutch Wadden Sea. Bed levels are given in m below NAP (Dutch leveling datum). The boxes indicate detail areas, shown in detail figures. Projection in Dutch Rijksdriehoek (RD) system.

SBW Waddenzee

Bed level (m NAP)



Bathymetry of the Amelander Zeegat region in the Dutch Wadden Sea, including the location of the wave buoys (circles), in the configuration of 2003–2006

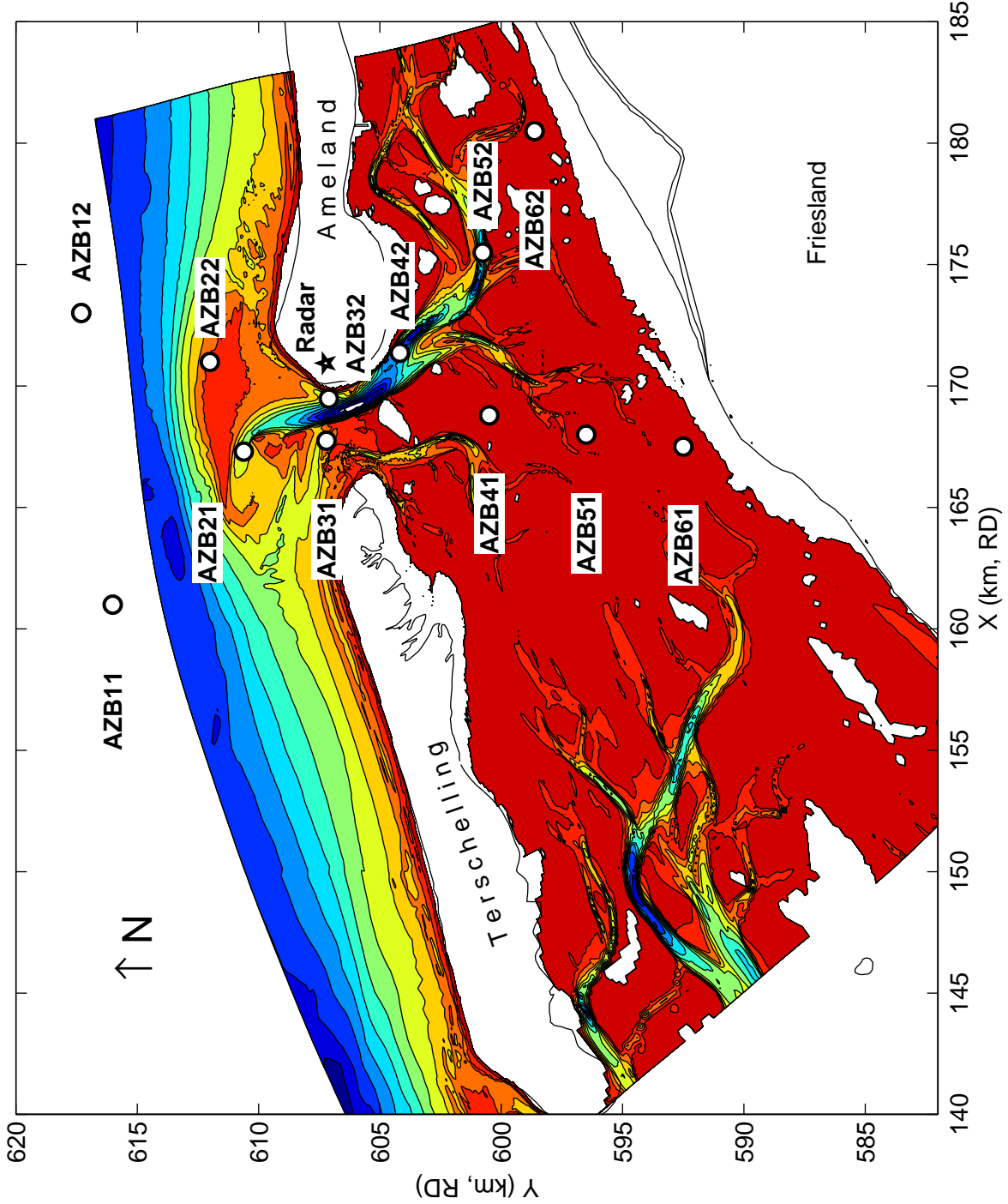
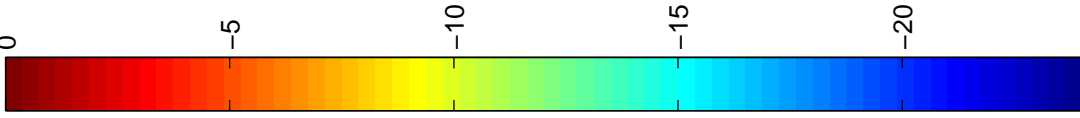
SBW Waddenzee

DELTAES

1202119.006

Fig. 2

Bed level (m NAP)



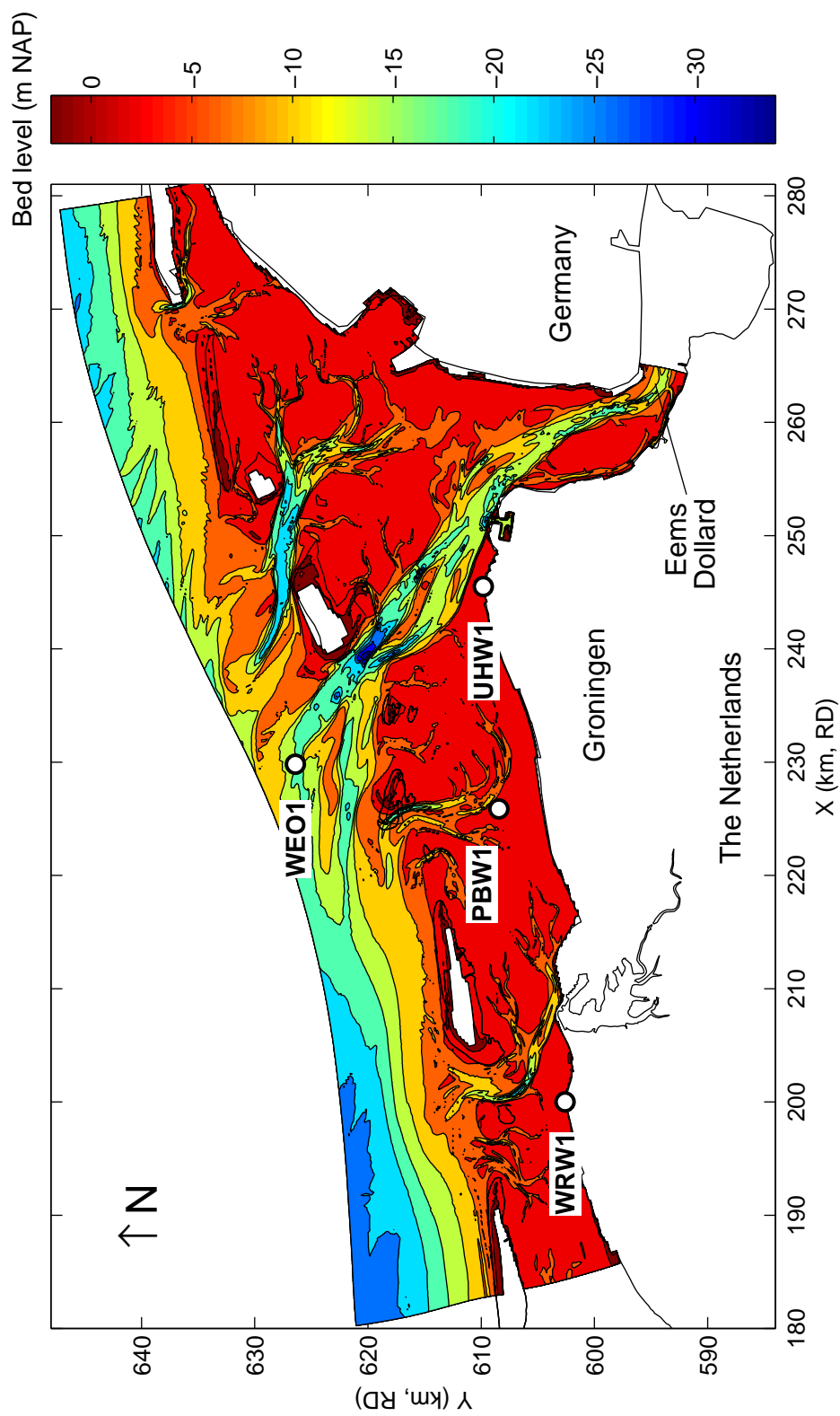
Bathymetry of the Amelander Zeegat region in the Dutch Wadden Sea, including the location of the wave buoys (circles) and the radar deployment on the lighthouse (star) in the configuration of 2007–present

SBW Waddenzee

DELTAES

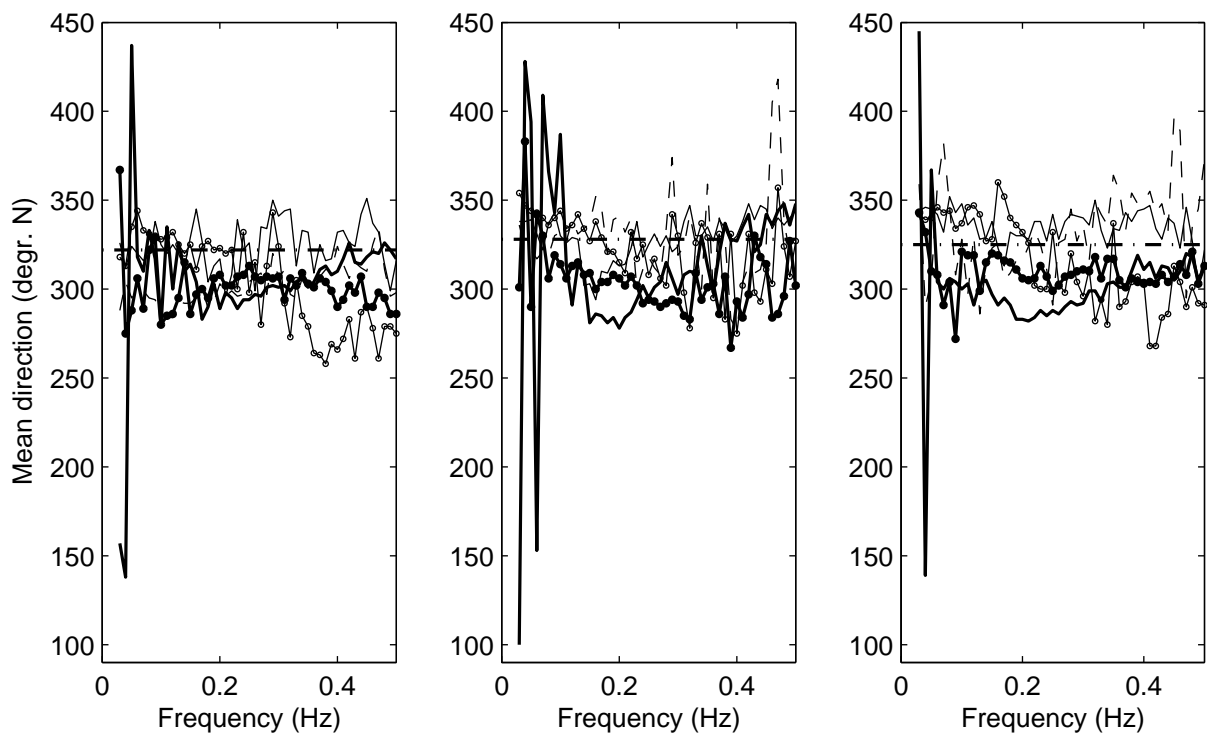
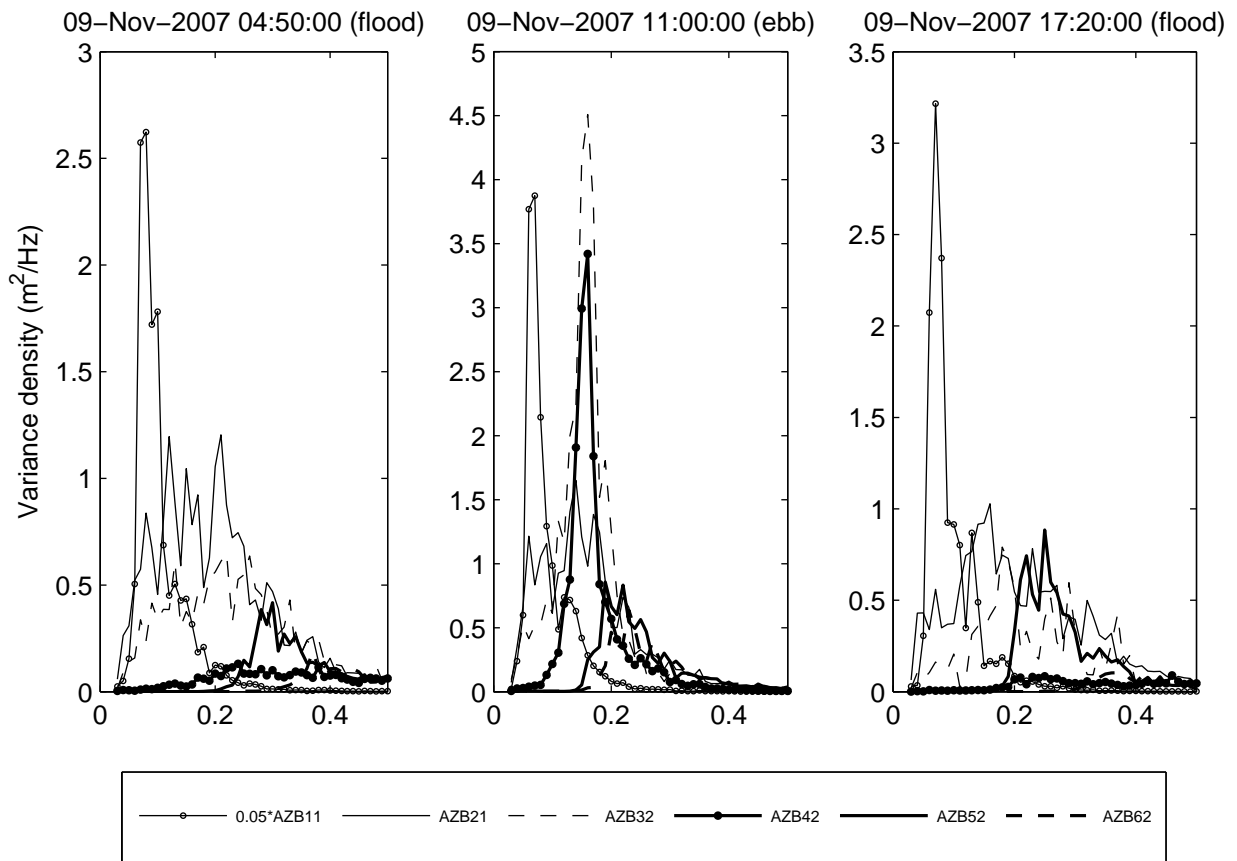
1202119.006

Fig. 3



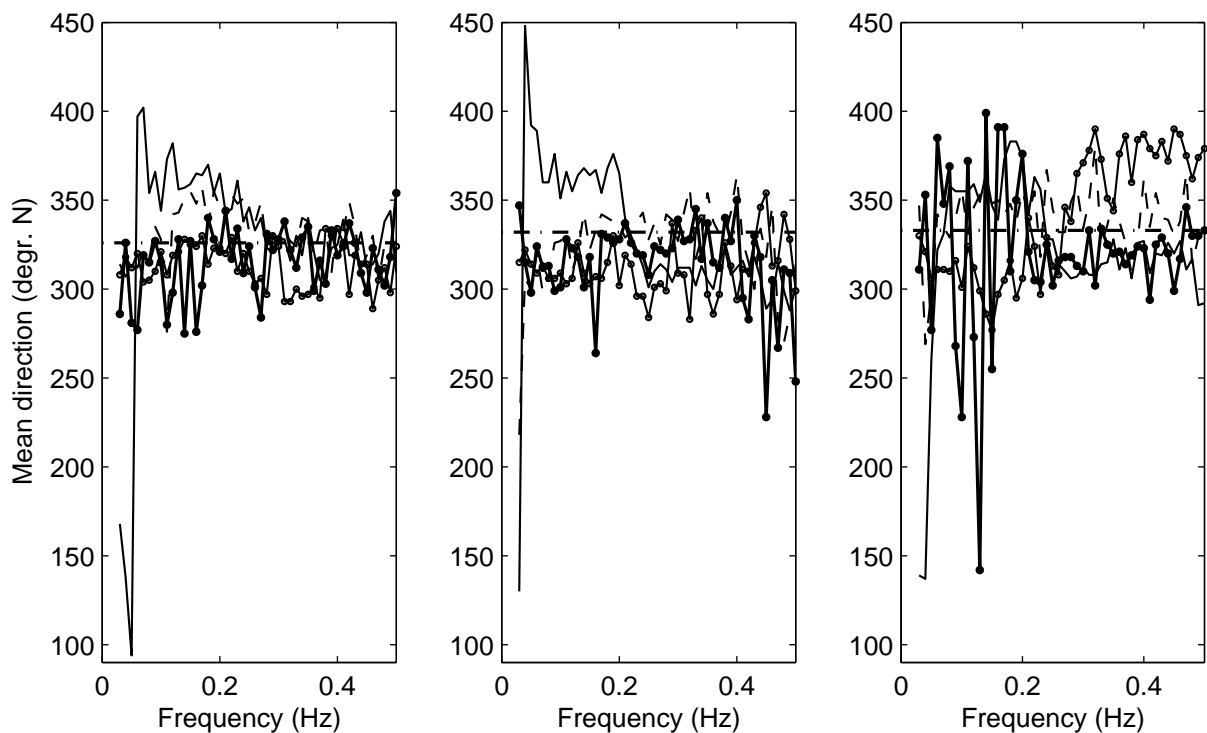
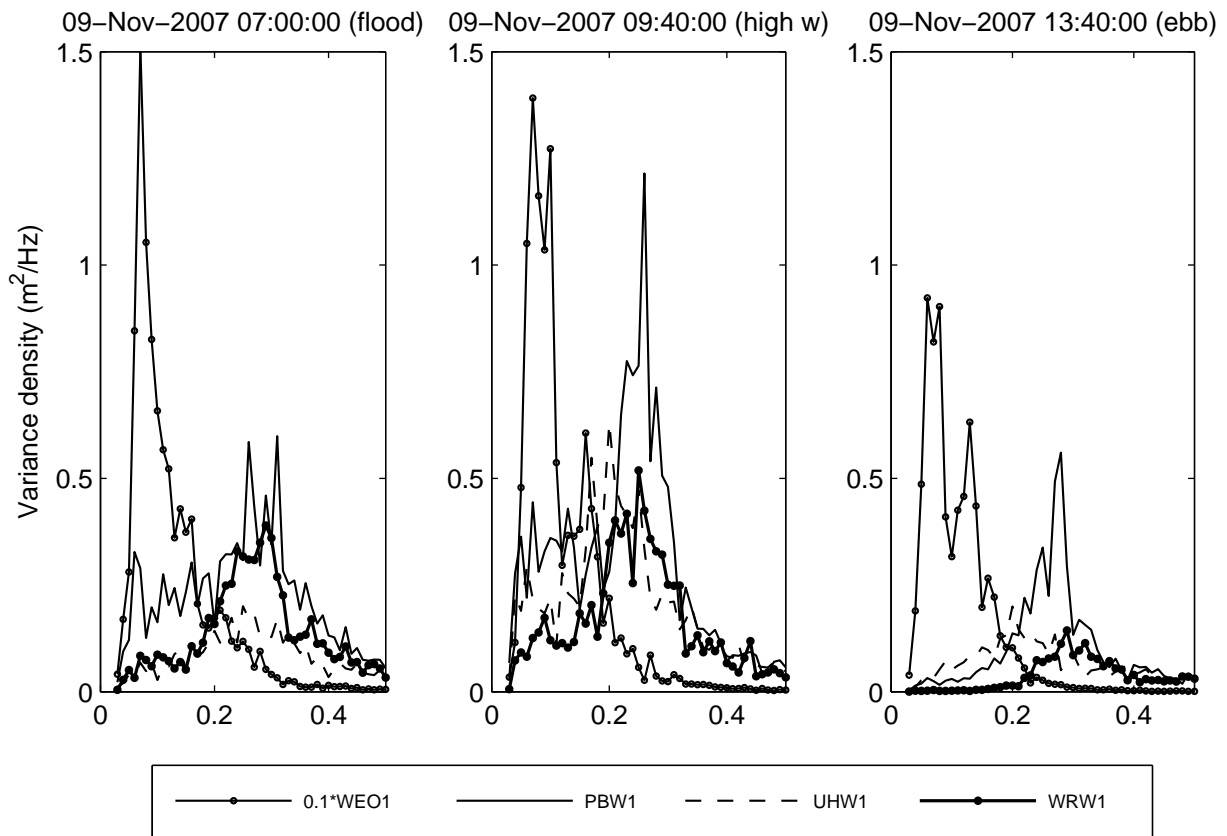
Bathymetry of the Dutch Eastern Waddenzee, including the location of the wave buoys (circles)

SBW Waddenzee



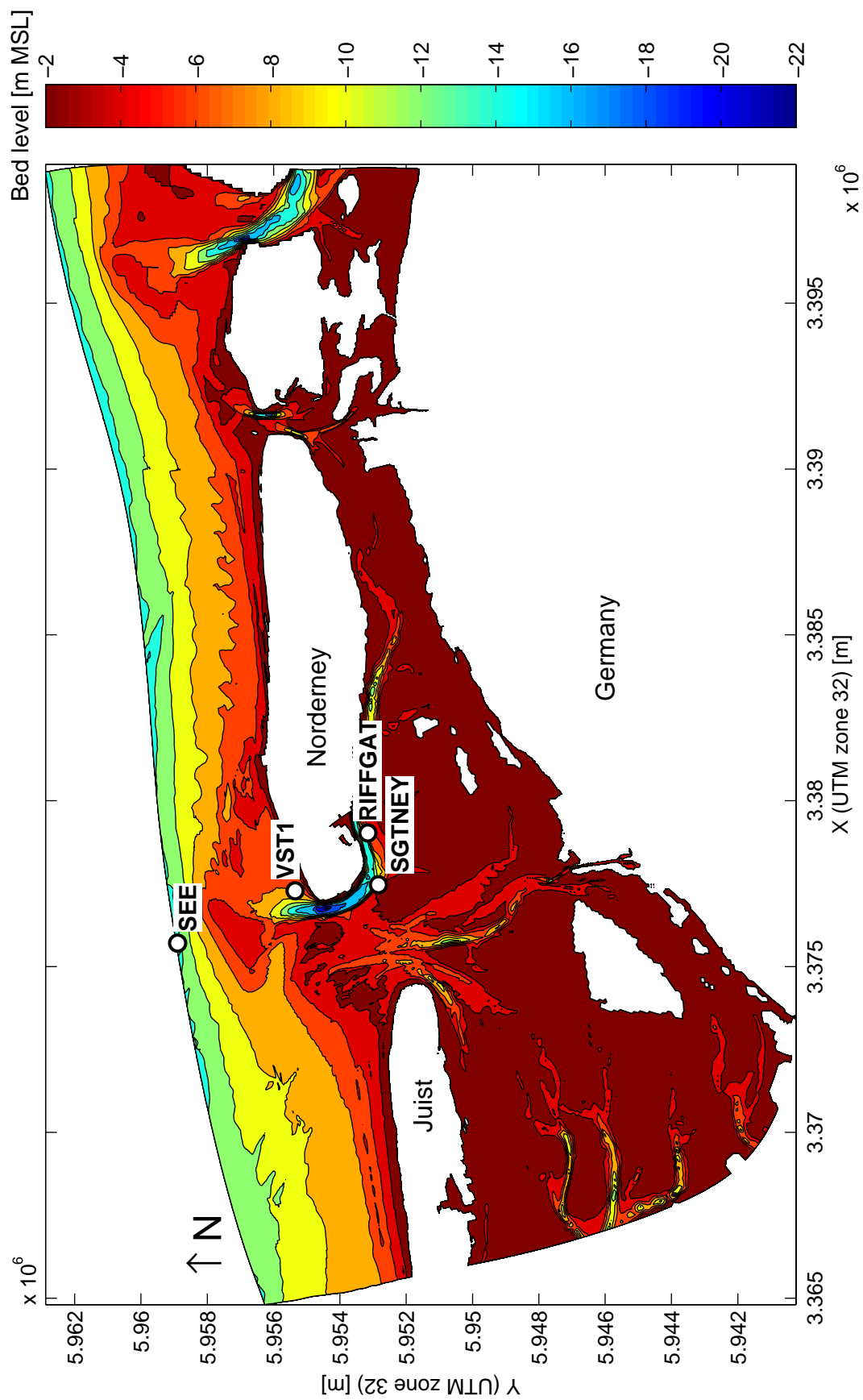
Observed spectra along the NW-SE array in the Amelander Zeegat at three stages during a tidal cycle at the peak of the storm of 8-9 November 2007. Dash-dot line in bottom panels indicates wind direction.

SBW Waddenzee



Observed spectra in the Eastern Dutch Wadden Sea at three stages during one half tidal cycle during the peak of the storm of 8–9 November 2007. Dash-dot line in bottom panels indicates wind direction.

SBW Waddenzee



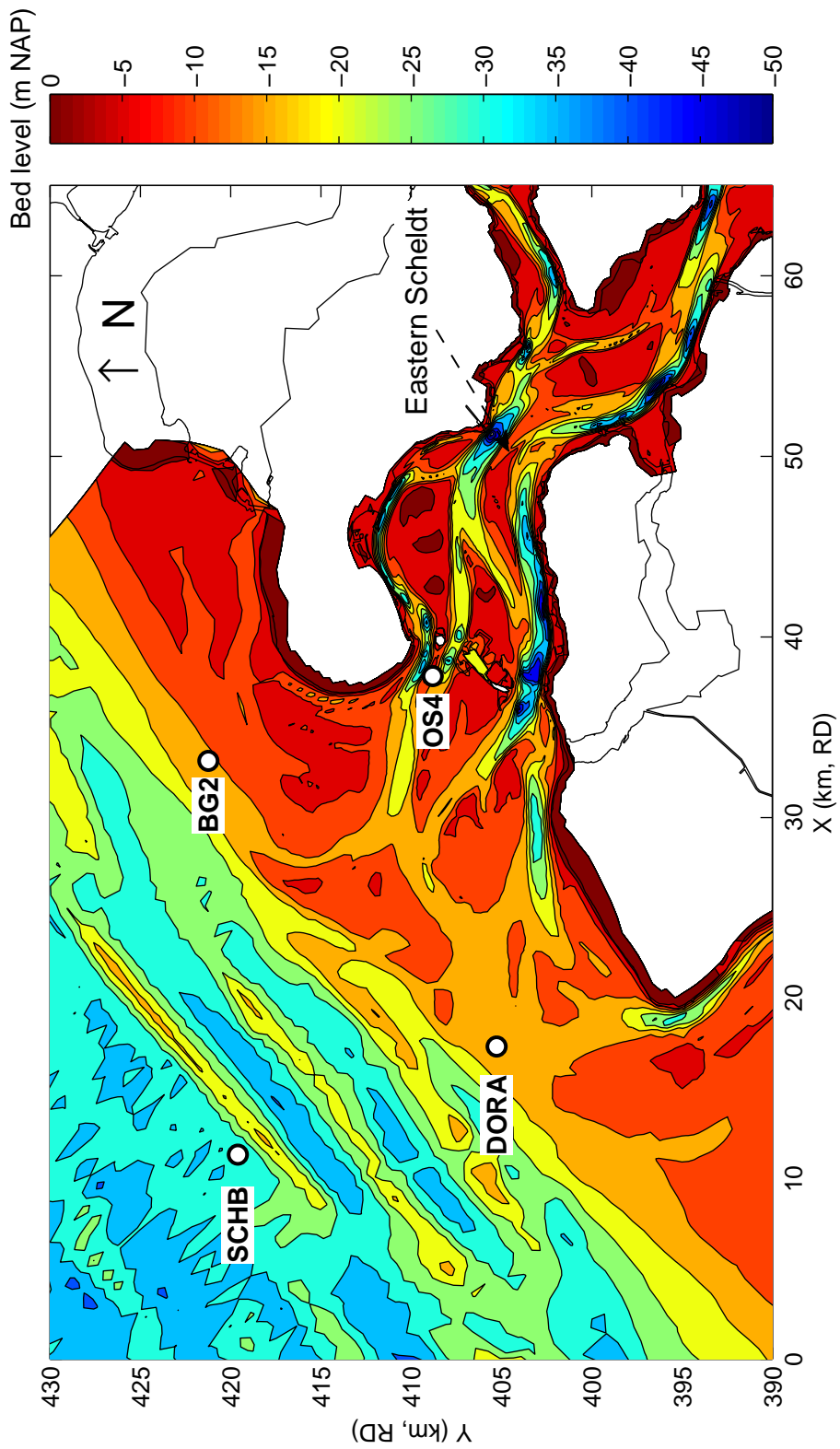
Bathymetry relative to MSL of the Norderney Seegat, including the location of the wave buoys (circles)

SBW Waddenzee

DELTA RES

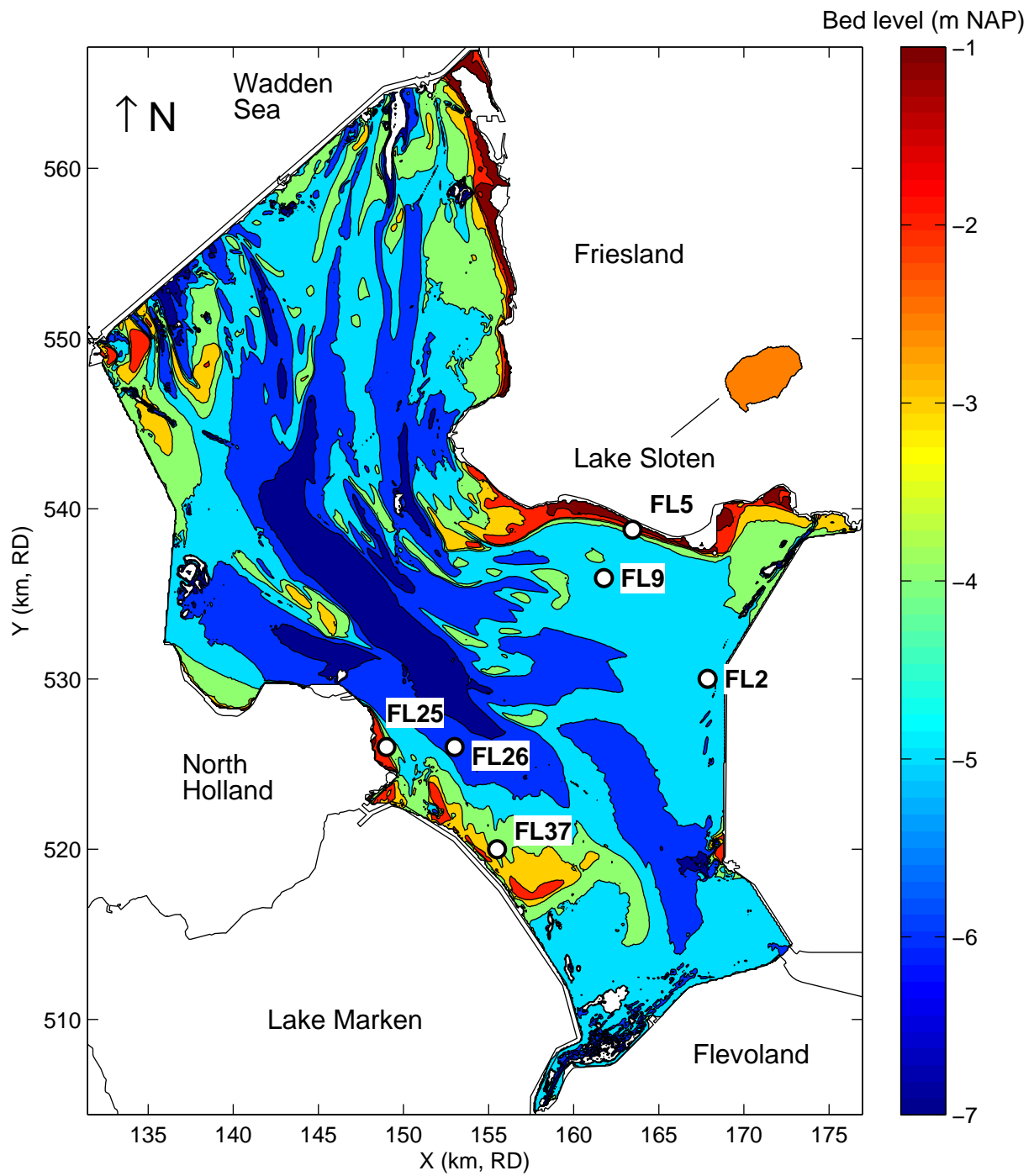
1202119.006

Fig. 7



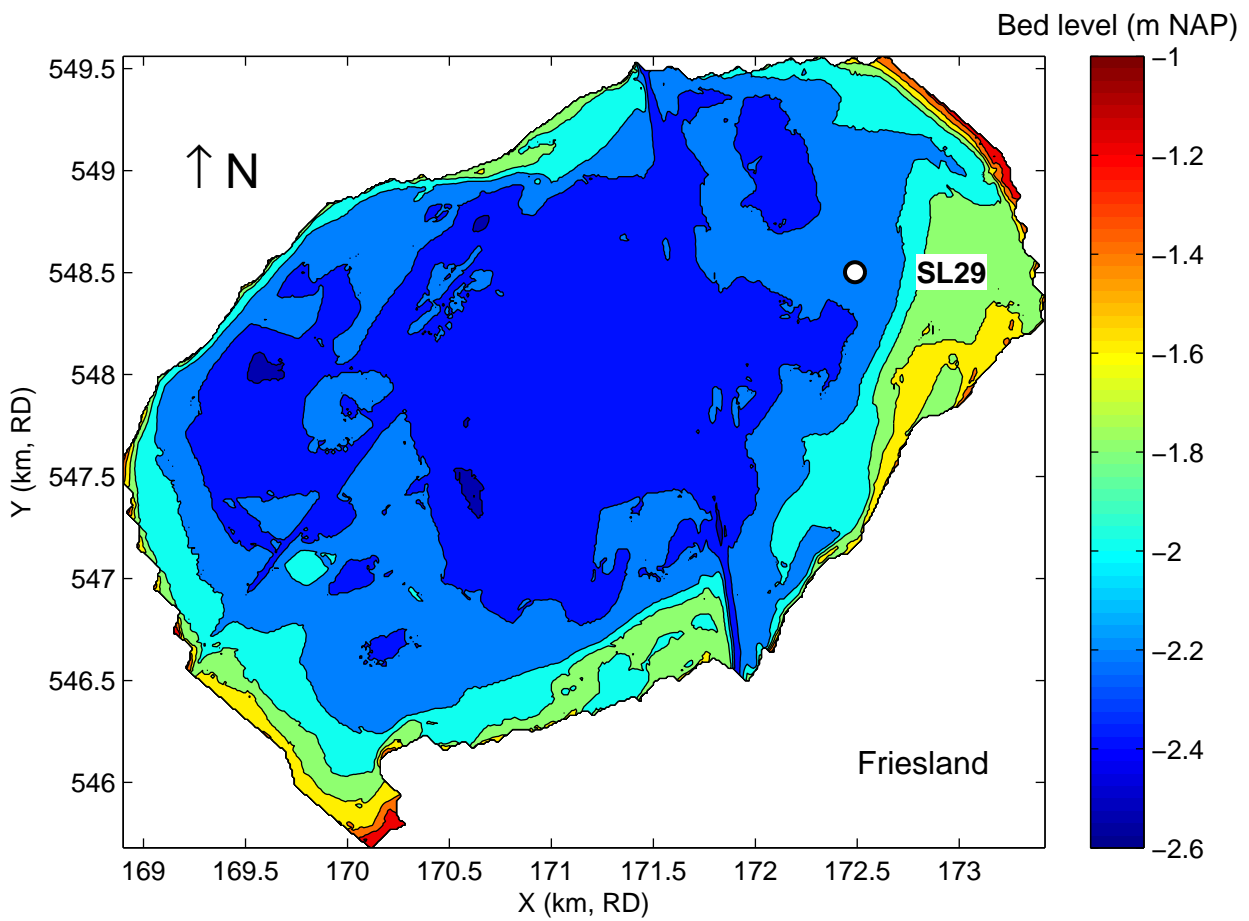
Bathymetry of the mouth of the Eastern Scheldt, including the location of the wave buoys (circles)

SBW Waddenzee



Bathymetry of Lake IJssel,
including the measurement locations (circles)

SBW Waddenzee



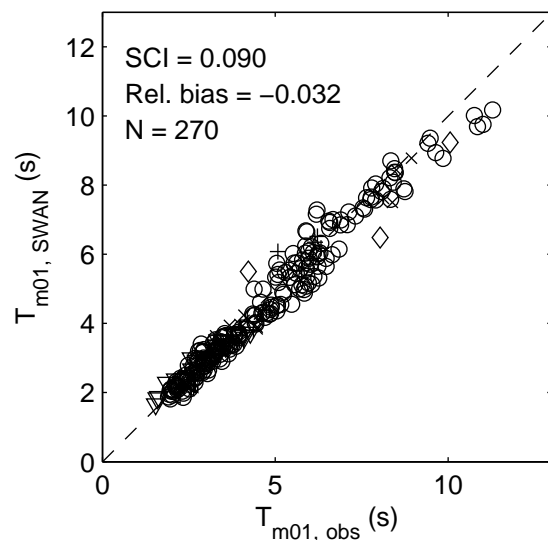
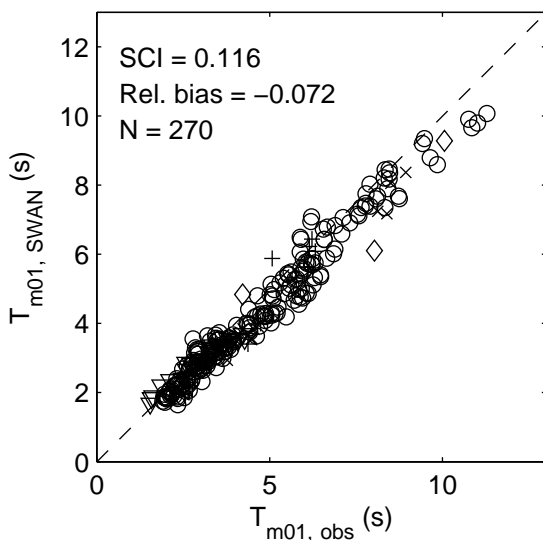
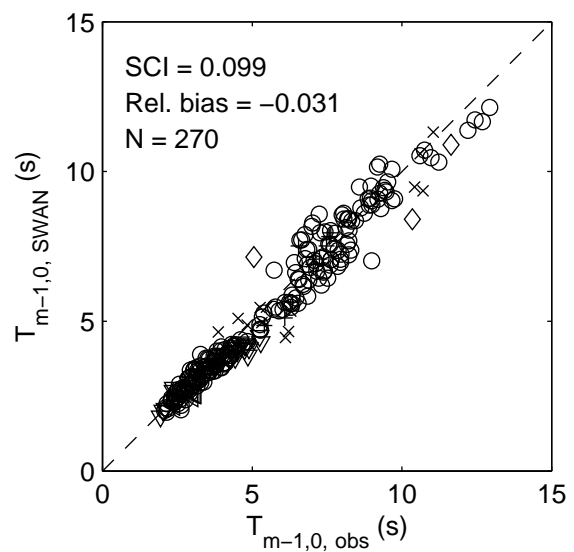
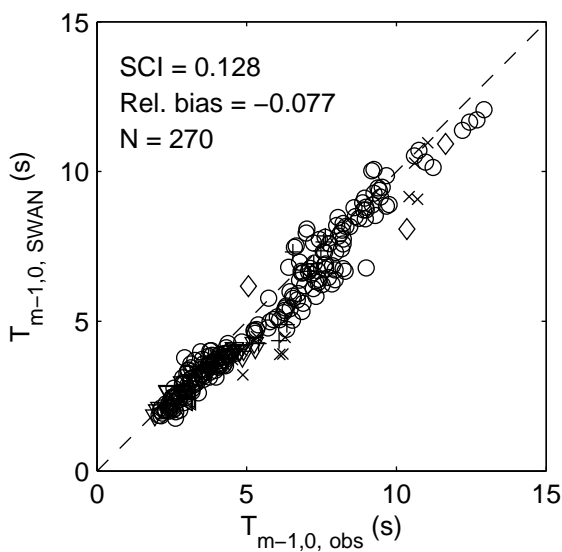
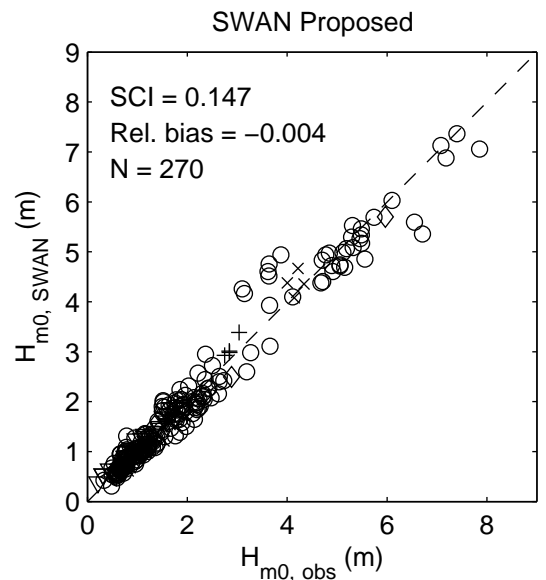
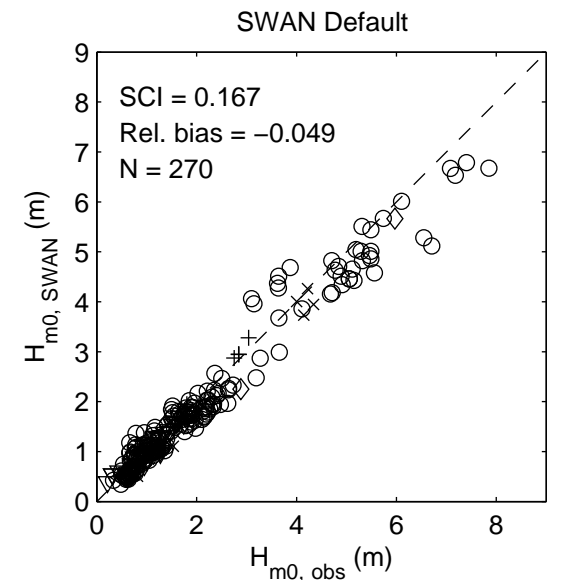
Bathymetry of Lake Sloten,
including the measurement location (circle)

SBW Waddenzee

DELTARES

1202119.006

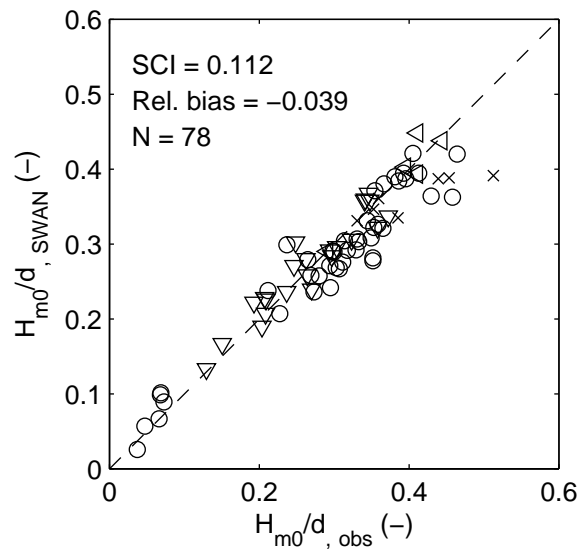
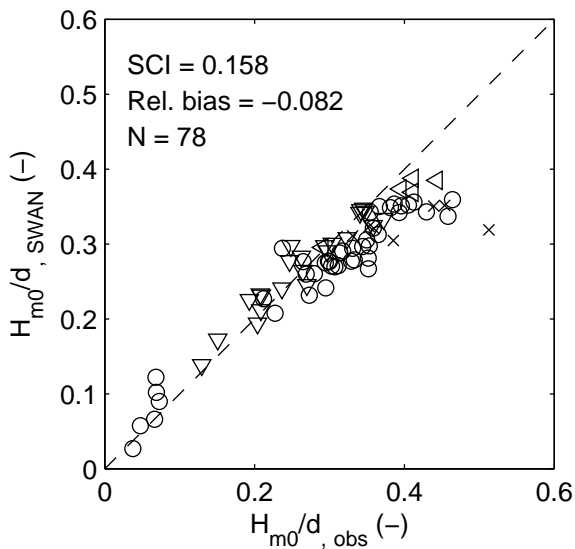
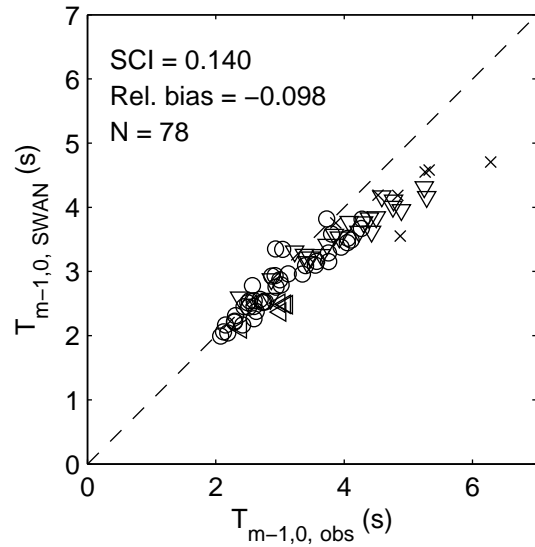
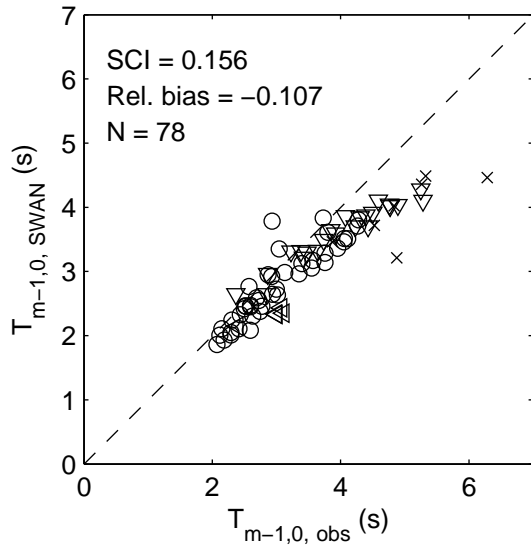
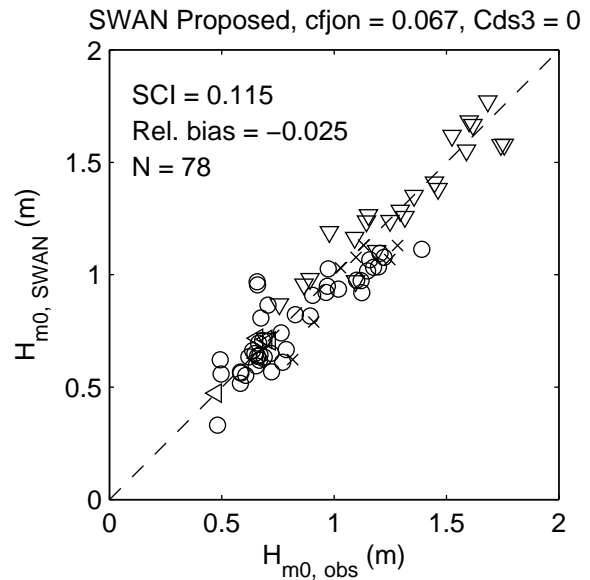
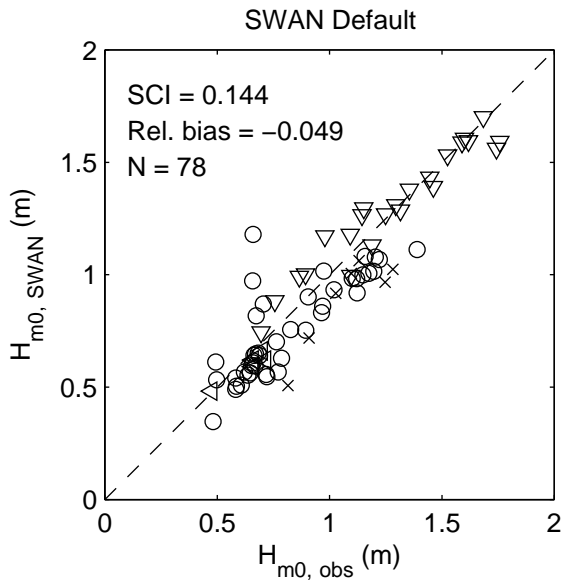
Fig. 10



- Amelanders Zeegat + Eastern Scheldt × Eastern Wadden Sea
- ▽ Lake IJssel ◁ Lake Sloten ◇ Norderney

Scatterplots of model results of wave height and wave period versus observations for all cases and location for the default model (left) and proposed model (right)

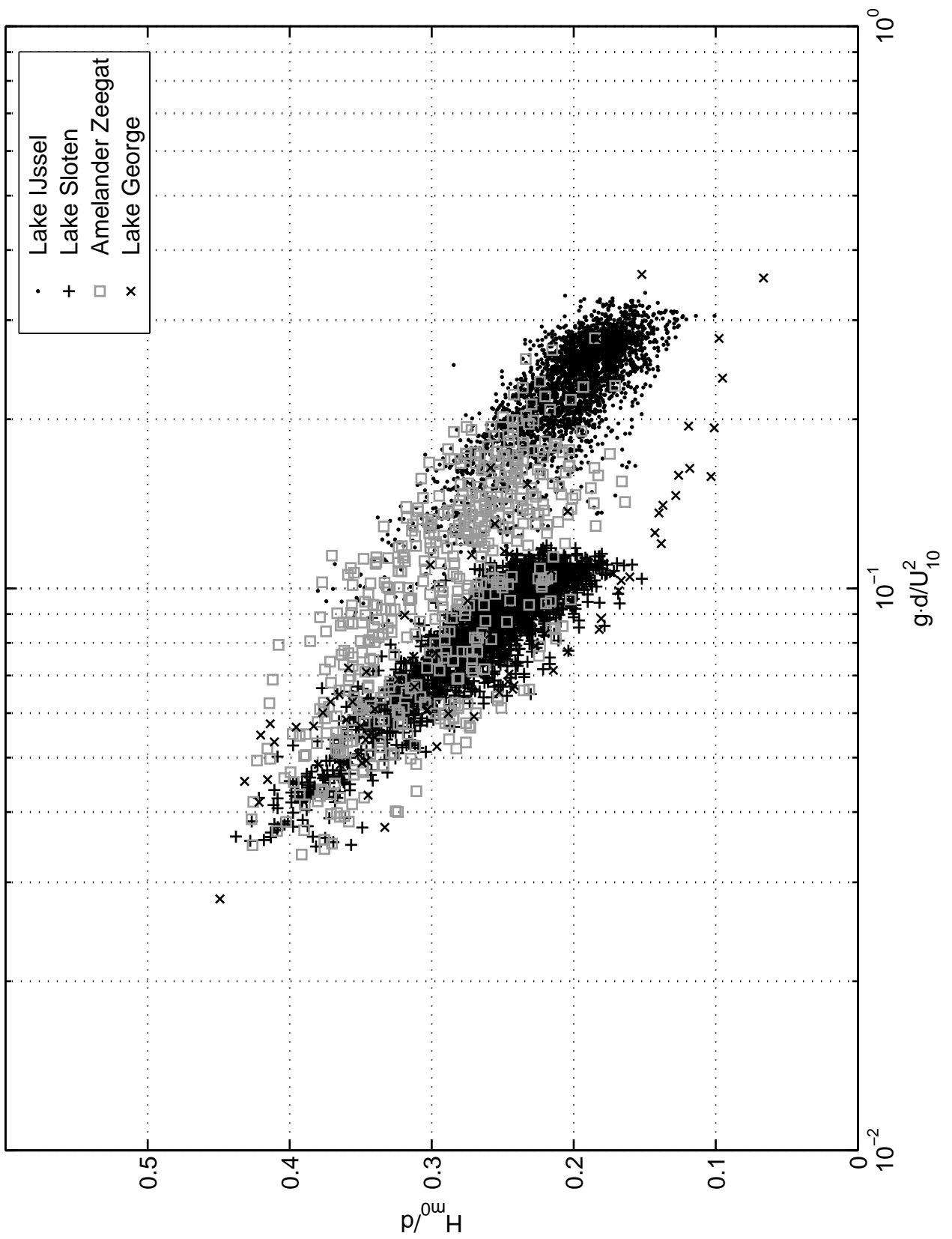
SBW Waddenzee



○ Amelanders Zeegat × Eastern Wadden Sea ▽ Lake IJssel ◁ Lake Sloten

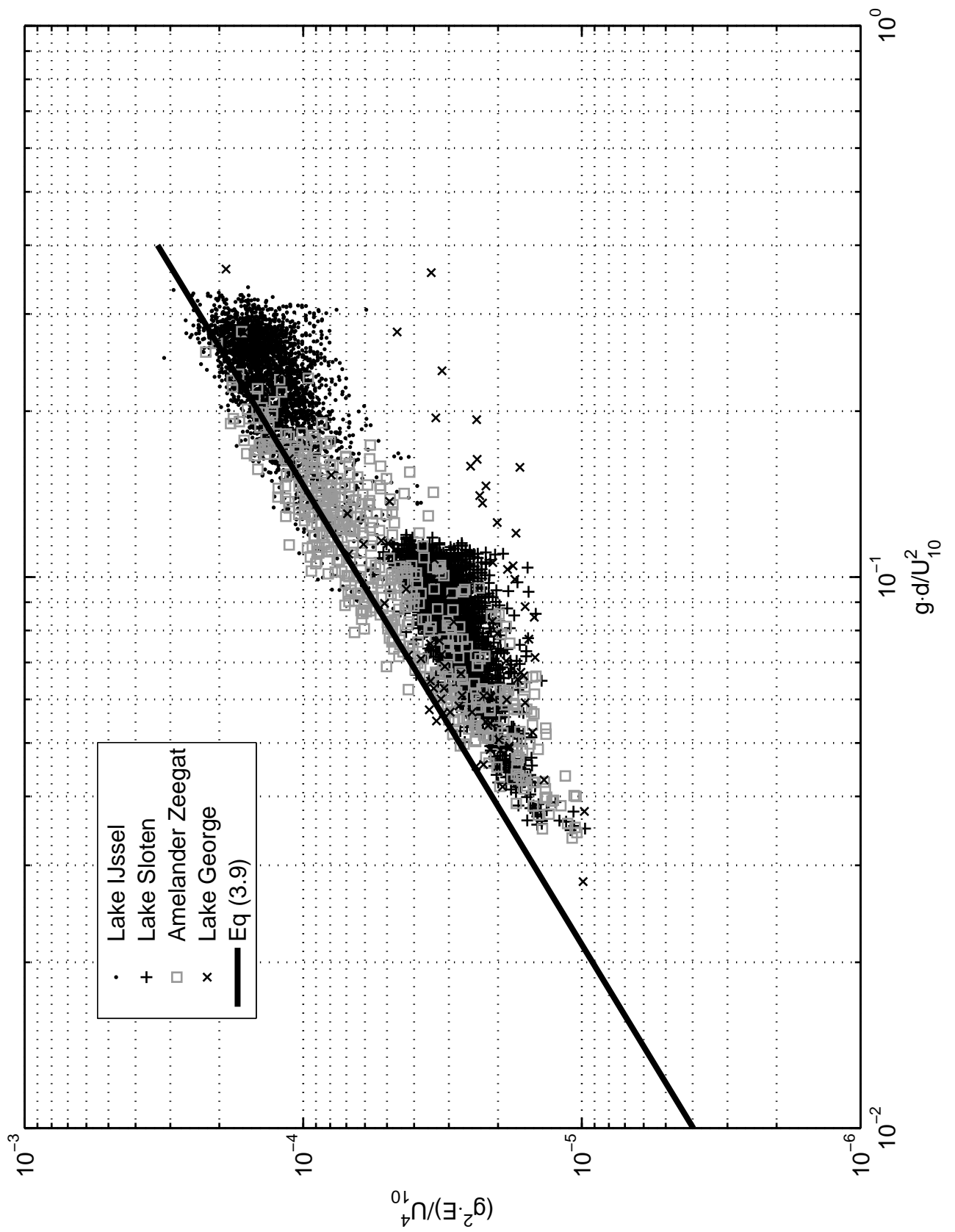
Scatterplots of model results of wave height and wave period versus observations for the cases of finite depth wave growth for the default model (left), and the proposed model with $cfjon=0.067 \text{ m}^2/\text{s}^3$ (right)

SBW Waddenzee



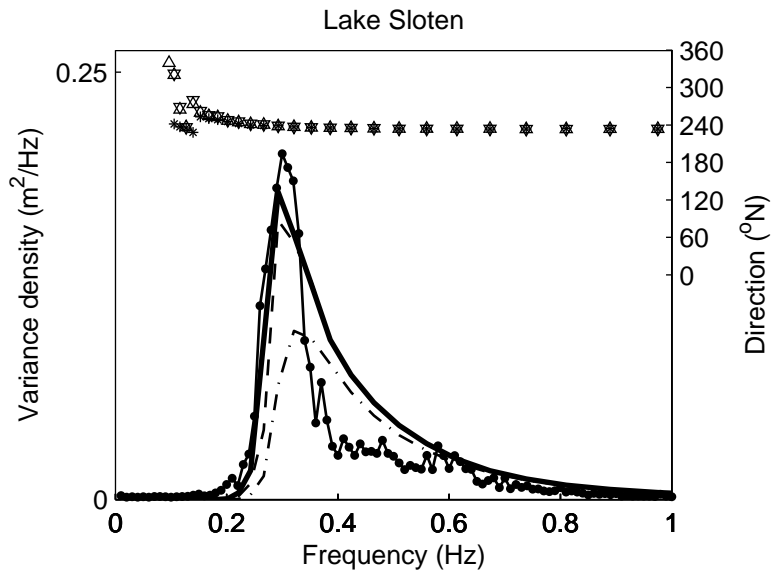
Nondimensional energy versus nondimensional depth (U_{10} -scaled)
for the finite-depth wave growth dataset

SBW Waddenzee



Nondimensional energy versus nondimensional depth (U_{10} – scaled) for the finite–depth wave growth dataset and Eq (3.9) by Young and Babanin (2006)

SBW Waddenzee



Default - · - · var., * dir. measured: ● — ● var.
 Proposed, - - - var., ▽ dir.
 cfjon = 0.067 m²/s³, Cds3 = 0
 Proposed ——— var., △ dir.

Variance density spectrum of observations and SWAN default and proposed results for the field case of Lake Sloten

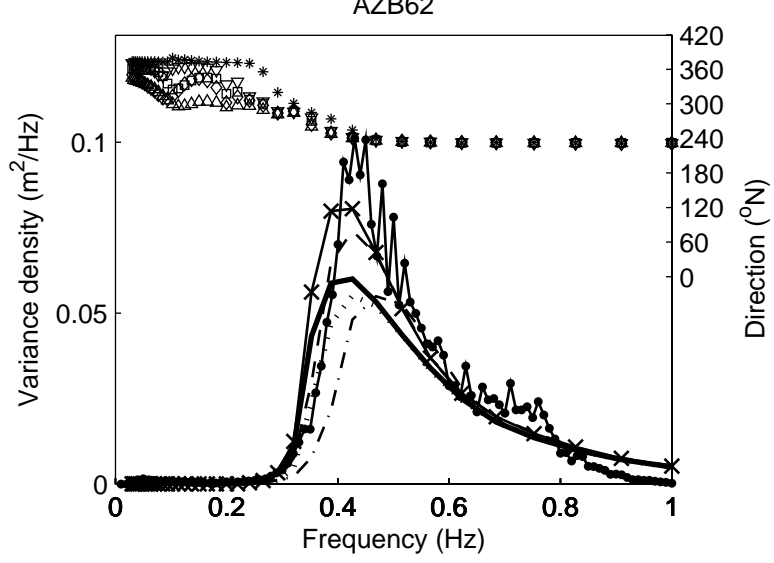
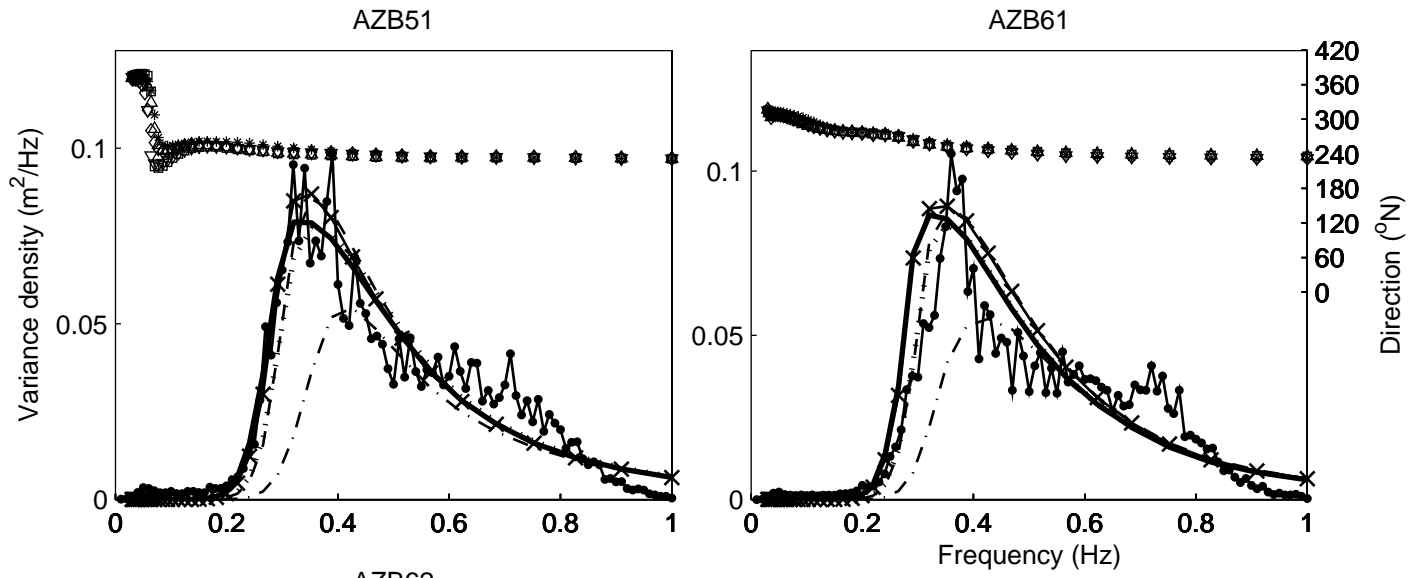
18/01/2007, 12:00

SBW Waddenzee

DELTAES

1202119.006

Fig. 15



Default	- - - var., * dir.	measured:	●—● var.
Proposed, cfjon = 0.067 m²/s³, Cds3 = 0	- - - var., ∇ dir.	Proposed, cfjon = 0.067 m²/s³ var., □ dir.
Proposed	— var., △ dir.	Proposed, Cds3 = 0	×—× var., ◇ dir.

Variance density spectra of observations and SWAN default and proposed results for the field case of Amelanders Zeegat

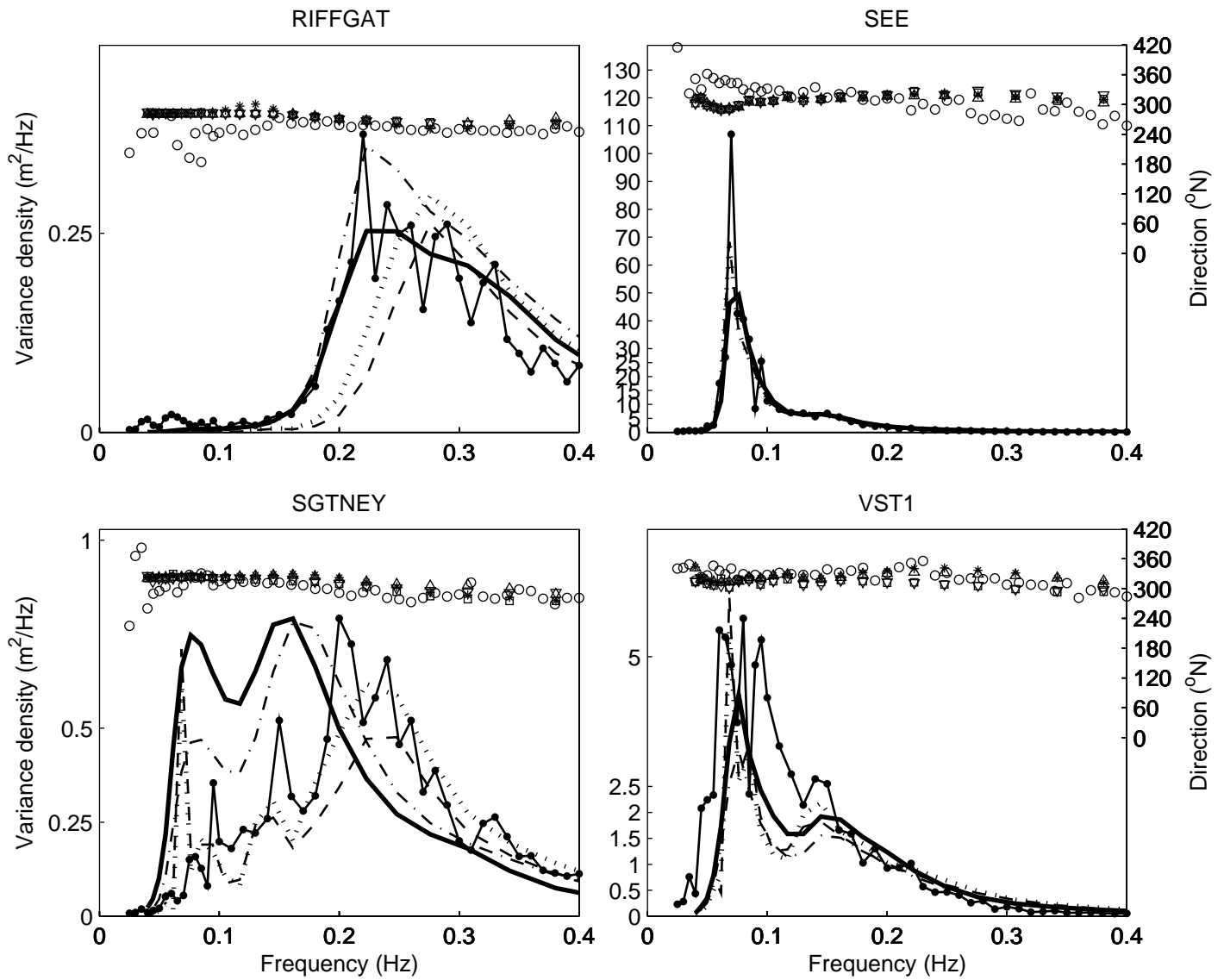
18/01/2007, 12:20

SBW Waddenzee

DELTAES

1202119.006

Fig. 16



Default, no currents 15 iterations - - var., □ dir. measured: ● — var., ○ dir.
 Default, no currents ····· var., ▽ dir.
 Default, with currents - · - · var., * dir.
 Proposed — var., △ dir.

Variance density spectra of observations and SWAN default and proposed results for the field case of the Norderney Seegat

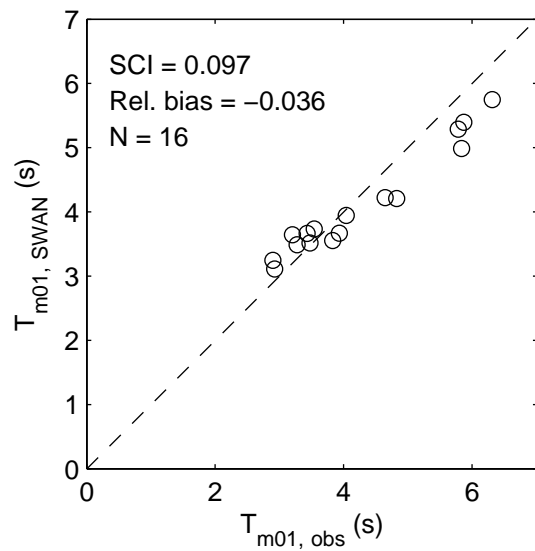
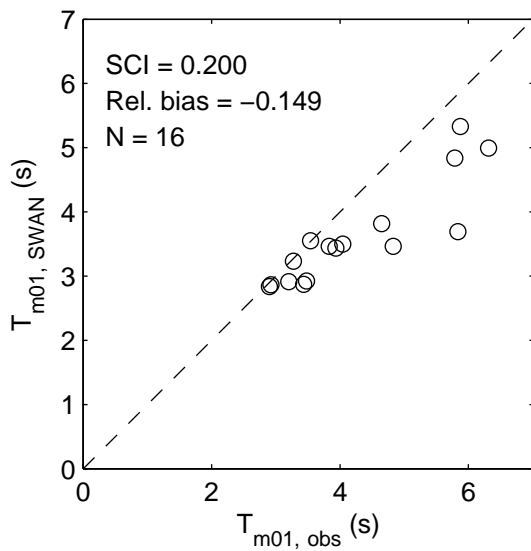
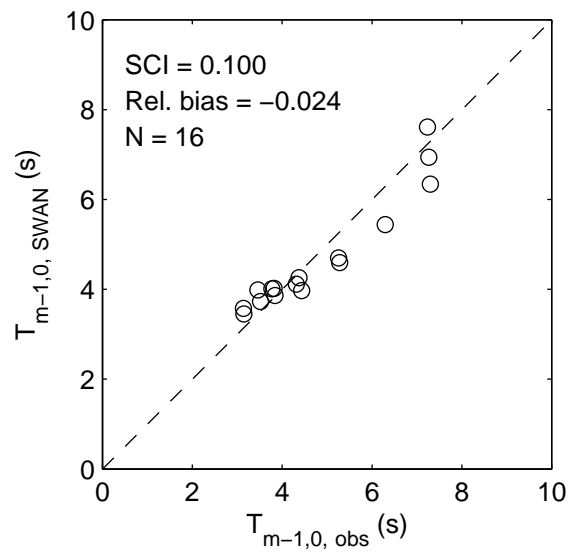
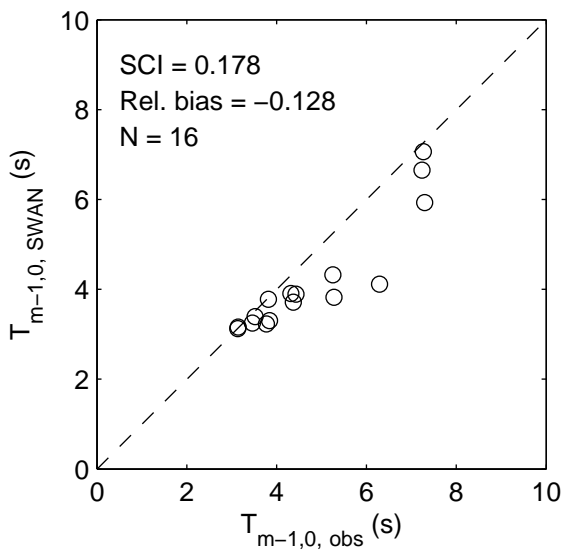
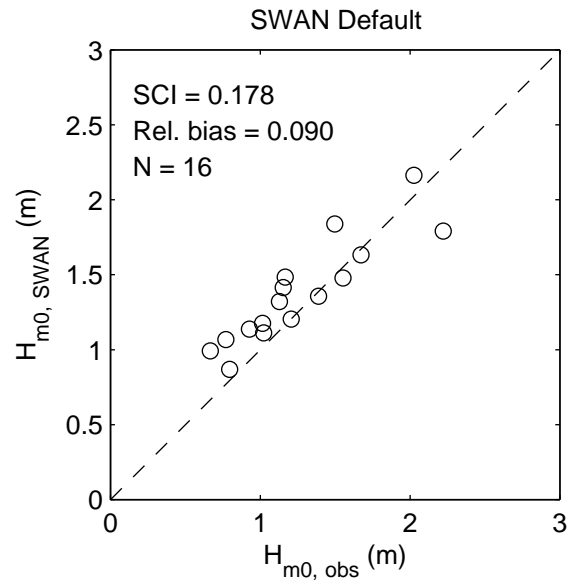
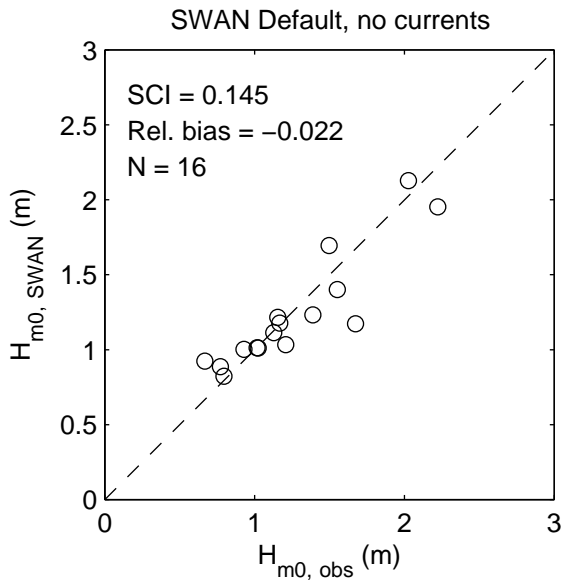
05/02/1999, 03:36

SBW Waddenzee

DELTAES

1202119.006

Fig. 17



○ Amelanders Zeegat

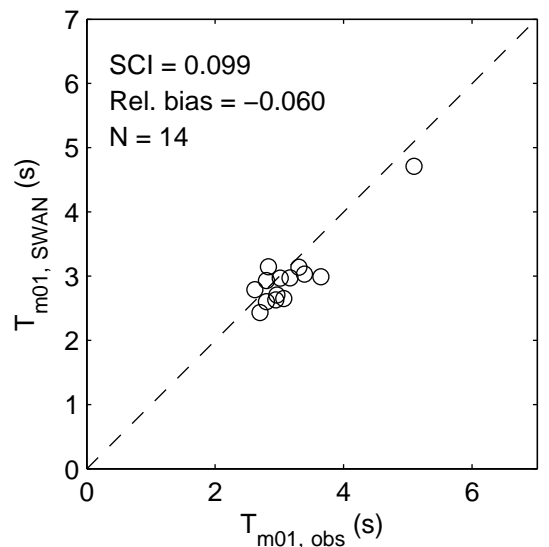
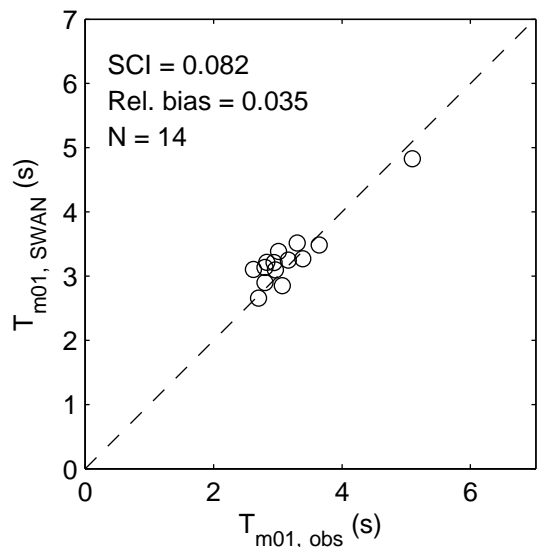
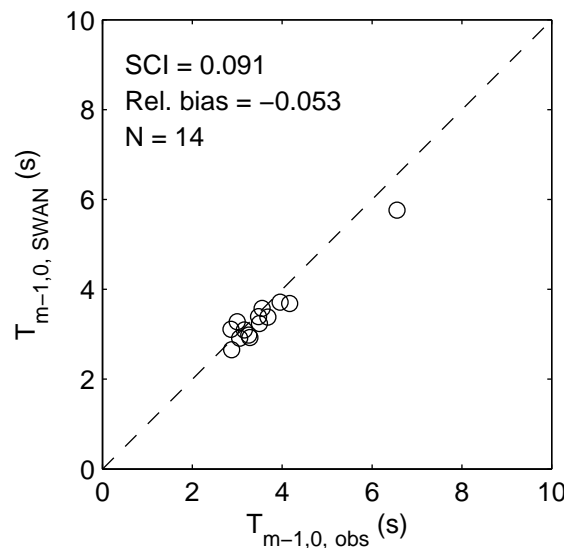
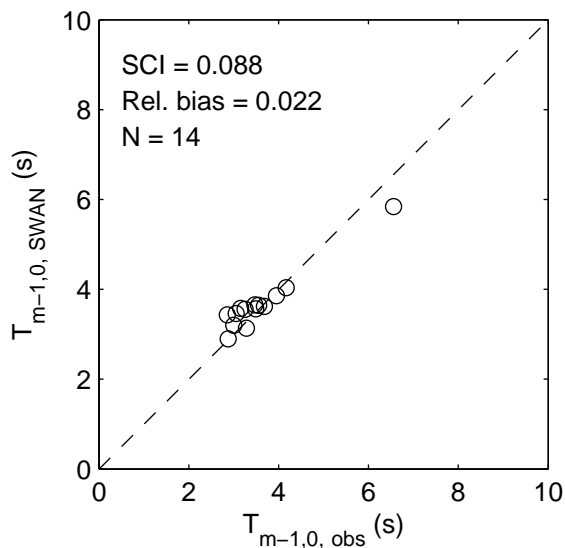
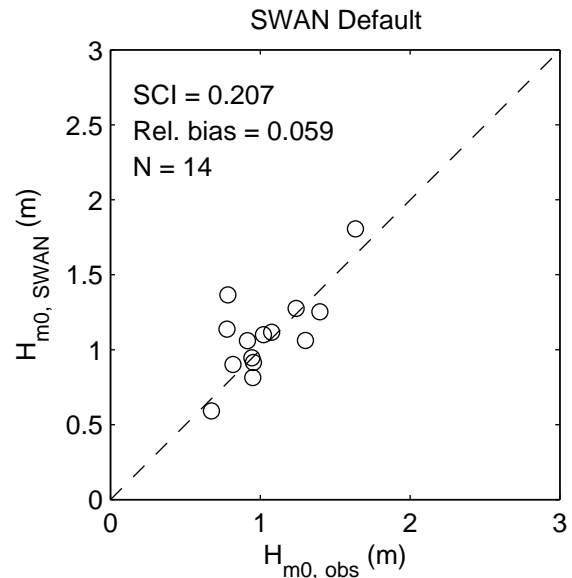
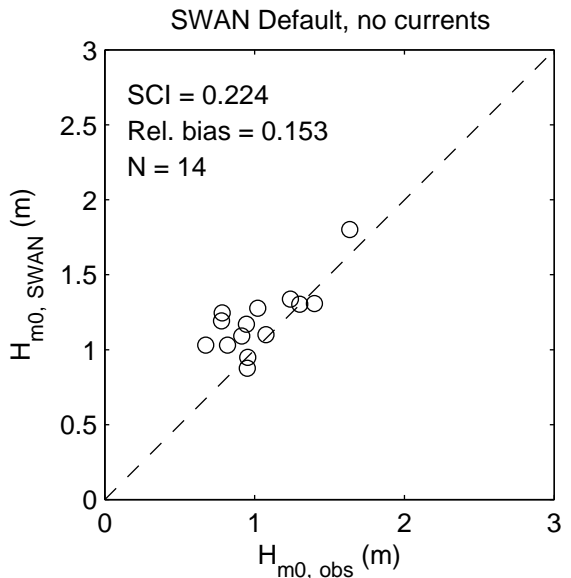
Scatterplots of model results of wave height and wave period versus observations for opposing currents in the Amelanders Zeegat. Left: Default model without currents. Right: Default model (with currents)

SBW Waddenzee

DELTAES

1202119.006

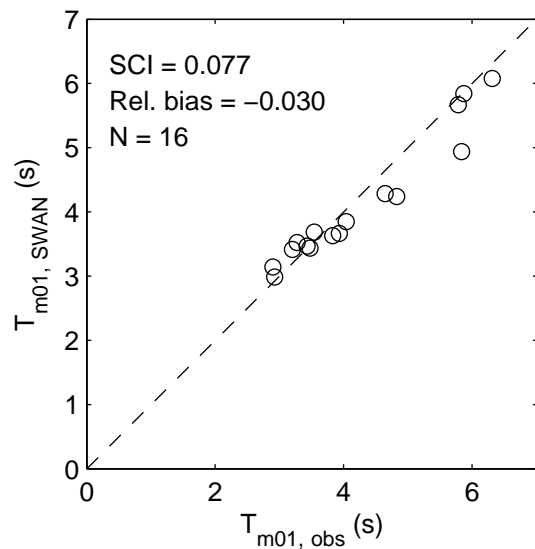
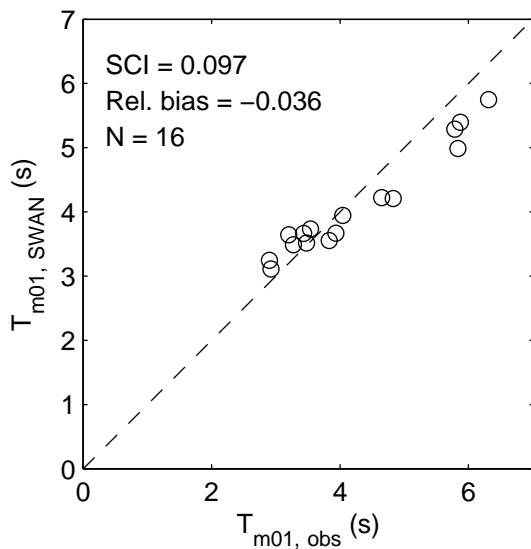
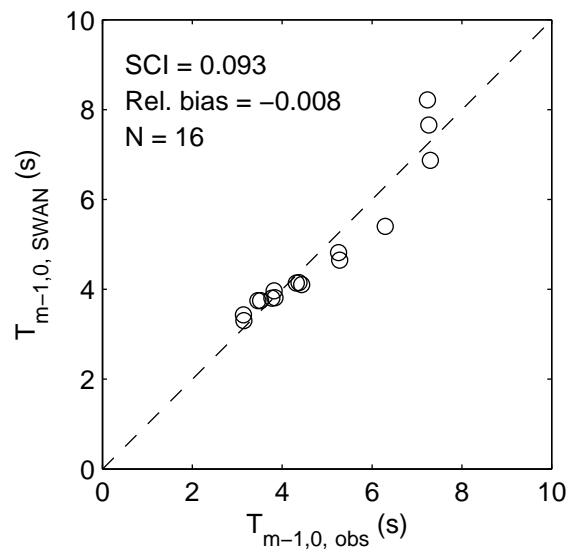
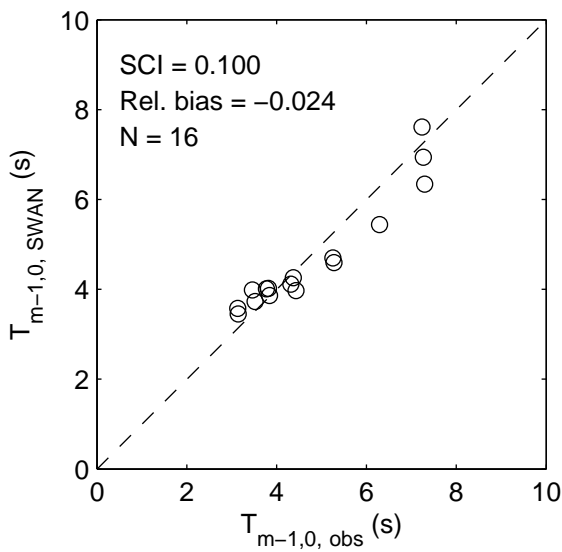
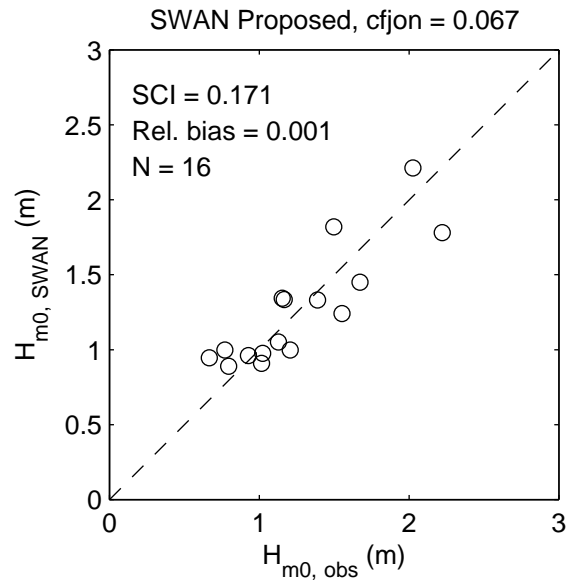
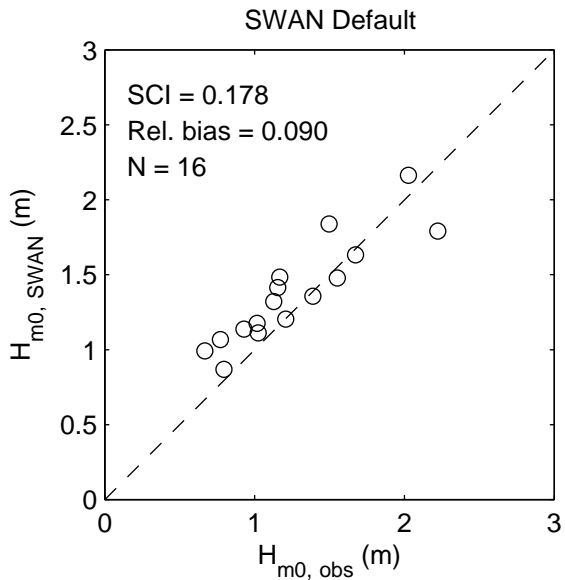
Fig. 18



○ Amelander Zeegat

Scatterplots of model results of wave height and wave period versus observations for following currents in the Amelander Zeegat. Left: Default model without currents. Right: Default model (with currents)

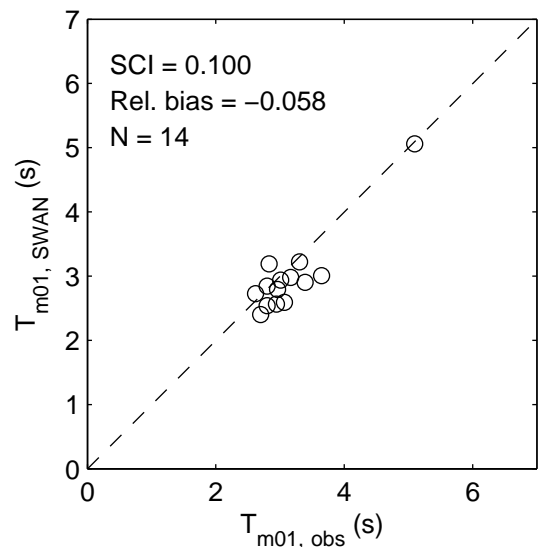
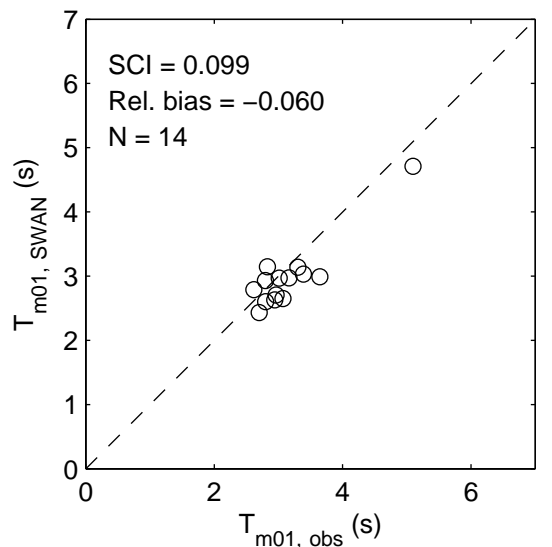
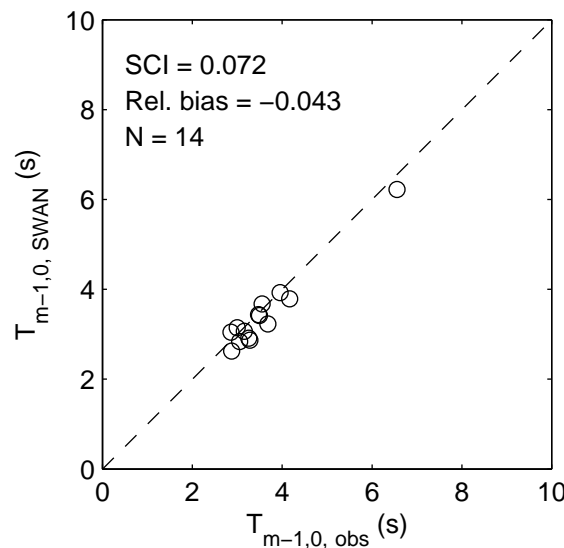
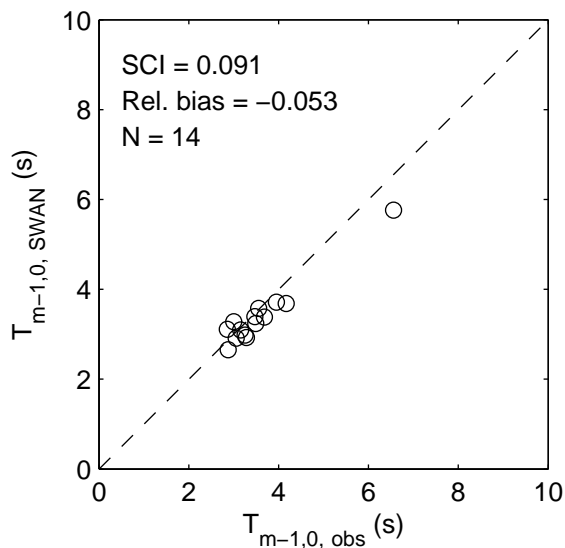
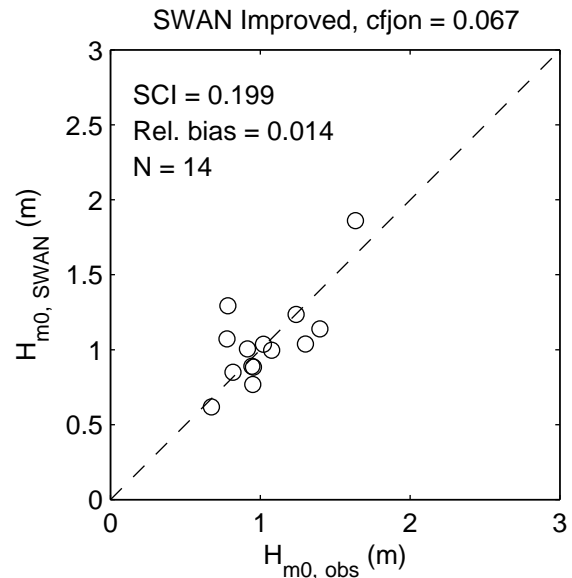
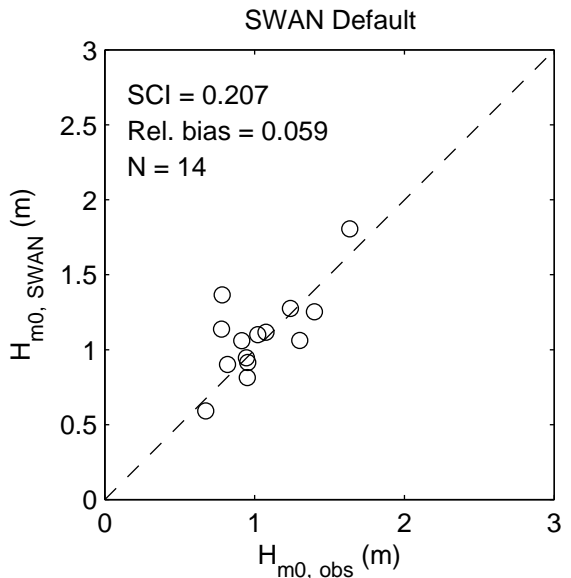
SBW Waddenzee	
1202119.006	Fig. 19



○ Amelanders Zeegat

Scatterplots of model results of wave height and wave period versus observations for opposing currents in the Amelanders Zeegat.
Left: Default model. Right: Proposed model, cfjon=0.067 m²/s³

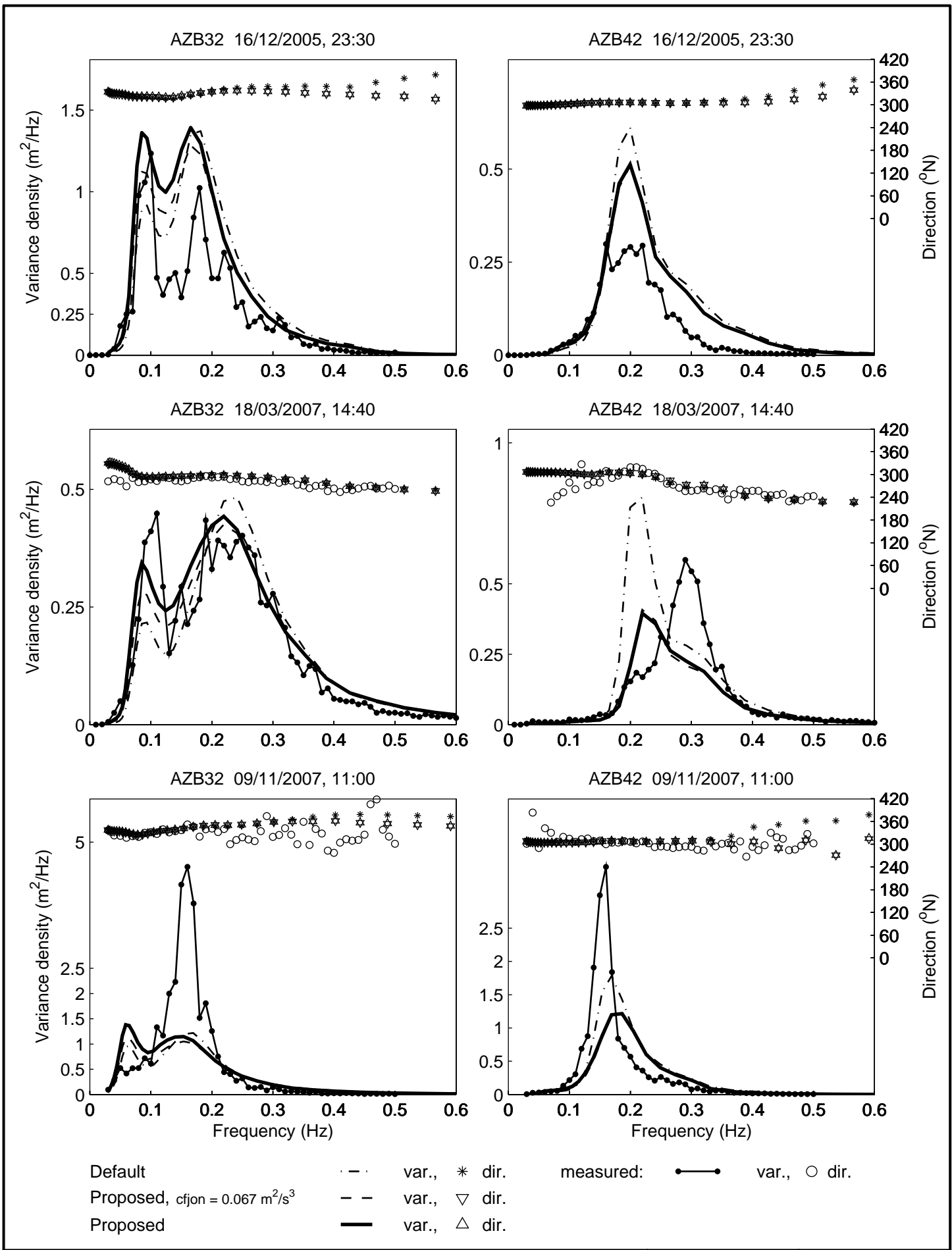
SBW Waddenzee



○ Amelander Zeegat

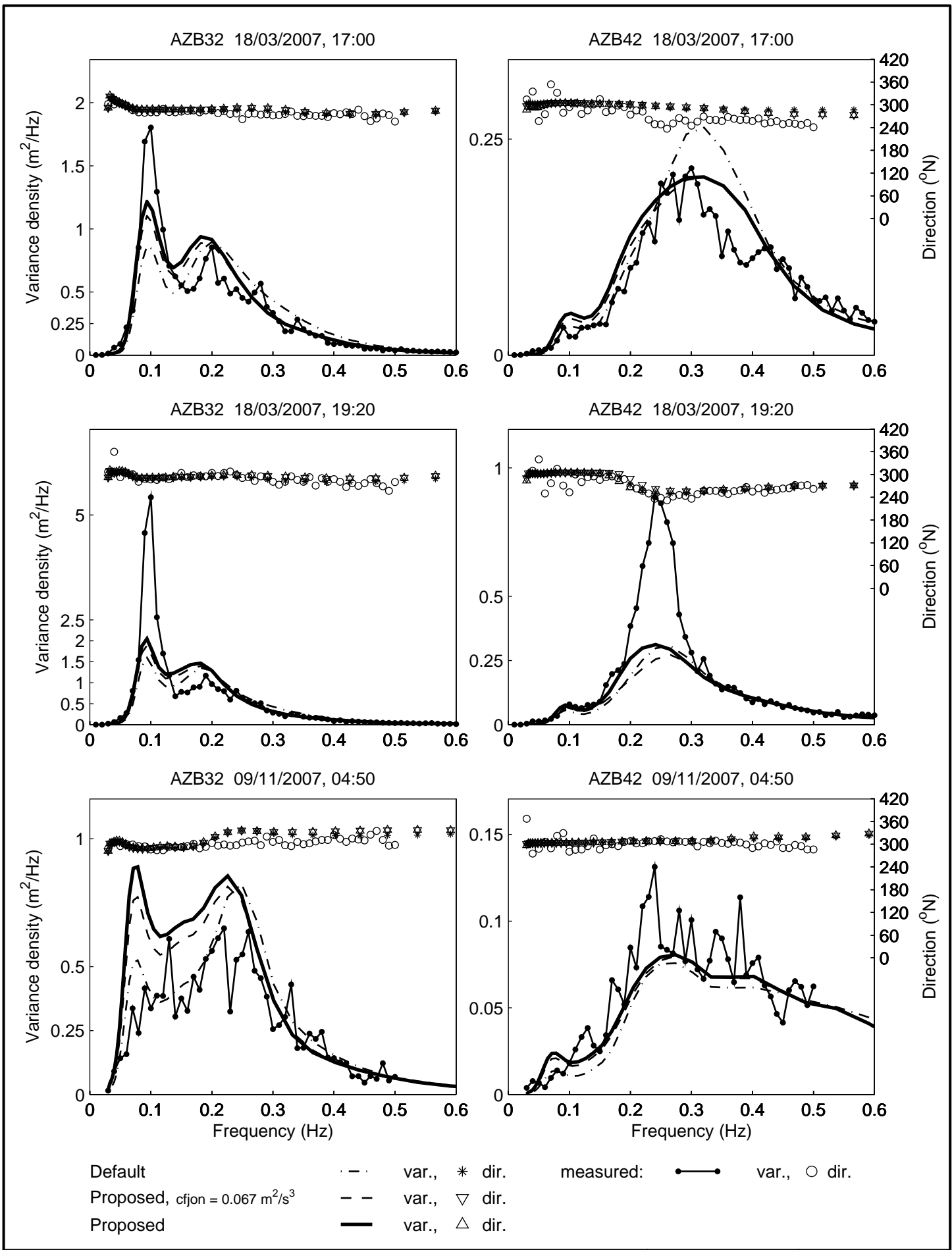
Scatterplots of model results of wave height and wave period versus observations for following currents in the Amelander Zeegat.
Left: Default model. Right: Proposed model, cfjon=0.067 m²/s³

SBW Waddenzee	
1202119.006	Fig. 21



Variance density spectra of observations and model results, for three cases of opposing currents in the Amelander Zeegat

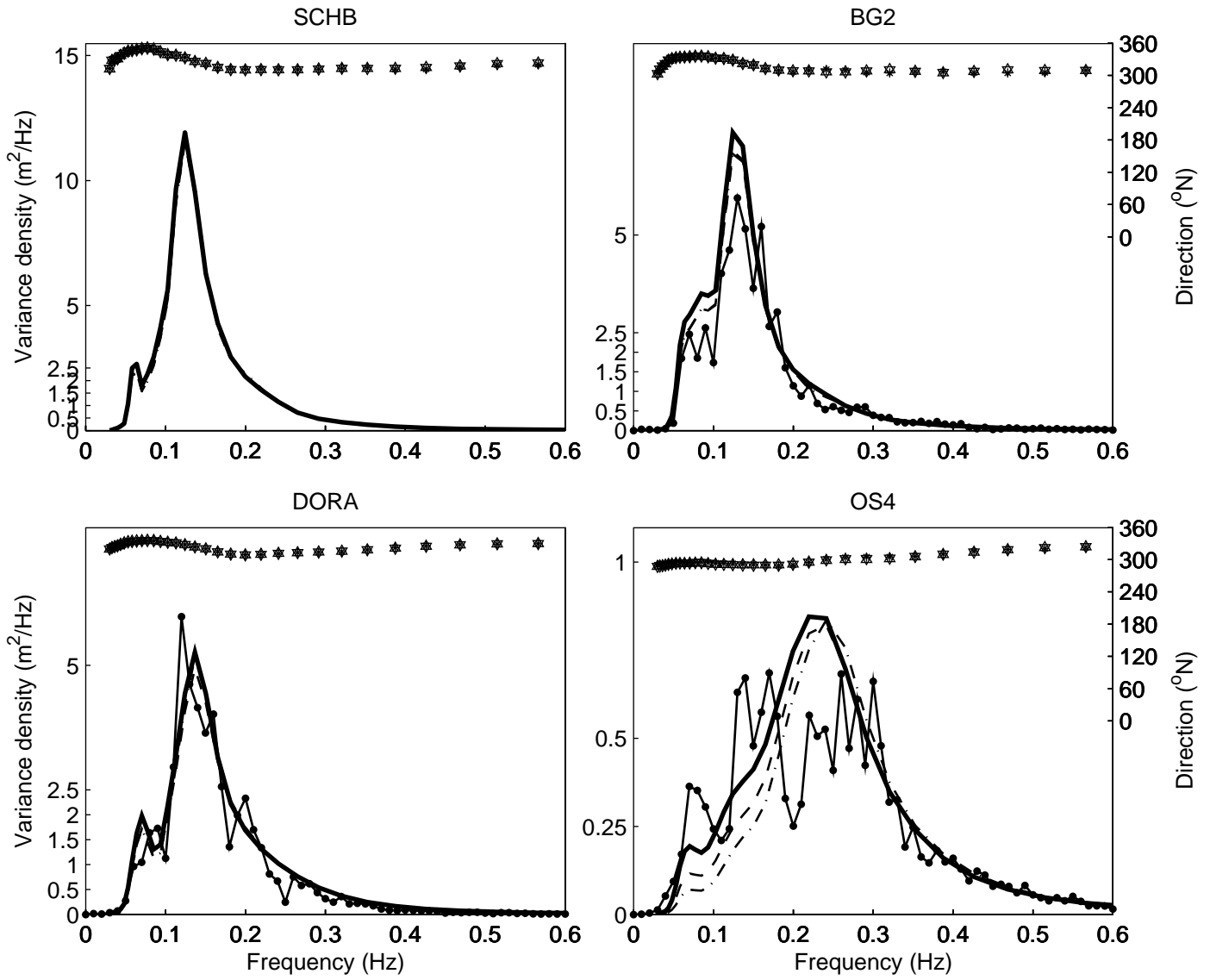
	opposing current	
	SBW Waddenzee	
DELTAES	1202119.006	Fig. 22



Variance density spectra of observations and model results, for three cases of following currents in the Amelander Zeegat

following current

SBW Waddenzee



Default · - · var., * dir. measured: ● — ● var.
 Proposed, $cfjon = 0.067 \text{ m}^2/\text{s}^3$ - - var., ▽ dir.
 Proposed — var., △ dir.

Variance density spectra of observations and model results,
for a case of North Sea wave penetration in the Eastern Scheldt

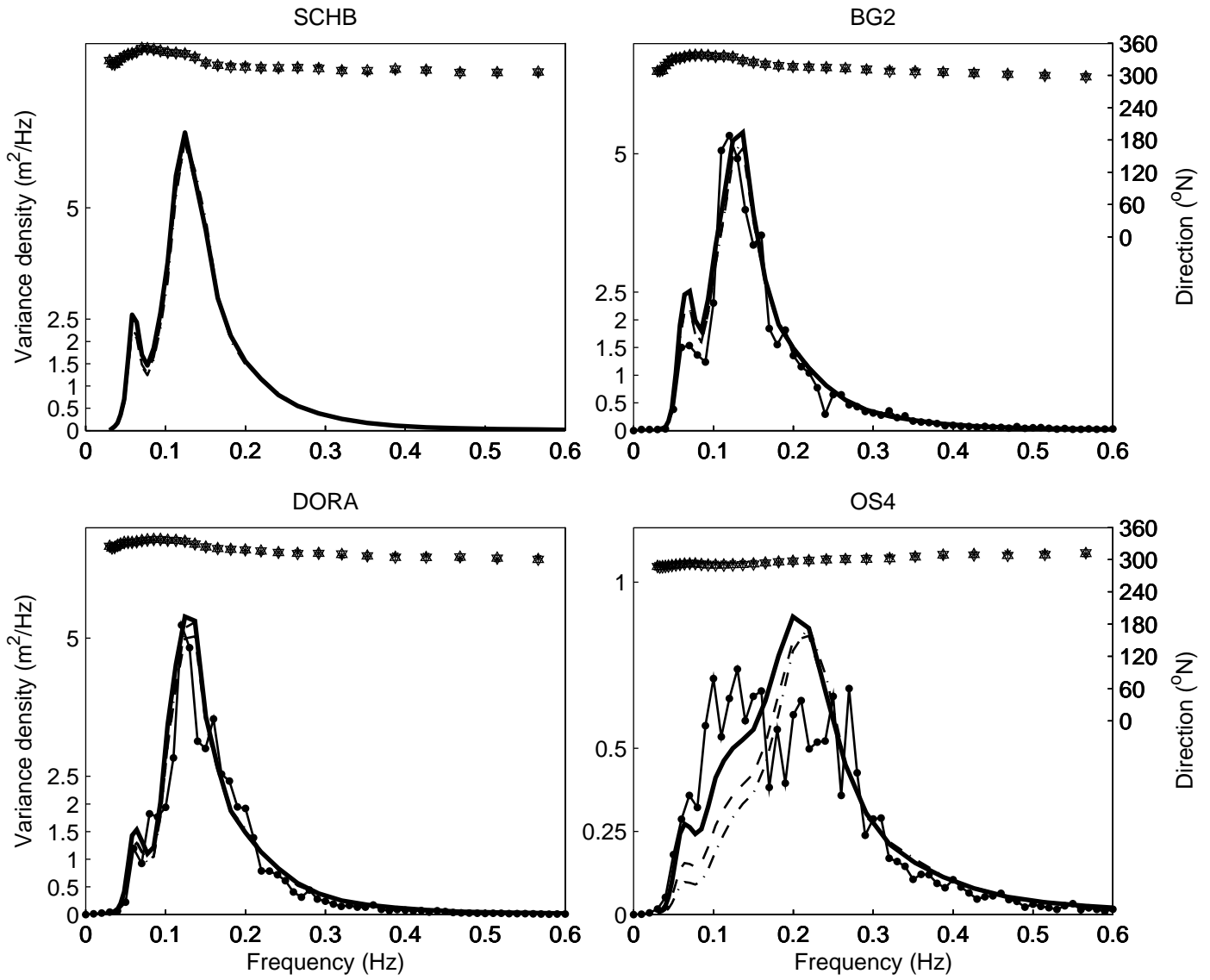
26/12/2001, 09:00

SBW Waddenzee

DELTAES

1202119.006

Fig. 24



Default · - · var., * dir. measured: ● — ● var.
 Proposed, $cfjon = 0.067 \text{ m}^2/\text{s}^3$ - - var., ▽ dir.
 Proposed — var., △ dir.

Variance density spectra of observations and model results, for a case of North Sea wave penetration in the Eastern Scheldt

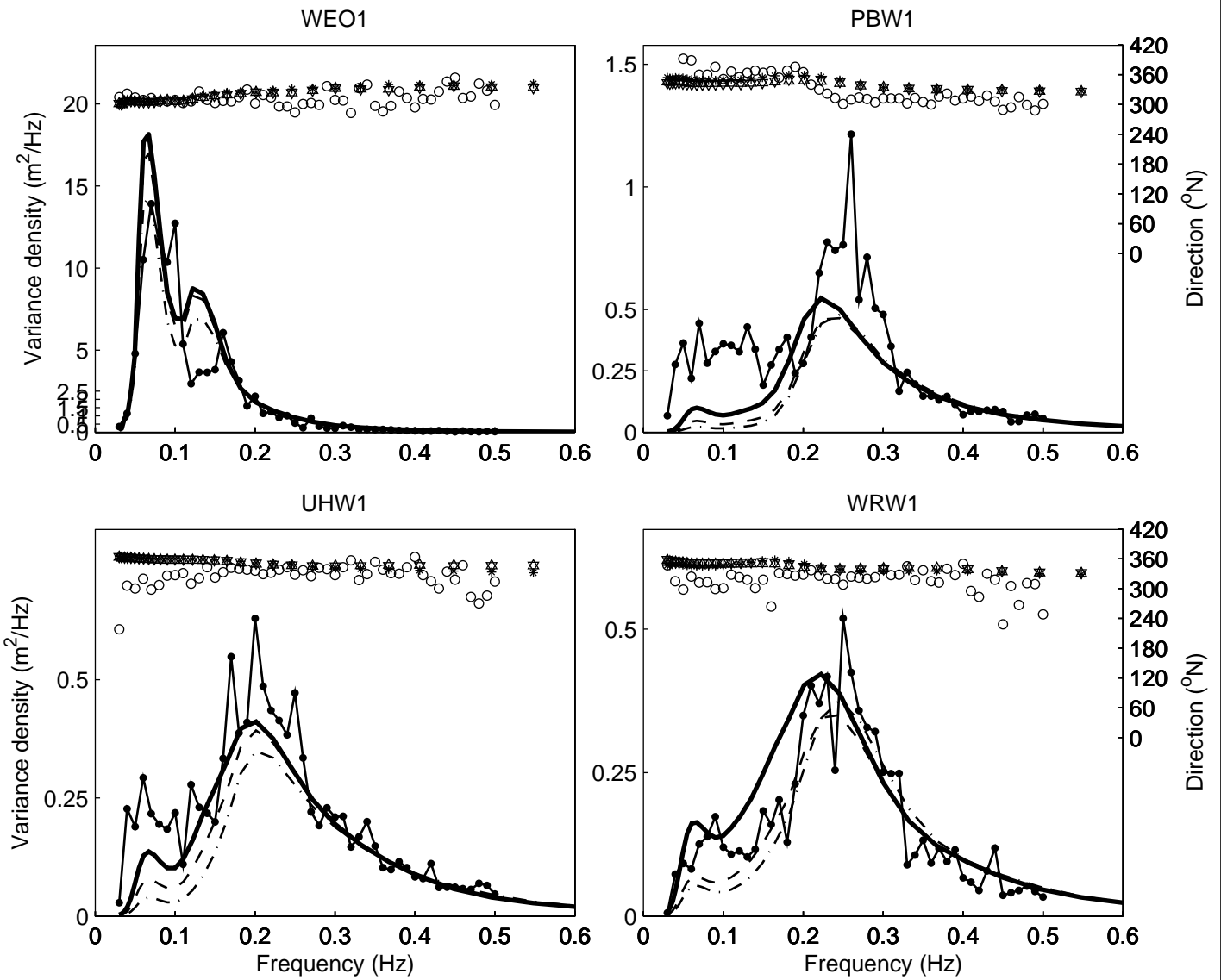
26/12/2001, 12:00

SBW Waddenzee

DELTAES

1202119.006

Fig. 25



Default - · - var., * dir. measured: ● - ● var., ○ dir.
 Proposed, $cfjon = 0.067 \text{ m}^2/\text{s}^3$ - - var., ▽ dir.
 Proposed — var., △ dir.

Variance density spectra of observations and model results,
for a case of North Sea wave penetration in the Eastern Wadden Sea

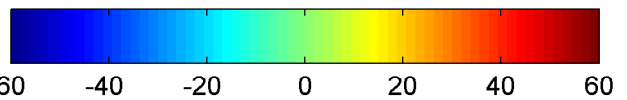
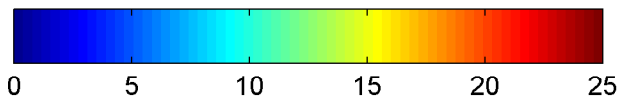
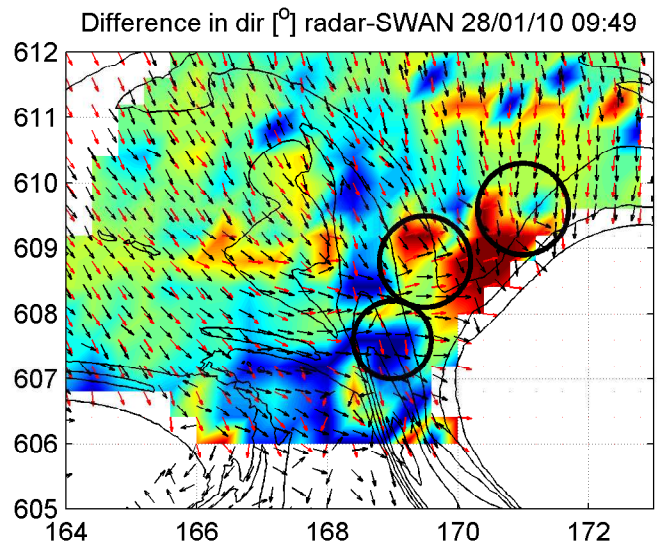
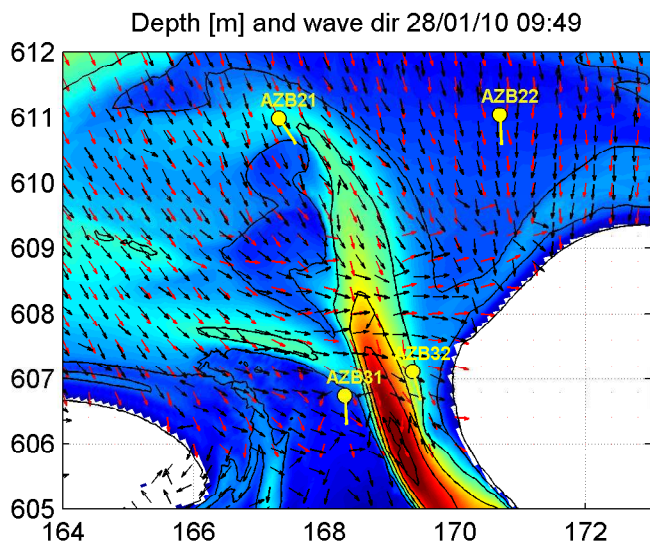
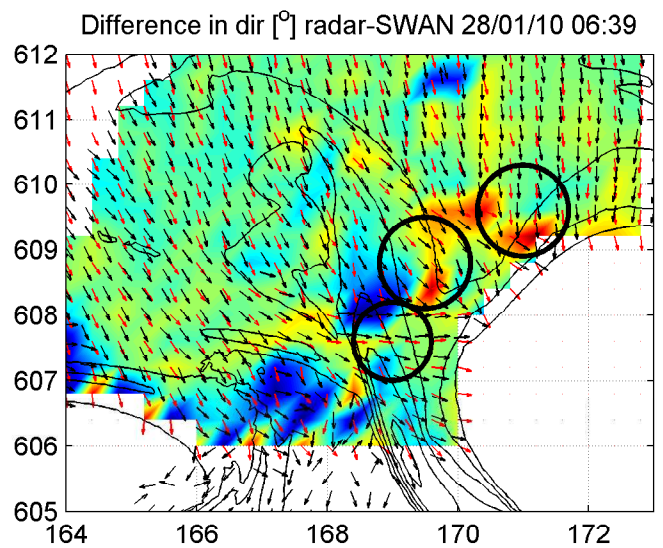
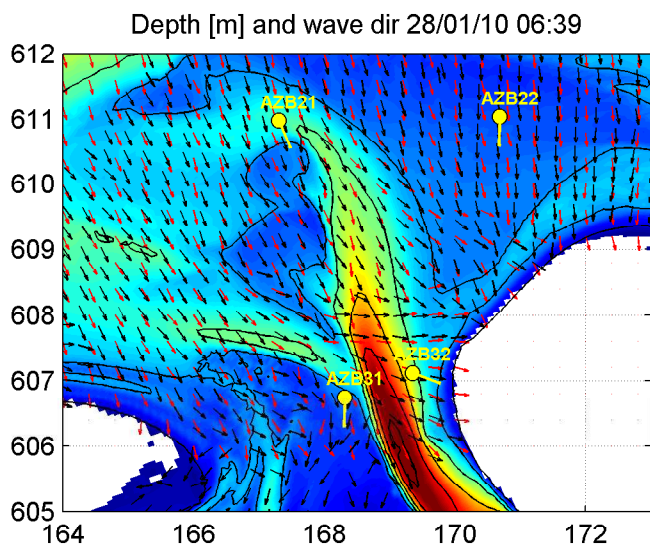
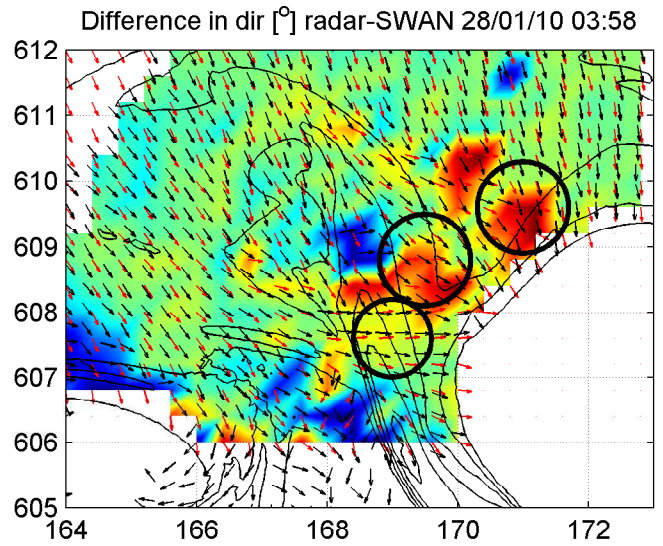
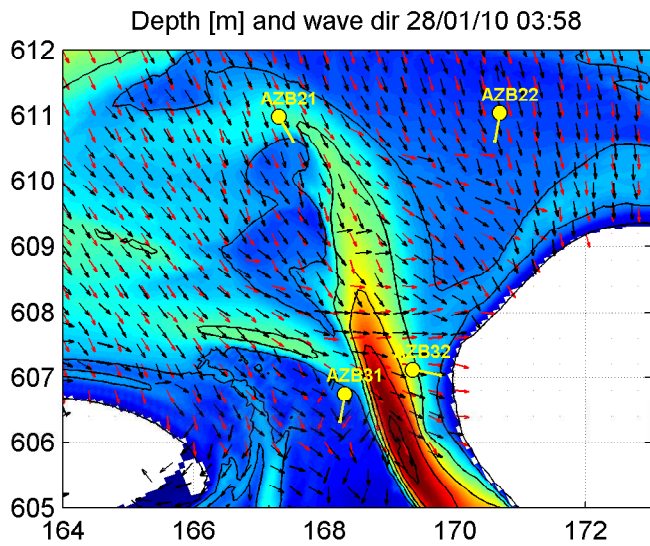
09/11/2007, 09:40

SBW Waddenzee

DELTAES

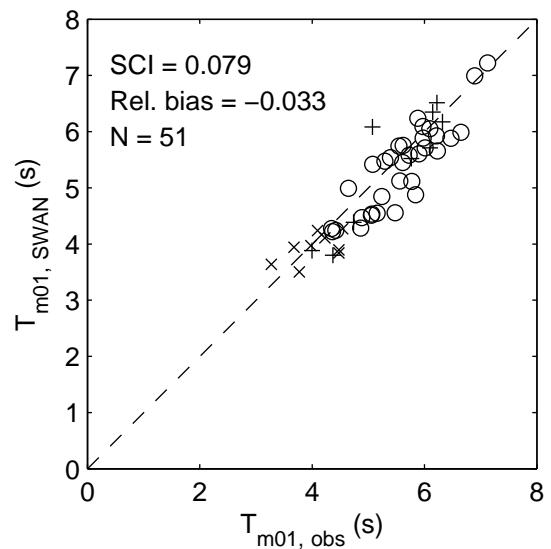
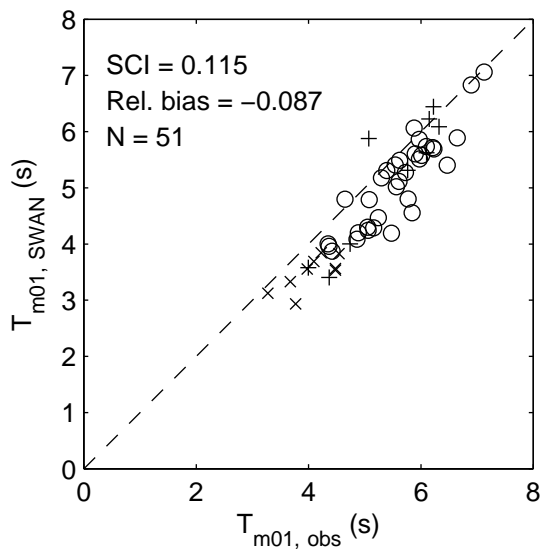
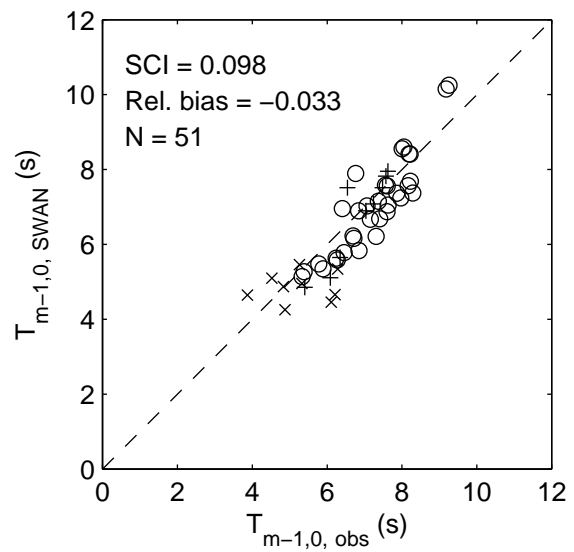
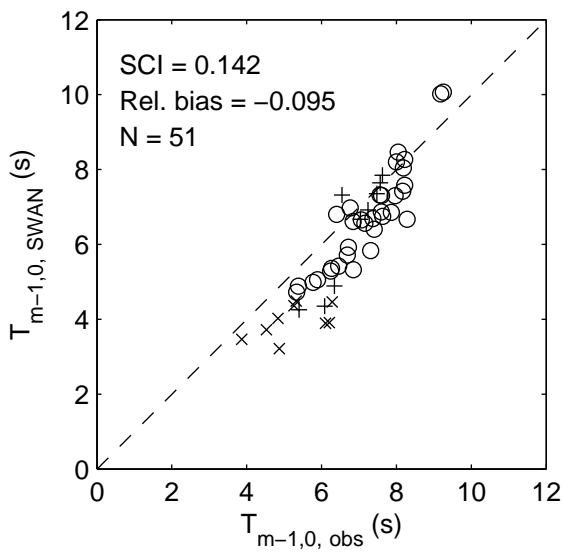
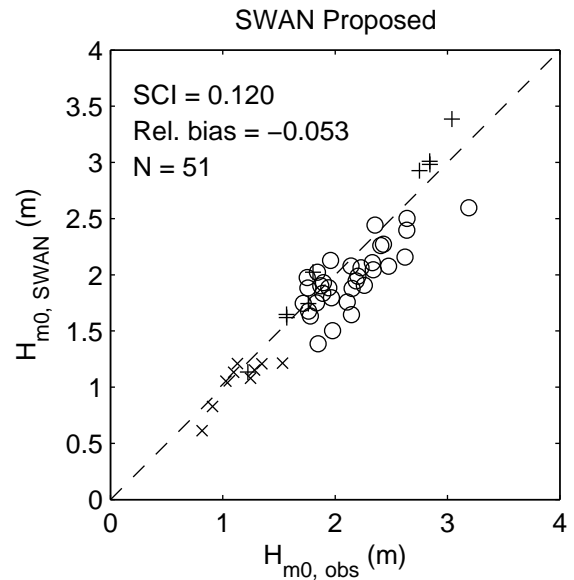
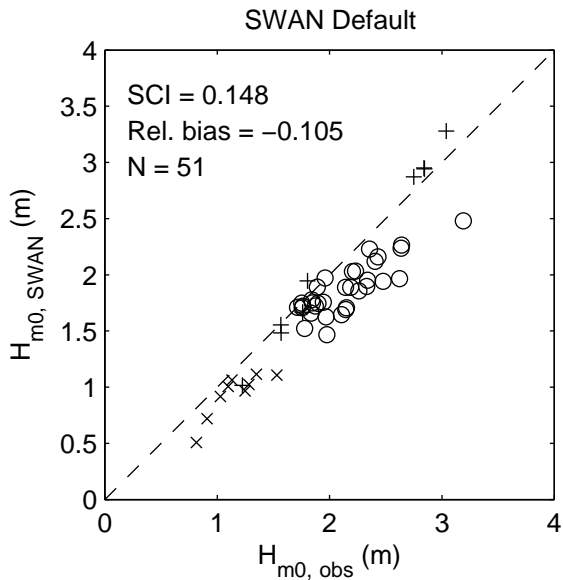
1202119.006

Fig. 26



Comparison dominant wave direction SWAN and radar
 left: depth; right: difference in dominant direction
 vectors: black=radar dominant dir; red=SWAN dominant dir

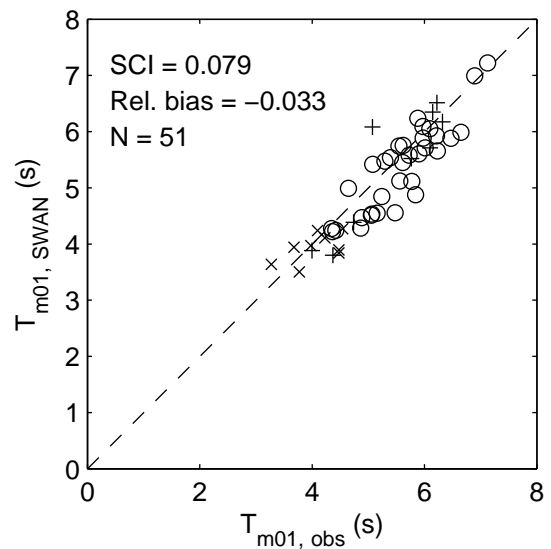
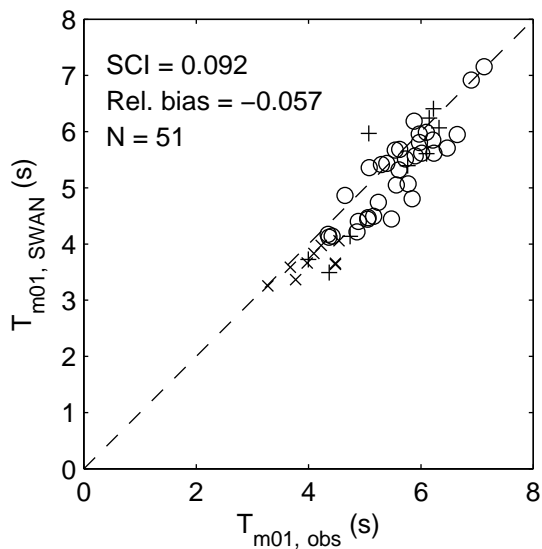
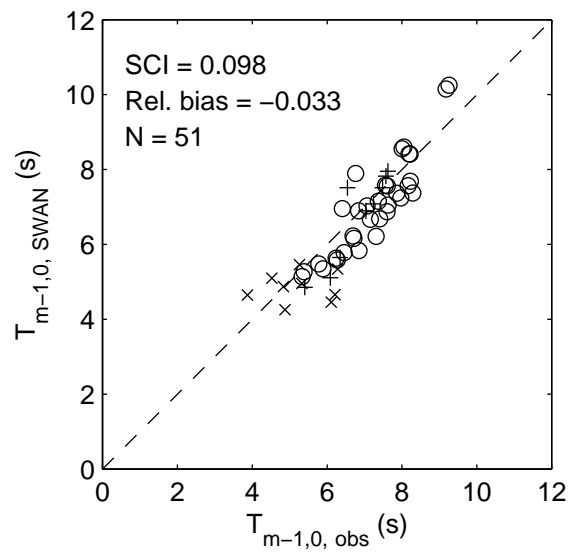
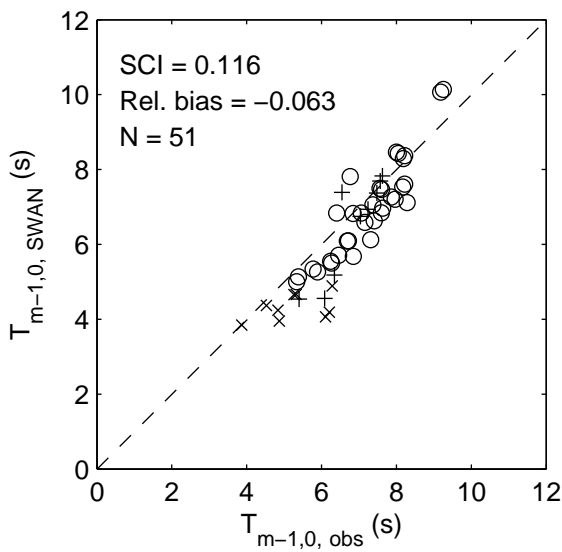
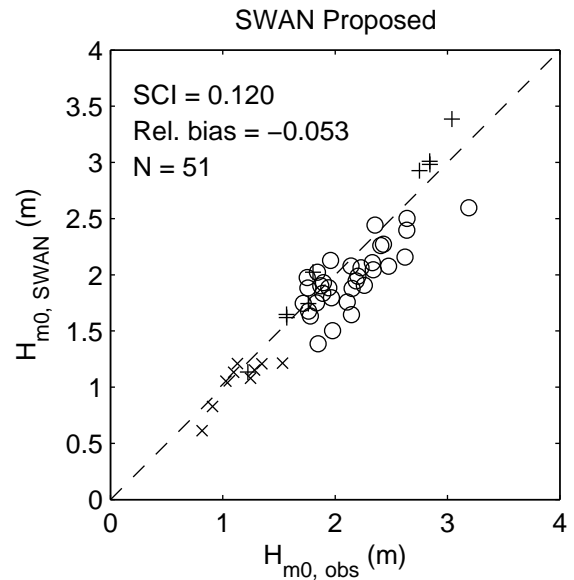
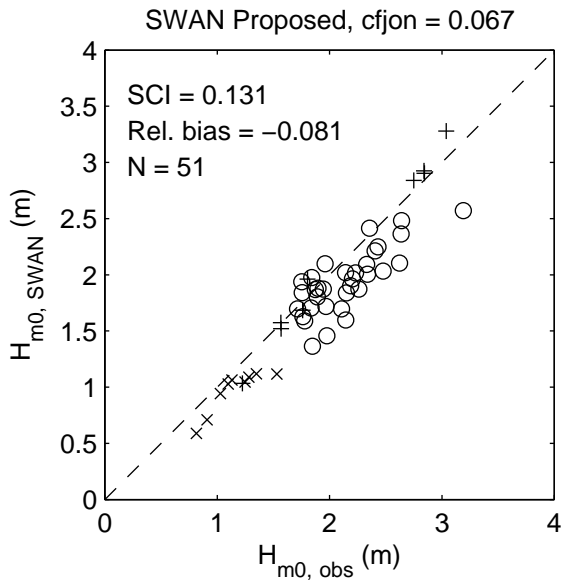
SBW Waddenzee



○ Amelanders Zeegat + Eastern Scheldt × Eastern Wadden Sea

Scatterplots of model results of wave height and wave period versus observations for cases of North Sea wave penetration.
Left: Default model. Right: Proposed model

SBW Waddenzee



○ Amelanders Zeegat + Eastern Scheldt × Eastern Wadden Sea

Scatterplots of model results of wave height and wave period versus observations for cases of North Sea wave penetration.
Left: proposed model with cfjon=0.067 m²/s³. Right: Proposed model

SBW Waddenzee